


PHD PROGRAM IN BIOENGINEERING AND ROBOTICS

ORGANIC AND CMOS BIOSENSORS FOR DETECTION OF TELOMERASE EXPRESSION

CORRADO NAPOLI

SUPERVISOR PROF. MASSIMO BARBARO

A DISSERTATION SUBMITTED IN PARTIAL FULFILLMENT
OF THE REQUIREMENTS FOR THE DEGREE OF
DOCTOR OF PHILOSOPHY IN BIOENGINEERING

UNIVERSITY OF GENOVA

jointly with

ISTITUTO ITALIANO DI TECNOLOGIA

UNIVERSITY OF CAGLIARI

XXX Cycle

To my family. . .

Acknowledgements

To thank in an appropriate manner all the people that have contributed to this work, would probably require another manuscript, perhaps longer than this one.
I would like to thank my thesis advisor, Prof. Massimo Barbaro: the support and the trust you gave me during these years were more than I expected.
My gratitude goes to Prof. Annalisa Bonfiglio and Prof. Piero Cosseddu: thank you for your advice, your help and for having taught me all I know about Organic Electronics.
Thanks to all my colleagues at EOLAB and DEALAB. It has been a pleasure to work with each and every one of you: Alessandra, Alberto, Andrea (both!), Caterina, Fabrizio, Federica, Giulia, Jose, Lorenzo, Roberto, Silvia (both, again!). Last, but not least, a special thanks to Stefano for the precious discussions and the unconditional support.
A special thank goes to Prof. Annalisa Vacca, Prof. Michele Mascia, Dr. Fabrizio d'Adda di Fagagna and Dr. Sofia Francia, for all their support to my research activity. Sofia, thank you for all the invaluable discussions and priceless suggestions.
I have to thank Prof. BenoÃőt Piro, Prof. Vincent Noel, Prof. Giorgio Mattana Dr. Marion Woytasik and Dr. Alexandra Tibaldi: thank you for the opportunity to work with you, it has been a great experience.
Finally, my gratitude goes to my friends, to Francesca and to my parents. For your support, your patience and your love. Thank you.

Cagliari, 13 February 2018

OUTLINE

Cell division plays a crucial role in the normal growth, maintenance and repair of human tissue. Telomeres are regions of repetitive nucleotides located at the end of linear chromosomes of most eukaryotic organisms, which protect DNA from illegitimate recombination, degradation, loss of essential gene and allow the cell to distinguish between double-strand breaks and natural chromosome ends. These structures are primarily involved in the regulation of cell proliferation: they progressively shorten after each division, until a critically short length is reached and the cell either dies by apoptosis or stops dividing and senesces. In 2009 the Nobel prize in Physiology or Medicine was awarded to Elizabeth H. Blackburn, Carol W. Greider and Jack W. Szostak for the discovery of telomerase: a ribonucleoprotein enzyme complex able to stabilize telomere's length. Allowing to sustain chronic and uncontrolled proliferation of cells, telomerase is a fundamental trait of cancer and is found to be active in more than 90% of tumors.

Clearly, the rising interest in the development of new tools for telomerase activity detection is accounted for their clinical implications, which range from the early detection of tumor onset, to the possibility of employing telomerase inhibiting drugs to treat cancer. The research activity discussed in this thesis, aims to introduce a novel approach for telomerase activity detection, in order to overcome the main limitations of the currently employed detection methods, which currently hinder their integration with standard electronics. After a thorough introduction on currently employed techniques, the employment of a particular reference-less Field-Effect Transistor based structure, namely Charge-Modulated Field-Effect Transistor (CMFET), will be discussed. In the perspective of design a device which can either be employed as a laboratory instrumentation or as disposable sensor, according to the technology employed for its fabrication, both the organic implementation of the sensor and a CMFET-based Lab-on-a-chip (LoC) design, will be addressed.

Contents

List of Figures

List of Tables

1 Telomerase expression regulation: detection and clinical implications

In this chapter, an overview of cells life-cycle regulatory mechanism will be presented. Telomeres and telomerase structure and function will be introduced, discussing the influence of telomerase activity in cells senescence and its correlation with the outbreak of neurodegenerative and malignant diseases. A briefly introduction to the commonly employed detection methods will be provided, with an accurate description of their main limitations.

Contents

Each human being experiences birth, life and death. As well, a butterfly starts its life as a very small egg and when it finally hatches, a caterpillar see the light. The worm grows until it reaches its full length and then it form itself into a chrysalis. Finally, when the caterpillar has done all of its forming and changing into the chrysalis, a butterfly emerge.

Both, even if lowly poetic or slightly macabre, are example of a life cycle. At a smaller level, the cell-cycle can be thought as the life cycle of a cell as well. In eukariote organisms it consists of four distinct phase, during which cells perform different, specific, functions depending on the type of cell; it grows, proliferate and eventually become senescent, ceases to carry out its functions and die. In the first phase of the cycle, *G1*, the cell grows, completes biosynthetic activities and increases its supply of proteins in preparation to the start of the second phase, *S*: DNA replication. During this stage, the genetic material of the cell is effectively doubled and, when even this task is completed, the cell enters the third phase, *G2*, during which it grows again, synthesizing more proteins and prepare itself for mitosis, *M*. During this last stage, the cell finally divides its nucleus, its copied DNA and cytoplasm to make two new cells. At first glance, this cycle appears endless. Even so, during G1, the cell could both continue the cycle proceeding with the DNA replication, or it could enter in a *resting* phase, *G0* during which the cell stops further divisions and leave the cycle. This particular phase of the cell-cycle, however, could be both reversible or irreversible: three G0 states exists and can be categorized depending on the mechanism underlying the cause which leads to this phase. In fact, some particular cells, such as stem cells, are believed to actively

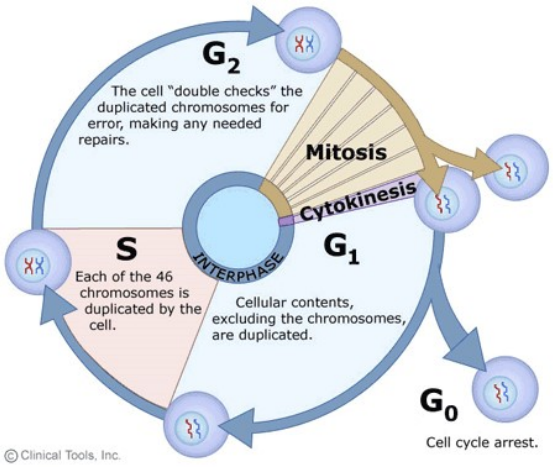

Figure 1.1 – Pictorial representation of the cell cycle.

and reversibly enter this resting phase [1], which is then a *quiescent* state. On the other hand, a cell can enter this stage in an irreversible way. A cell which reached a mature (terminally differentiated) state, such as neurons or cardiac muscle cells, continue to perform its function remaining metabolically active. Otherwise, a dysfunctional cell can cease proliferation and be permanently withdrawn from the cell cycle.

1.1 A biomarker for cancer and neurodegenerative diseases diagnosis

To ensure the proper division of the cell, eukaryotes have evolved a network of regulatory process to control the progression of the cell cycle: *cell cycle checkpoints*, aremechanisms by which the cell actively halts progression of the cell cycle until it can ensure that an earlier process, such as DNA replication or mitosis, is complete [2]. One of the most critical checkpoints in the cell cycle is DNA damage, as unfixed damage can introduce mutations during DNA replication, leading to potential changes in cell behavior. Epidemiological studies demonstrated that damages to cellular DNA can cause cancer [3], but it should also be used to cure the same illness. A wide variety of therapeutic approaches currently used to treat malignancies target the DNA, including radiation therapy and many chemo-therapeutic agents. Nevertheless, DNA damage is responsible for most of the side effects of therapy as well. Although there is still a limited understanding of how the processes of cell-cycle arrest and the process of DNA repair are coordinated, increasing evidence suggests that cellular senescence plays a crucial role in suppressing malignant tumour formation [4]. Cellular senescence occurs both as a consequence of a DNA damage, and as because of the limited replicative lifespan of the cell as well. This phenomenon, called *replicative senescence*, appears to be a fundamental characteristic of somatic cell. Leonard Hayflick and Paul Moorhead investigated the limited capability of normal human cells to divide [5]. Their experiment demonstrated that a counting mechanism intrinsically presents in each single cell, allows to stop cell division after a fixed number of divisions. Such a regulatory mechanism is called *Hayflick limit*. Probably one of the most important consequences of this study, has been the investigation of the mechanisms which underlies the existence of the Hayflick limit. In particular, it has been demonstrated that replicative senescence is a consequence of the progressive shortening

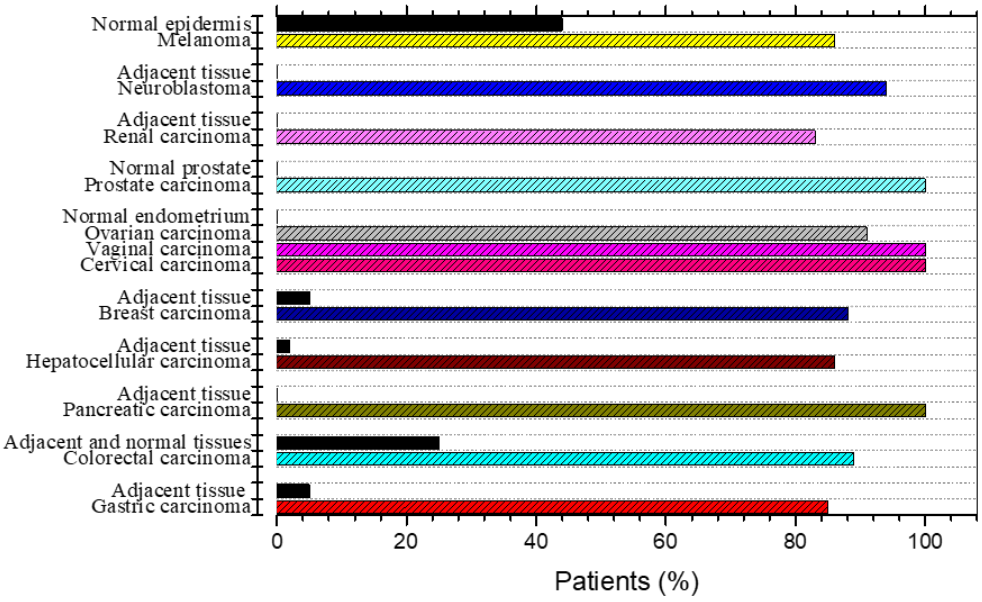

Figure 1.2 – Telomerase activity in cancer [10].

of the distal DNA filaments. These chromosomes terminal structures, called *telomeres*, do not carry genetic information but act as a protective caps of chromosomes, preventing lost of genetic information or end-to-end fusions. In addition, their progressive shortening provide a natural hindrance to tumor progression [6]. The strong correlation between these two mechanisms, leads to a number of study which eventually demonstrated the correlation between the activity of a ribonucleoprotein complex, called *telomerase*, and outbreaks of tumors [7][6]. Tumoral illnesses share the common phenotype of uncontrollable cell growth and proliferation [8][9]; the limited capability of a normal cell to divide as a consequence of such behavior, in fact, acts as a natural control mechanism against uncontrolled proliferation of cells. In particular, studies performed in late 90's, revealed that while telomerase activity has been found in approximately 85% of the most common cancers, most normal human cells are telomerase silent [10][11] (figure 1.2). Even if telomerase do not drive the oncogenic process, it is permissive and required for the sustain growth of most advanced cancers. Detection and quantification of telomerase activity represents therefore an attractive tool both for early detection of cancer, and as a prognostic indicator of patient outcome, since the level of its activity is not high but increases with cancer progression [10][12]. As a consequence, in the last decade, the

study of telomerase inhibitor has become relevant to develop therapies for malignant proliferative diseases.

In addition to its role in the diagnosis and treatment of cancer, telomerase was demonstrated to play a role in age-related [13][14] and neurodegenerative diseases [15][16] as well. In particular, preliminary results seem to confirm the first hypothesis of correlation between the insurgence of these pathologies and a down-regulation of the enzyme [13], suggesting that its catalytic subunit assumes a protective function in adult human brains [16], thus shedding new light on the role of telomerase in this field of research.

1.2 Telomeres and telomerase: structure and function

The well-known double-strand helix structure of DNA, suggested by Watson and Crick, is composed of two strands formed by a sequence of nucleotides. A nucleotide is composed of a nucleoside, which consists in a nitrogenous base and a phosphate group, and a pentose sugar.

Each nucleoside is composed of one of five nucleobases: cytosine (C), adenine (A), guanine (G) and thymine (T) in DNA, or uracil (U) instead of thymine in RNA.

Each strand is made up of a sequence of nucleotides joined together in a chain of covalent bonds, forming a sugar-phosphate backbone, and it is bound with its complementary strand (A bound to T and G bound to C) with hydrogen bonds to form a double strand DNA. This structure is anti-parallel, that is the 5' end of one strand is paired with the 3' end of its complementary, as shown in figure 1.4.

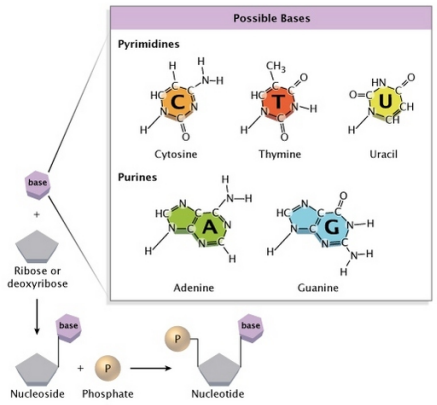

Figure 1.3 – Structure of a nucleotide. A five-carbon sugar and a nitrogenous base is a nucleoside. A nucleoside and a phosphate group form a nucleotide. Image courtesy of *Nature.com*.

The outer edges of the nitrogen-containing bases are exposed and available for poten-

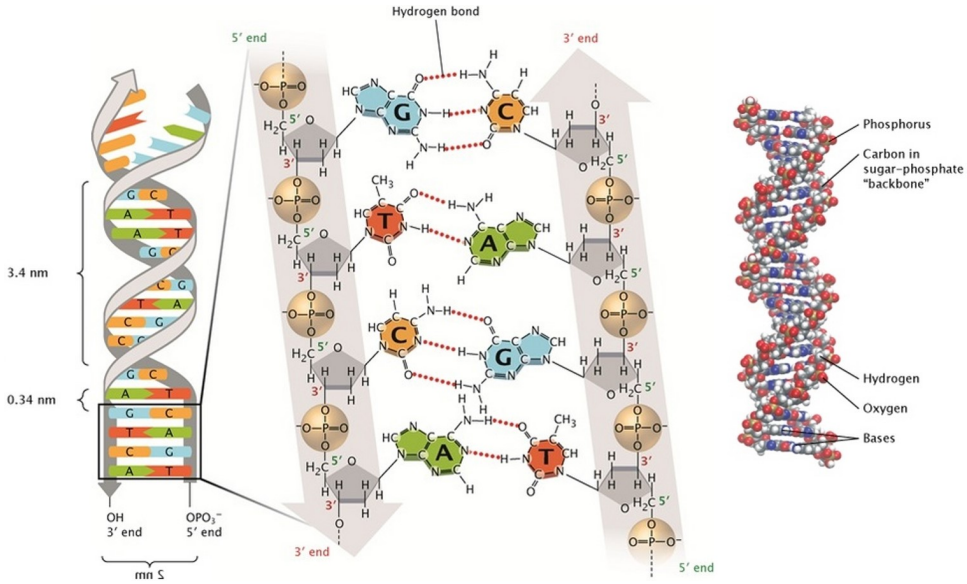

Figure 1.4 – DNA structure is composed of two anti-parallel strands, so that the 3' and the 5' end of the two strands are aligned. Image courtesy of *Nature.com*.

tial hydrogen bonding as well, in order to provide an access to the DNA for other molecules, including proteins.

A key step in the aforementioned cell life cycle, is represented by the DNA replication: during this stage, the genetic information of the cell is effectively copied so that it can be transferred to the new cell. DNA replication, however, is a semi-conservative process and, therefore, needs that the double-strand is unwound in order to be performed. Strands unwinding is carried out by a specfic enzyme, called helicase, which divide the double-strand into two separate strands which can be copied due to the work of polymerases. Such a process is somehow hindered from a particular characteristic of all DNA polymerases, which are able to synthesize DNA strands only in the 5'-3' direction. These enzymes, in fact, need both a template strand and a primer to proceed with the oligonucleotide synthesis, because they can add a nucleoside triphosphate molecule containing deoxyribose (dNTP) only on the 3'-OH end of an existing strand. As a consequence, the process requires a DNA primase which synthesizes an RNA primer so that it can be used as a starting point from DNA polymerases to proceed further, synthesizing polymers of nucleic acids.

Figure 1.5 schematically represents the problem which arise during DNA synthesis

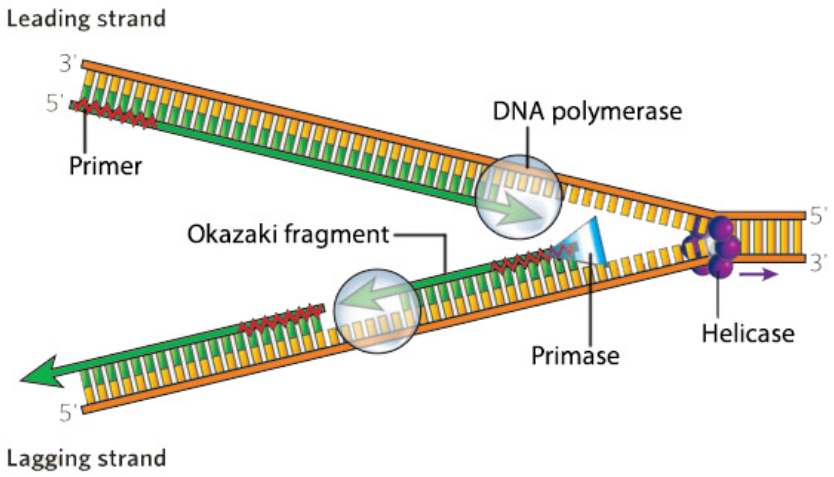

Figure 1.5 – DNA replication: the double strand is unwound by an helicase and the two strands are then copied by a DNA polymerase. The synthesis proceed continuously in the leading strand, while is performed in short separated segments in the lagging strand. Image courtesy of *Nature.com*.

starting from two unfolded strands: as DNA molecule is anti-parallel, the two strands are oriented in opposite directions. Therefore only one of them, the *leading strand*, can be synthesized in a continuous manner. On the contrary, the other one, the *lagging strand*, is synthesized in short separated segments, also called *Okazaki fragments*, each of which needs its own RNA primer. At the end of the replication process, arises the so called *end replication problem*: because of the above mentioned mechanism, the last small sequence of nucleotides at the very 5'-end of the lagging strand is lost, because of the impossibility of the enzyme to replace the 5'-end RNA primer. As a result, the leading strand is progressively shorten as cell division proceeds, and in absence of an appropriate control mechanism, part of cell genetic information would be lost at each division.

Telomeres are non-coding structures formed of repetitions of a G-rich sequence (*TTAGGG* in humans) of six nucleotides located at the end of eukaryotic chromosomes, which main function is to maintain chromosome stability, avoiding end-to-end fusions and the accumulation of chromosomal aberrations. In 1985, Carol Greider investigated the activity in Tetrahymena extracts that could add nucleotides to a synthetic oligonucleotide that contained four copies of the Tetrahymena telomere. She was then able to purify an enzyme able to catalyze the synthesis of telomeres-repeated sequence at the end

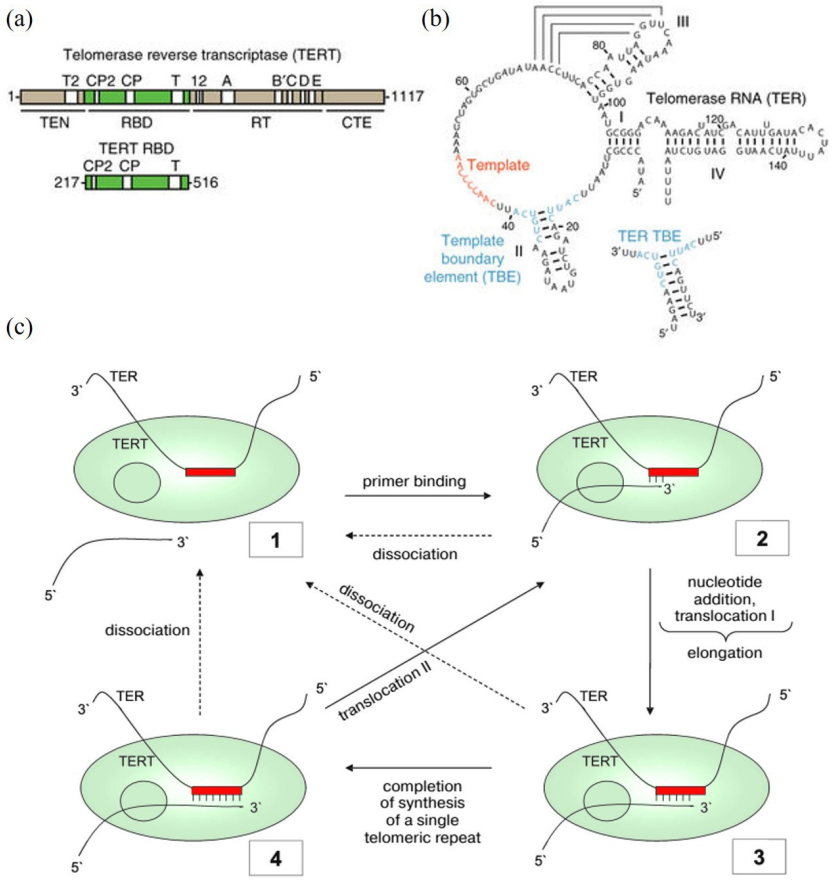

Figure 1.6 – (a) Telomerase Reverse Transcriptase (TERT) structure. (b) Secondary structure model for telomerase RNA. (c) Telomerase reaction cycle: 1) enzyme is not bound to primer; 2) primer annealing; 3) elongation stage; 4) completion of a single telomeric repeat synthesis. Dotted arrows point to possible processes of primer dissociation during enzyme functioning [18]

of such oligonucleotides [17], thus solving the end replication problem. The enzyme, which was later named telomerase, is an highly-specialized reverse transcriptase able to synthesize DNA from an RNA template. Its structure comprises a RNA component (TER), which contains a template region complementary to the telomeres sequence, and different, functionally important, secondary structure elements involved in template region restriction, protein subunit binding, and partially carrying out catalytic and other functions [18]. A telomerase reverse transcriptase (TERT) subunit contains a catalytically important domain resembling that of reverse transcriptases, as well as only telomerase-specific domain necessary for TER and DNA substrate binding and for functional activity of telomerase [18]. Telomerase reaction cycle is shown in figure

1.6c. The enzyme interacts with the DNA not only at its 3'-end, but also in its 5'-end in the so called "*anchor site*". There is not enough data on the anchor site function and localization, but is supposed to be responsible to form stable interactions with DNA to prevent enzyme-DNA dissociation during telomeres elongation process. Such a process, after primer binding, consists of elongation, traslocation and a dissociation stage. As depicted in figure 1.6c, telomerase is able to add one or several telomeric repeats during a single act of attachment to oligonucleotide substrate [19]. In the case of consecutive transition of the enzyme from through each stage, telomerase adds one telomeric repeat to the primer. Transition from stages 4-2 in figure 1.6c, corresponds to translocation II, i.e. to addition of several telomeric repeats without separation from the primer.

Telomerase activity is proportional to the total amount of DNA that it synthesizes, however it is important to underline that its components may perform functions that are independent of the arrangement of the active complex. In fact, enzyme expression and activity are not always correlated and while targeting complex activity is interesting because of the before mentioned correlation with the onset of malignant illnesses, the enhancement of the human TER is not always correlated with the enzyme activity [20]. Targeting the enzyme activity, and not its presence or enhancement of the transcription expression, could therefore be useful both in clinical application for diagnostic purposes and to develop telomerase inhibitors as potential anti-cancer drugs.

1.3 Detection of Telomerase expression regulation

In the early Nineties, research emphasized the connection between telomerase activity and proliferation of cancer cells [6], and assays for direct detection of telomerase activity were based on the exploitation of an oligonucleotide of telomere sequence, used as a substrate for elongation by telomerase. The incorporation of a deoxynucleotide triphosphate (dNTP) mixture allows to detect such an activity by means of optical measurements. These methods, however, have a low-sensitivity and require a relatively high levels of radioactive precursors. Nowadays, the most common methods for the detection of telomerase activity are based on modifications of a protocol proposed by Kim et al. [7], named *Telomerase Repeat Amplification Protocol*. The assay replaces the oligonucleotide used in the previous approach with a substrate primer (TS) of a non-

telomeric sequence, which will be extended with telomeric repeats as shown in figure 1.7. The amplification of the telomerase-mediated extensions was then performed using *Polymerase Chain Reaction* (PCR) with a reverse primer (CX). Finally, the detection was originally intended to be performed through electrophoretic separation. Such a technique, needs a relatively large amount of DNA (tens of ng) in order to be performed and interactions between primers could produce both the appearance of false positive signals and the onset of a background signal when using a concentrated extracts from tumor samples. Most recent modifications attempt to overcome these issues, modifying the biological components of the assay. For example, the use of two primers in order to reduce false positive signals, or the implementation of internal standards [22] to take into consideration the presence of Taq polymerase inhibitor into the samples [23] [24] can be cited. Aside from this, however, TRAP-based techniques suffer of some other drawbacks originated from the amplification step. In fact, because of the low sensitivity of electrophoretic detection method, a three stage procedure comprising an amplification step subsequent to primer elongation is unavoidable. PCR amplification, in its turn, is a time-consuming step and from a practical viewpoint represents a critical hindrance to the development of a fast and automatizable assay. PCR consists of a series of different steps, performed in 20-40 cycles in a thermal cycler (figure 1.8b). During each cycle, the

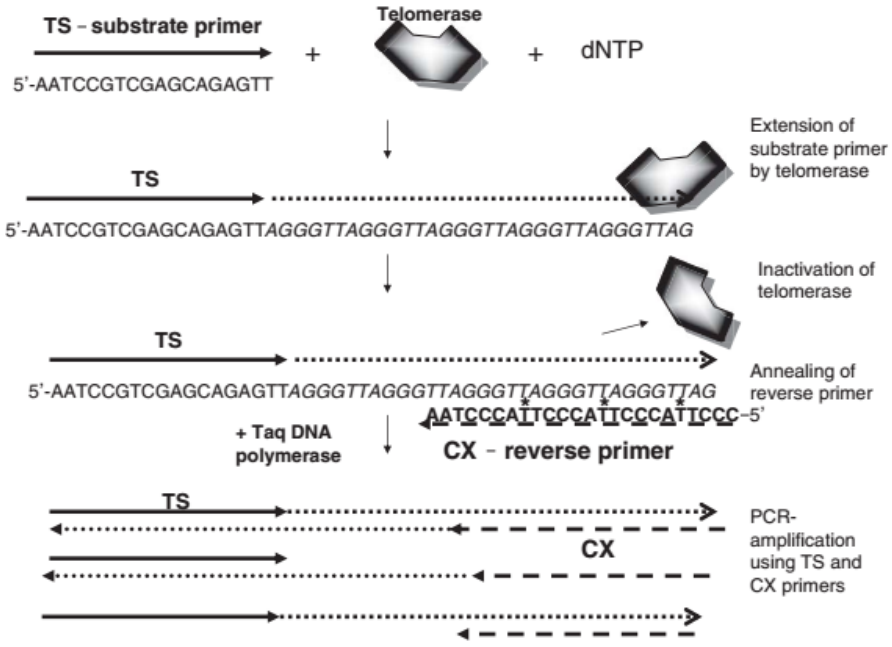

Figure 1.7 – Scheme of TRAP assay. [21]

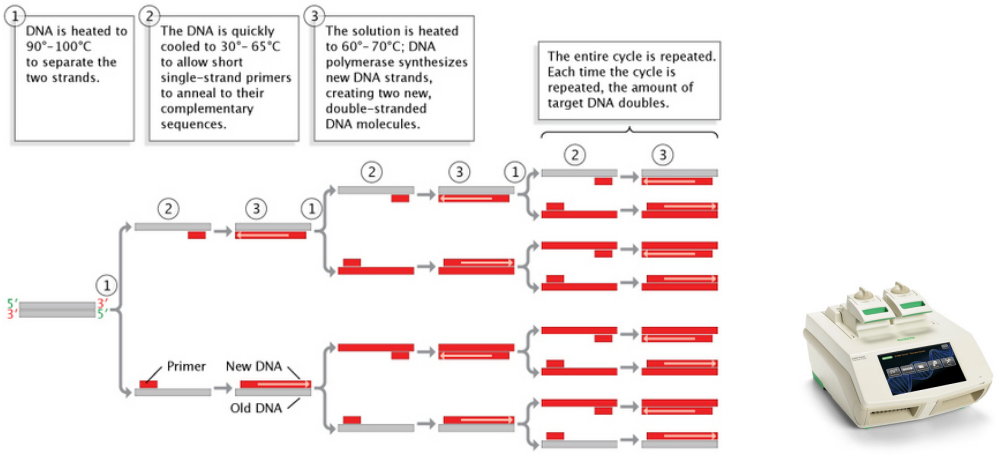

(a) Schematic representation of PCR step. Image courtesy of *Nature.com*

(b) Bio Rad thermal cycler. Image courtesy of *www.bio-rad.com*

Figure 1.8

temperature repeatedly changes. The firs step (*denaturation*) is performed at 90-100 °C for 20-30 seconds. During this step, hydrogen bonds of double stranded DNA molecules have been broken and DNA melts. The subsequent step (*anneling)* is performed at 30-65 °C for 20-40 seconds, and promotes DNA fragments binding with a complementary DNA primer necessary for the polymerase reaction. Finally, the elongation of the DNA target region to amplify (template), is elongated due to the work of DNA polymerases. The temperature used during this process depends on the specific polymerase used and is usually comprised within 60 and 70 °C. During a final step the reaction chamber is cooled at 4-15 °C.

In addition to the inherent complexity of the basic procedures before explained, and to the time needed to perform the whole process, the assay is usually complicated by a number of specific protocols are required in order to limit the amplification of spurious DNA products. Improvements in telomerase activity detection methods are nowadays a prolific field of investigation. Researchers' effort focuses on the possibility to avoid both the amplification stage and the electrophoresis detection, in order to improve both the reliability and the sensitivity of the procedure. A number of different approaches have been investigated during the last decade, exploiting recent progresses in the fields of bio- and nano-technologies.

Bibliography

[1] T. H. Cheung and T. A. Rando, "Molecular regulation of stem cell quiescence," *Nature Reviews Molecular Cell Biology*, vol. 14, no. 6, pp. 329–340, 2013.

[2] S. J. Froelich-Ammon and N. Osheroff, "Topoisomerase poisons: Harnessing the dark side of enzyme mechanism," 1995.

[3] P. R. Doll R, "The causes of cancer: Quantitative estimates of avoidable risks of cancer in the united states today," *Journal of the National Cancer Institute*, vol. 66, no. 6, pp. 1192–1308, 1981.

[4] J. Campisi, "Cellular senescence: Putting the paradoxes in perspective," 2011.

[5] L. Hayflick and P. Moorhead, "The serial cultivation of human diploid cell strains," *Experimental Cell Research*, vol. 25, no. 3, pp. 585–621, 1961.

[6] C. M. Counter, A. A. Avilion, C. E. Lefeuvrel, N. G. Stewart, C. W. Greider, C. B. Harley, and S. Bacchettil, "Telomere shortening associated with chromosome instability is arrested in immortal cells which express telomerase activity," *The EMBO Journal*, vol. 1, no. 1, pp. 921–1929, 1992.

[7] N. Kim, M. Piatyszek, K. Prowse, C. Harley, M. West, P. Ho, G. Coviello, W. Wright, S. Weinrich, and J. Shay, "Specific association of human telomerase activity with immortal cells and cancer," *Science*, vol. 266, no. 5193, pp. 10114–10118, 1994.

[8] A. Balmain, "Cancer genetics: from Boveri and Mendel to microarrays.," *Nature reviews. Cancer*, vol. 1, no. 1, pp. 77–82, 2001.

[9] P. A. Futreal, L. Coin, M. Marshall, T. Down, T. Hubbard, R. Wooster, N. Rahman, and M. R. Stratton, "A census of human cancer genes," *Nature Reviews Cancer*, vol. 4, no. 3, pp. 177–183, 2004.

[10] J. W. Shay and S. Bacchetti, "A survey of telomerase activity in human cancer," *European Journal of Cancer*, vol. 33, no. 5, pp. 787–791, 1997.

[11] N. W. Kim, "Clinical implications of telomerase in cancer," *European Journal of Cancer Part A*, vol. 33, no. 5, pp. 781–786, 1997.

[12] M. Hashim, M. Sayed, N. Samy, and S. Elshazly, "Prognostic significance of telomerase activity and some tumor markers in non-small cell lung cancer," *Medical Oncology*, vol. 28, pp. 322–330, Mar 2011.

[13] M. Jaskelioff, F. L. Muller, J.-H. Paik, E. Thomas, S. Jiang, A. C. Adams, E. Sahin, M. Kost-Alimova, A. Protopopov, J. Cadiñanos, J. W. Horner, E. Maratos-Flier, and R. A. DePinho, "Telomerase reactivation reverses tissue degeneration in aged telomerase-deficient mice," *Nature*, vol. 469, no. 7328, pp. 102–106, 2011.

[14] R. M. Cawthon, K. R. Smith, E. O'Brien, A. Sivatchenko, and R. A. Kerber, "Association between telomere length in blood and mortality in people aged 60 years or older," *Lancet*, vol. 361, no. 9355, pp. 393–395, 2003.

[15] E. Eitan, E. R. Hutchison, and M. P. Mattson, "Telomere shortening in neurological disorders: An abundance of unanswered questions," 2014.

[16] A. Spilsbury, S. Miwa, J. Attems, and G. Saretzki, "The Role of Telomerase Protein TERT in Alzheimer's Disease and in Tau-Related Pathology In Vitro," *Journal of Neuroscience*, vol. 35, no. 4, pp. 1659–1674, 2015.

[17] C. W. Greider and E. H. Blackburn, "Identification of a specific telomere terminal transferase activity in tetrahymena extracts," *Cell*, vol. 43, no. 2 PART 1, pp. 405–413, 1985.

[18] D. M. Shcherbakova, M. E. Zvereva, O. V. Shpanchenko, and O. A. Dontsova, "[Telomerase: structure and properties of the enzyme, characteristics of the yeast telomerase]," *Mol Biol (Mosk)*, vol. 40, no. 4, pp. 580–594, 2006.

[19] C. Kelleher, M. T. Teixeira, K. Förstemann, and J. Lingner, "Telomerase: Biochemical considerations for enzyme and substrate," 2002.

[20] T. Pasrija, R. Srinivasan, D. Behera, and M. S., "Telomerase activity in sputum and telomerase and its components in biopsies of advanced lung cancer.," *Scientific reports*, vol. 43, no. 9, p. 1476âĂŞ1482, 2007.

[21] J. Fajkus, "Detection of telomerase activity by the TRAP assay and its variants and alternatives," 2006.

[22] I. Szatmari and J. Aradi, "Telomeric repeat amplification, without shortening or lengthening of the telomerase products: a method to analyze the processivity of telomerase enzyme.," *Nucleic acids research*, vol. 29, no. 2, p. E3, 2001.

[23] I. Szatmari, S. Tokes, C. B. Dunn, T. J. Bardos, and J. Aradi, "Modified telomeric repeat amplification protocol: a quantitative radioactive assay for telomerase without using electrophoresis," *Anal Biochem*, vol. 282, no. 1, pp. 80–88, 2000.

[24] H. Uehara, G. Nardone, I. Nazarenko, and H. RJ., "Detection of telomerase activity utilizing energy transfer primers: Comparison with gel- and ELISA-based detection," *BioTechniques*, vol. 26, no. 3, pp. 552–558, 1999.

2 Biosensors for Telomerase expression regulation detection

Telomerase activity has been shown to be an effective biomarker, strictly correlated with the outbreak of tumoral illnesses and neurodegenerative diseases. Standard detection mechanisms suffers of several limitations, which hinder their integration with standard electronics. In this chapter, the main advantages, issues and still-opened challenges of several biosensing techniques will be reviewed, with particular focus on the application to detection of telomerase activity.

Contents

Detection of telomerase activity has been demonstrated to be a useful diagnosis tool for cancer, as the majority of tumors showed a pronounced expression of its catalytic activity [1] [2]. Furthermore, its inhibition has been considered as a new, relatively safe, anticancer strategy [3].

Conventional primer extension-based assays suffer from some limitations, mainly related to the large sample requirements, and low sensitivity of the technique. TRAP method and its modifications need an almost unavoidable PCR step and gel electrophoresis. The main drawbacks with this approach are due to its rather complex experiment protocol, a long testing time as well as the issues related to the possible presence of PCR inhibitor in the sample under test. For example, saliva usually contains RNase and therefore the contamination of a TRAP assay is unavoidable when using samples of oral origin. Furthermore, the analysis of TRAP results is usually accomplished observing PCR amplification products after gel electrophoresis. Obviously, such an evaluation is both subjective, often not clear and barely scalable. The fast pacing progresses obtained in this research field place an additional restrain to the clinical application of these techniques, which proven to be less flexible in terms of capability to handle a growing amount of samples, and require highly specialized operators in order to be performed.

Overcoming these shortcomings through the employment of alternative approaches to the biochemical-based assays should be a valuable choice to take into consideration. In particular, the employment of a device which could combine the advantages offered from different transduction methods and the selectivity which is proper of biological elements, could be considered as a valuable candidate for the proposed investigation.

2.1 Biosensors: introduction, definition and their applications

Accordin to IUPAC, a biosensor is an analytical device which uses a specific biochemical reactions mediated by isolated enzymes, immunosystems, tissues, organelles or whole cells to detect chemical compounds usually by electrical, thermal or optical signals [4]. The usual aim of such a device is to produce an output signal which is proportional to the concentration of a specific chemical or set of chemicals. In particular, the combination

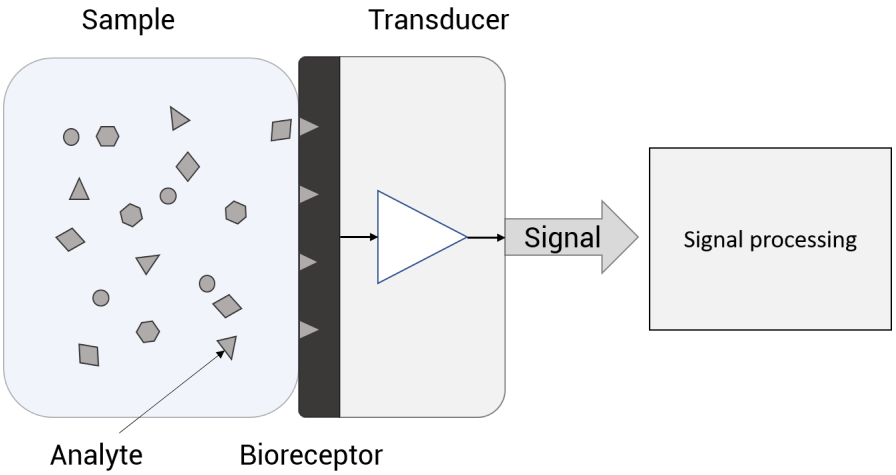

Figure 2.1 – Generalized schematic of a biosensor.

of a biological sensing element (*bioreceptor*) either intimately connected to or integrated with a physico-chemical detector (*transducer*), allows the exploitation of both the specificity and sensitivity of the biological systems with the computing power of modern signal processing elaboration. The modern concept of a biosensor can be led back to the idea of Leland C. Clark Jr. and Lyons [5]. A generalization of the concept introduced by Clarke and Lyon with the glucose sensor, is depicted in figure 2.1. Over the years many combinations of bioreceptors and transduction mechanisms have been proposed and, according to IUPAC [4] and figure 2.1, biosensors classification can be based either by the employed bioreceptor or their transduction mechanism, as summarized in Table 2.1. The remarkable high specificity confered by the bioreceptor, is one of the key factor of the success experienced by these devices. In particular, bioreceptors are responsible for binding the analyte of interest to the sensor for the measurement. Therefore, a careful choice of either the biological element, and the immobilization technique used to bind it

Table 2.1 – Biosensor classification.

Bioreceptor	**Transducer**
Enzyme	Electrochemical
Antibody	Optical
Oligonucleotides	Mass-Based
Cell	Other
Tissues	
Biomimetic	

to the transducer is required.

The most common forms of bioreceptors used in biosensing are:

- **antibodies**, which are one of the key element of an *immunosensor*. The specific interaction between the *antigen* and the correspondent antibody can be exploited to detect the immunologic reaction both in an *indirect* and in a *direct* way, as molecules are labeled with a radioactive or a fluorescent probe, or the transduction is obtained exploiting the modification in the electrical properties of the molecule respectively;

- **enzymes** are often chosen as bioreceptors because of the high selectivity with respect to enzyme binding and catalytic activity and because of their properties to catalyze a large number of reaction. The recognition of the analyte can be performed both through the detection of the product of their catalytic reaction or through the activation/deactivation of the enzyme due to the interaction with the analyte;

- **cells** are an interesting bioreceptor since they are sensitive to various kind of stimulants. Moreover, their capability to attach to the surface doesn't require complex immobilization techniques.

- **nucleic acids**: usually referred to as *genosensors*, this category of devices rely on the principle of *complementary base pairing*. As a DNA strand is a sequence of four kind of nucleotides (*adenine, guanine, timine, citosine*) and only adenine-timine and guanine-citosine bonds are allowed, only one specific sequence which is *complementary* to a specific DNA strand. Both *direct* and *indirect* detection of the bonding reaction (*hybridization*) can be performed.

There are many potential applications for biosensors as a diagnostic tools. The main requirements for this approach to be valuable in terms of research and commercial applications are the identification of a suitable biological recognition element for the target molecule which is under investigation, and the potential for disposable portable detection systems to be preferred to sensitive laboratory-based techniques in some situations.

Telomerase activity detection has drawn the attention of researchers working in various fields, mainly because of its role in early diagnosis of tumors. Therefore, as for PCR-based and TFR-based methods, several different approaches and transduction methods have been developed during the last decade, to perform the detection of telomerase activity through the employment of a biosensor, trying to exploit the advantages offered by the growing field of nanotechnologies.

2.2 Optical transduction

Optical biosensors probably represent the most common type of biosensor and, in the last decade, they experienced a wide diffusion even in commercial application [6] because of their high specificity and selectivity. Depending on the employed transduction mechanism, they can be broadly divided in two categories: those which perform a *label-free* detection, and *label-based* detection techniques. The former approach exploits the detection of a signal generated by the interaction between the analyte and the transducer, while the latter requires the use of a marker to detect the presence of the target. A further and more accurate classification of optical biosensor can be achieved considering more in deep the type of transduction employed:

- **surface plasmon resonance** (*SPR*) allows detecting the adsorption of an analyte on the surface of a planar metal or nanoparticles, monitoring a resonant electromagnetic waves (*surface plasmon polaritons*) which propagate on a metal-dielectric interface in a parallel direction with respect to such a surface. Since the wave depends on the metal-dielectric interface properties, it can be used to monitor the interaction between an analyte and its biospecific receptor immobilized on the metal surface.

- **evanescent wave fluorescence** exploits the propagation properties of an evanescent wave confined in a waveguide or optical fiber. Being the the decay of such a wave an exponential function of the distance from the waveguide/fiber surface, monitoring the surface properties exciting an evanescent wave is thus possible;

- **fluorescence**, **bioluminescence** and **chemiluminescence** measure photon emission at a particular wavelength. The excitation source can be a photon emis-

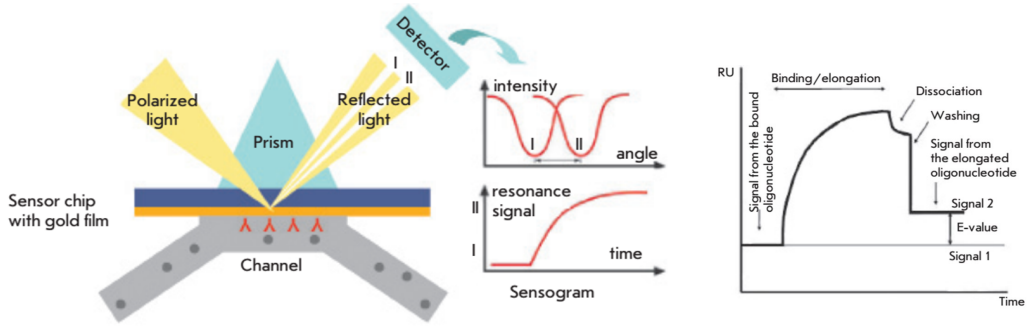

(a) (b)

Figure 2.2 – Surface plasmon resonance for telomerase activity detection. (a) schematic working principle for the detection of macromolecules and (b) the corresponding sensogram [7].

sion (*fluorescence*) at a different (usually lower) wavelength, a chemical reaction (*chemiluminescence*), or a chemical reaction occurring in a living organism (*bioluminescence*).

- **surface-enhanced Raman scattering** exploits the amplification of the intensity of the vibration spectra of a molecule which is in close proximity to a gold or a silver metallic surface.

As label-based techniques can be affected by systematic errors arising from the interaction of the marker with the process under investigation, a label-free approach is obviously preferable. Therefore, in the following, particular attention will be drawn to the latter approach.

Optical biosensors for telomerase activity detection

According to the previously mentioned methods, several optical biosensing techniques can be used to study the surface properties of a metal, or the emission of a molecule in the proper conditions.

Figure 2.2a shows the schematic working principle of surface plasmon resonance, employed for the evaluation of telomerase activity.

An emitting source of polarized light is directed on a metal surface through a prism and

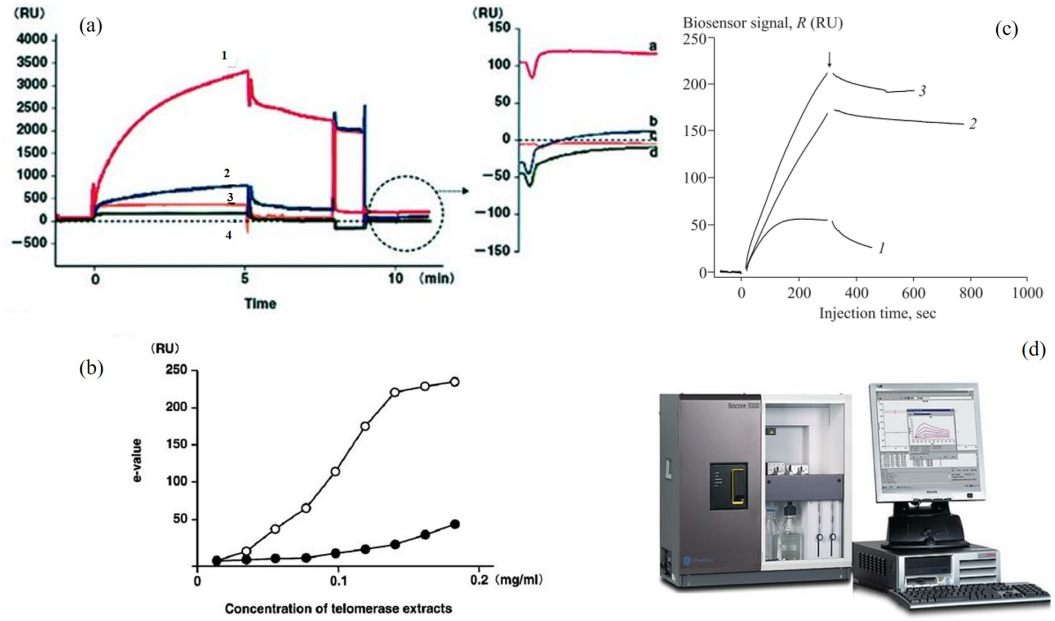

Figure 2.3 – (a) Sensorgram of telomerase activity measurement as presented in [8]. The output curve of telomerase-positive cell line with (1) and without (2) the addition of dNTPs is reported. A negative control with heated inactivated telomerase (3) and a sample without telomerase (4) are showed; (b) Output curve as a function of the enzyme concentration for colon cancer cell line (open circles) and normal fibroblast cell line (closed circles) [8]; (c) enhanced output signal proposed by Rad'Ko et al. [7], obtained using untreated probes (1), streptavidin (2) and gold nanoparticles (3) conjugated probes; (d) Biacore 3000 system.

the reflected light is measured by a detector as a function of the varying incidence angle, as shown in the inset of figure 2.2a. When surface plasmon resonance is induced by the emitting light, a minimum in the corresponding intensity plot is reached. As the refractive index in the near vicinity of the metal surface changes, the corresponding angle at which the intensity reach a minimum value is observed, as schematically represented in the top right inset of figure 2.2a. The kinetic of molecules interaction with the surface, can be studied in real-time monitoring the variation of the refracting index (i.e, the incidence angle) as a function of time. The corresponding plot, shown in the bottom right inset of figure 2.2a is a so called *sensorgram*.

Maesawa et al. [8] employed this method to study the telomerase activity, and a sensorgram similar to that proposed in figure 2.2b is obtained. In a first step, a 5'-Biotin-conjugated oligonucleotides was immobilized on the sensing area of the chip, pretreated with streptavidin. The signal (resonance unit, RU) was then measured using a commercial

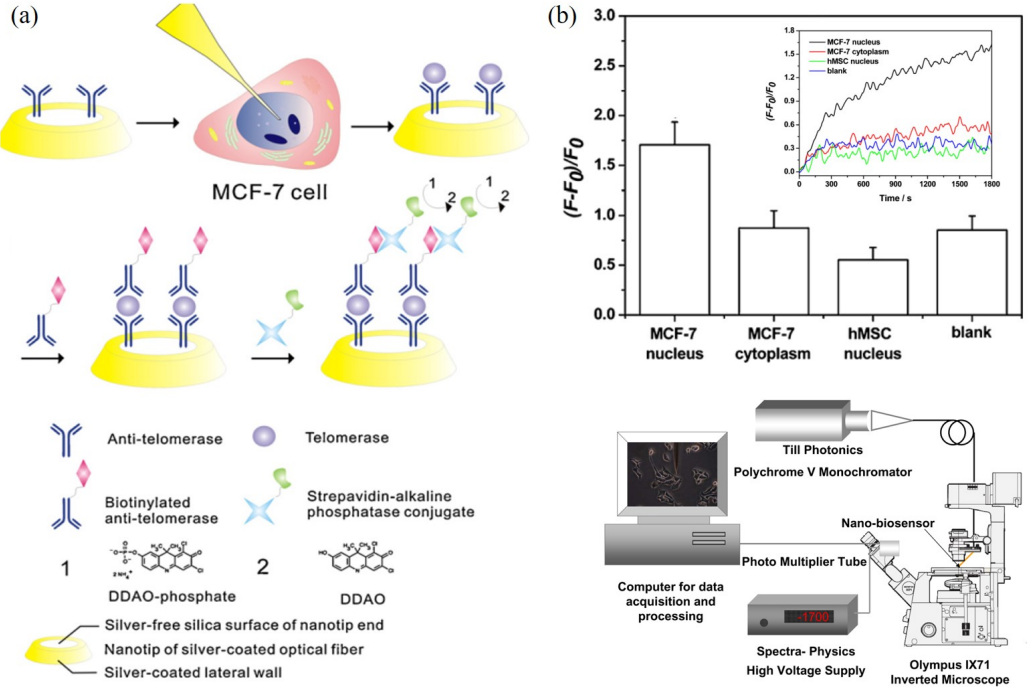

Figure 2.4 – (a) Schematic representation of the method proposed by Zheng et al. [9], for the detection of telomerase activity at single cell level; (b) relative fluorescence intensity variation after the introduction of DDAO-phosphates in liquid (i.e., telomerase activity), with respect to the cell used for the analysis; (c) block diagram of the system used for the fluorescence measurements [9].

Biacore system (figure 2.3d). After the addition of a telomerase-positive cell line, the sensorgram showed a steep increase of the output signal which gradually lower its slope. In this first step, both probes-enzyme interaction and probes elongation process are measured. As a negative control, a heat-inactivated telomerase extract were used (curve 3). Also, in buffer with lack of dNTPs (curve 2), only a slight elongation was observed, while in absence of telomerase extract (curve 4), no elongation was observed. The sensitivity of the assay was then assessed (figure 2.3b) using colon cancer cell line (open circles) and normal fibroblast cell line (closed circles). Signal intensity can be further increased by treating the sensor with telomerase-synthesized DNA with antisense oligonucleotides with respect to the telomeres, covalently bonded with streptavidin and gold nanoparticles, such as suggested in Rad'Ko et al. [7]. Figure 2.3c shows the enhanced signal of probes conjugated with streptavidin (curve 2) and with gold nanoparticles (curve 3) with respect to untreated probes (curve 1).

Other approaches involve the use of optical fiber biosensor, such as suggested in Zheng et al. [9]. In this work, fluorescence imaging where recorded with the apparatus shown in figure 2.4, and telomerase activity was monitored at single cell level. A silver nanotip was coated with polyclonal rabbit anti-telomerase: an antibody which, in this assay, allows the recognition of specific antigen-antibody interaction with telomerase. A MCF-7 breast cancer cell nucleus was then penetrated and telomerase expression was evaluated after the introduction of biotinylated antibody and streptavidin-alkaline phosphatase conjugate. The former, binds with telomerase immobilized on the near proximity of the nanotip, then the latter catalyzes the cleaving of diammonium salt (DDAO-phospate) by alkaline phosphatases to produce a large amount of DDAOs with fluorescence at 610 nm excitation. A summary of the proposed detection strategy is reported in figure 2.4a. In order to reduce the interference caused by different probes, rather than evaluate absolute fluorescence intensities, the ratio $(F - F_0)/F_0$ was introduced. F_0 and F are detected fluorescence intensity upon addition of DDAO-phosphates at $0s$ and $1800s$, as shown in the inset of figure 2.4b. The average ratio for MCF-7 cancer cell nucleus is significantly larger than that of the negative control (hMSC nucleus), confirming the positive response of cancer cells and demonstrating that successful detection of telomerases in a single living cell by the optical nanobiosensor.

Previously presented examples, show the broad diffusion experienced by optical biosensors. The constant evolution of such technologies, however, is fast outpacing the average skill level of biosensor's user. For example, analyze telomerase activity at single cell level, not only requires bulky and costly instrumentation, but also supervised operation of a specialized operator. A simpler method could be implemented using label-based approaches, but could arise of systematic errors caused by the interaction between the label and the process under analyses. Finally, commercially available systems and devices, could require complex methods to increase assay's sensitivity, thus impeding both an automation of the analysis routine, and the production of cost-effective devices. In this connection, a direct label-free detection of telomerase activity could be achieved exploiting the electrical properties of both DNA and enzyme molecules, thus allowing the production of simple and low-cost devices.

2.3 Electrochemical biosensors

A variety of new integrated chemical sensors realized using chemically selective membrane technology have yielded the capability of performing electrochemical analyses in real time, in remote applications, at reasonable cost. Biochemical sensors, such the glucose sensor proposed by Clarke and Lyon, have received a great deal of attention due to interest in biomedical applications and their ease of use. The advantages of integrating biomedical transducers include miniaturization for the purposes of implantation, and the capability of including additional integrated circuitry for *in-situ* signal conditioning and control. Electrochemical techniques can be roughly divided in four types:

- voltammetric/amperometric methods, which measure a current as a function of an applied potential;
- impedimetric methods, which measure resistive and capacitive properties of material upon perturbation;
- conductometric methods, which measure the change in the electrical conductivity of a sample solution as the composition of the solution changes during a chemical reaction;
- potentiometric methods measure the potential of the system while a negligible current flows through it.

Conductometric measurements suffer from some drawbacks due to the low-specificity of the technique itself. In fact, the conductance is a non-specific property, concentration of other electrolyte can affects the measurement. Potentiometric measurements can be subjected to various difficulties, arising from liquid junction potentials, electrochemical noise due to high electrode impedance, and sensitivity to buffer capacity. Furthermore, a 59-mV/decade concentration change logarithmic response is obtained in a potentiometric mode, therefore limiting the sensitivity and precision of the technique. Because of this, most of systems overcome these issues operating in an amperometric or impedimetric mode. For this reason, in the following section the attention will be focused on these two techniques.

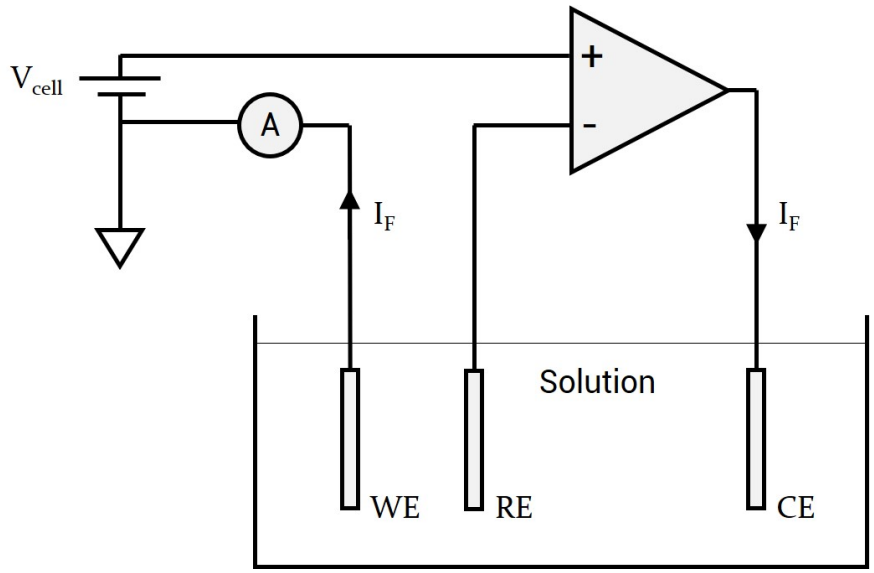

Figure 2.5 – Block diagram of a three-electrode amperometric electrochemical cell.

Figure 2.5 depicts the conceptual drawing of a three-electrode electrochemical cell and a *potentiostat*, which is a device capable to control the potential across the cell and measure the corrent flowing through it. In this setup, the half-cell reactivity of an analyte is investigated measuring the current flowing through the *Working Electrode* (WE). While this electrode serves as a platform on which an electrochemical reaction take place, a *Reference Electrode* (RE) is used to measure the solution potential. In order to maintain constant the RE potential, no current should be sinked or sourced from the electrode and, therefore, a *Counter Electrode* (CE) closes the electrical path of the system.

A deep understanding of molecules interaction with an electrode immersed in a solution is essential not only for the comprehension of the electrochemical analyses and their application to the detection of telomerase activity, but also to figure out many phenomena which take place at the interface between a charged metal and an electrolyte. Therefore, in the following, together with the state-of-the-art on electrochemical devices the characteristics of the electrochemical cell will be thoroughly examined.

Electrochemical biosensors for telomerase activity detection

As previously mentioned, biochemical reactions can be investigated by means of electrochemical techniques. In fact, the application of a potential to the cell, can cause a current

flow due to the electrons transfer between the electrode and the solution. These reactions are called *oxidation-reduction* (redox) reactions. The current that arises from electrolysis by means of a redox process is limited by the mass transport rate of the reactant molecules from the bulk solution to the electrode interface. These processes can be studied both monitoring the current flowing through the electrode, and evaluating how such reaction modify the electrical properties of the cell. In particular, voltammetric/potentiometric and impedimetric have been extensively employed as electrochemical sensors for the detection of clinically relevant biomolecules and processes related to their activity.

Voltammetry

Voltammetry is a category of electrochemical method which measures the current as a function of the applied potential. In particular, the most widely used methods consist in the application of a continuously time-varying potential to the working electrode, thus allowing the study of the oxidation (reduction) process of electroactive species, molecules adsorption and capacitive current due to the formation of a double-layer structure. The current which flows through the working electrode and the counter electrodes due to a redox reaction is called *faradaic current*. According to the literature, a current due to the analyte's reduction has a positive sign and is a *cathodic current*, while an *anodic current* is due to an oxidation and its sign is negative.

This approach has been extensively used since the beginning of 80's, to study nucleic acids interaction [10, 11, 12], as an alternative to study telomeres structure [13] and to directly detect telomerase activity [14, 15, 16, 17]. The methods is based on the application of a sufficiently large potential difference between the anode and cathode of an electrolytic cell. A linear (Nernst) diffusion layer of fixed thickness δ is assumed when a steady-state mass-transport rate of analyte is attained, then a mass-transport limited current will flow in the external circuit, as shown in figure 2.6b. These currents are given by

$$I_l = -zFAD_{ox}C_{ox}/\delta \tag{2.1}$$

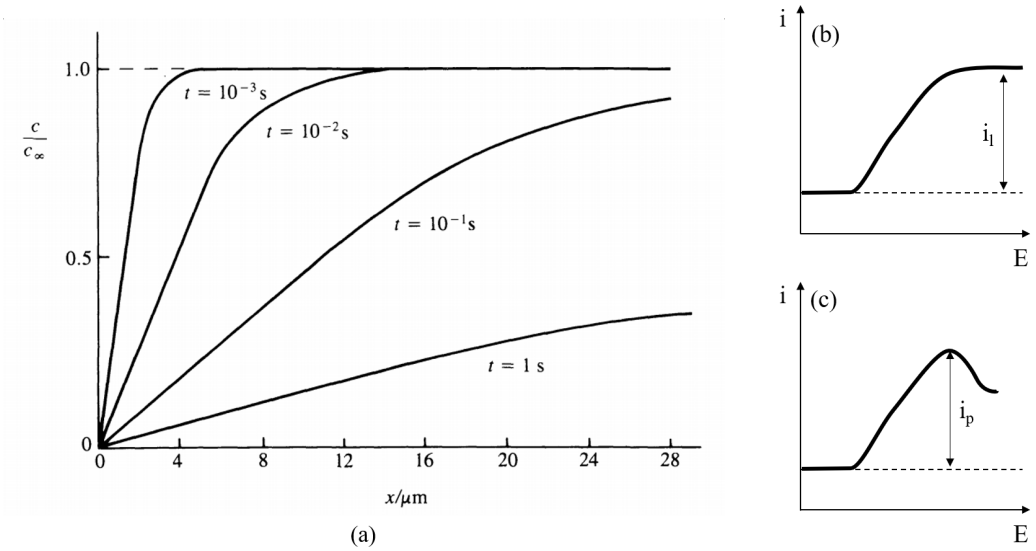

Figure 2.6 – (a) Variation of concentration with distance at a planar electrode for various values of t; (b) limiting current as defined in 2.1 and 2.2; (c) peak current arising in the absence of convection or migration.

for cathodic processes, and

$$I_l = zFAD_{red}C_{red}/\delta \tag{2.2}$$

for anodic processes. Here z is the number of moles of electrons transferred per mole of reactant, F is the Faraday constant = 96 487 $C/mole$, A is the electrode area in square meters, $D_{ox}(D_{red})$ is the diffusion coefficient in m^2/s for the oxidized (reduced) species, and $C_{ox}(C_{red})$ is the bulk concentration in $moles/m^3$ of the oxidized (reduced) species in the test solution.

As the reaction progresses, all the reactants at the surface electrode will be consumed, resulting in a decrease of their concentration in proximity of the surface, thus leading to the formation of a gradient of concentration, such as depicted in figure 2.6.

As a consequence, to support further electrolysis, reactants should diffuse from the bulk of the solution, or proceed because of forced convection (i.e., mechanical stir), natural convection (i.e., thermal gradient), or migration (i.e., motion forced by an electric field). In the absence of convection or migration, when diffusion is the only relevant form of mass-transport, the diffusion layer δ increases in time. Therefore, the diffusion gradient

decreases and, when the amount of reactants at the working electrode interface is not enough to balance the electrochemical reaction, the current decreases in magnitude thus leading to the occurrence of a peak, as shown in figure 2.6b. The curves $I = f(E)$ obtained with such an analysis are called *voltammograms* and vary their form depending on the applied potential.

In particular, Eskiocak et al. [17] studied a method based on the measurement of guanine oxidation signal to directly transduce telomerase activity, exploiting the fact that half of the telomeres sequence is made up of guanine. The procedure uses a *Differential Pulse Voltammetry* (DPV), which is a series of regular voltage pulses superimposed on the potential linear sweep or stairsteps and a disposable *Carbon Graphite Electrode* (CGE) as a working electrode. As a first step, the reaction mixture including a 36 bp internal control was subjected to 33 cycles of PCR amplification. Then, the amplified product of PCR (amplicons) was transduced by means of DPV, using the current peak of the guanine oxidation as analytical signal, as shown in figure 2.7a. Amplicons immobilization in the CGE was performed dipping the graphite leads into a solution containing the fragments, through an adsorption process. The electrode was then rinsed in order to wash non-specifically bounded molecules from the surface. The functionalized electrode was then immersed in acetate buffer solution and the guanine oxidation signal was measured by using DPV, scanning from 0.8 V to 1.4 V. In order to quantify the obtained signal, in each measurement the length of the graphite lead was measured by a ruler and the volume of blank/DNA solution was optimized. Figure 2.7a summarizes the working principle of this assay, while figure 2.7b shows the results obtained with this method. The authors claims that telomerase activity could be detected in extracts containing as low as 100 $ng/\mu L$ of protein, and protein concentration correlated significantly with guanine oxidation signal. However, the telomerase extract employed is a purified enzyme from a commercial kit. Therefore, accounting for the sensitivity of the assay in a clinical diagnostic tool is not straightforward. Moreover, the need for a PCR preliminary step, does not overcome the limitations imposed by this procedure.

It is worth explicitly noting that this approach implicitly assumes that the test solution does not contains additional electroactive species that are capable of undergoing oxidation/reduction at the same applied potential as the analyte. Otherwise, a more complex system, comprising a suitable selective membrane must be employed in order to isolate

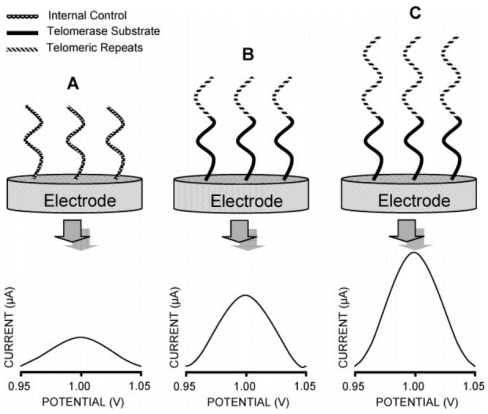

(a) Schematic illustration of guanine oxidation signals of PCR products from (A) primer-dimer and heat inactivated negative controls, telomerase positive cell extracts with (B) moderate, and (C) strong telomerase activity.

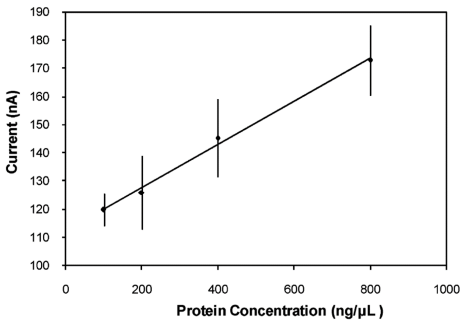

(b) Detection of telomerase activity by guanine oxidation signals with increasing concentrations of the telomerase positive cell extract.

Figure 2.7 – Schematic illustration of the detection method and of the results obtained by Eskiocak et al [17].

the species of interest.

Mori *et al.* presented an *Electrochemical Telomerase Assay* (ECTA) [15], to measure telomerase activity. The proposed method improved Eskiocak approach avoiding the need for a PCR step or a subsequent gel electrophoresis. As in the previously presented work, this method measures the current variation as a function of the potential applied between two electrodes. In this work, ferrocenylnaphthalene diimide (FND) was used as probe. Gold electrodes fabricated by sputter coating were used as disposable working electrode. As FND is easily adsorbed at gold surface, telomerase substrate primer immobilization was performed with 6-mercaptohexanol, used as a blocking agent for the gold surface. Electrochemical measurement were performed using a three-electrode potentiostat, using an Osteryoung Square Wave Voltammetry. Figure 2.8 illustrates the working principle of the assay: after telomeres immobilization on the gold electrode, FND probe were added in solution. Electrochemically active FND binds with the DNA strand, thus leading to a current which is correlated with telomerase activity. In particular, the current variation (ΔI) represent the elongation of the telomeres due to telomerase activity.

Figure 2.9a shows results obtained by ECTA. the high sensitivity of the assay, demonstrat-

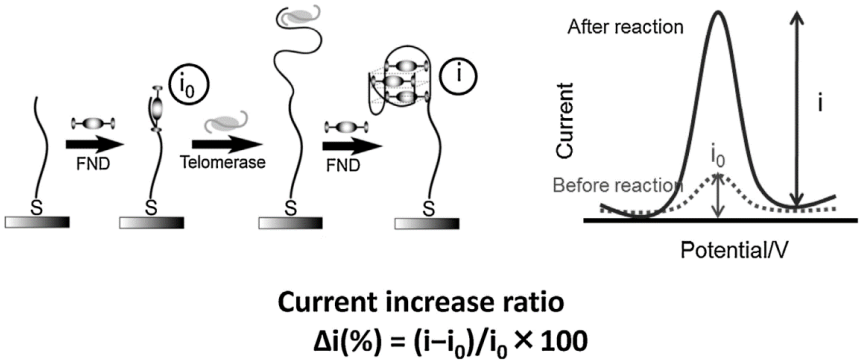

Figure 2.8 – Schematic illustration of the working principle proposed in Hayakawa et al [16].

ing that its sensitivity is as low as 8 ng of protein (equivalent to about 10 cancer cells), while TRAP requires at least 20 times more protein. Despite its high sensitivity, the output signal of the assay saturated with a relatively low amount of cancer cells present in the sample and therefore can not be used as a quantitative assay. In Hayakawa et al. [16] ECTA was employed to perform a pilot study to assess a screening system for oral cancer. Results showed in figure 2.9b show the capability of the assay to discriminate between positive and negative samples. However, as previously stated, because of the high sensitivity of the assay it is not possible to distinguish between cells derived from the tumor itself or from the oral cavity.

Chronocoulometry

As previously discussed, voltrammetric methods measure the current as a function of a variable potential, while amperometric techniques held constant the potential between the reference electrode and the working electrode.

In 2012, Sato and Takenaka [18], proposed a chronocoulometric technique for a PCR-free telomerase assay. In chronocoulometry, the potential is swept stepwise and the charge used in an oxidation or reduction reaction is measured and plotted versus to time. The simplest example of chronocoulometry analysis is the Cottrell experiment. In this procedure, the voltage is swept with a square wave starting at a potential E_i, where insignificant electrolysis takes place. At $t = 0$, the potential is shifted to E_f, which is

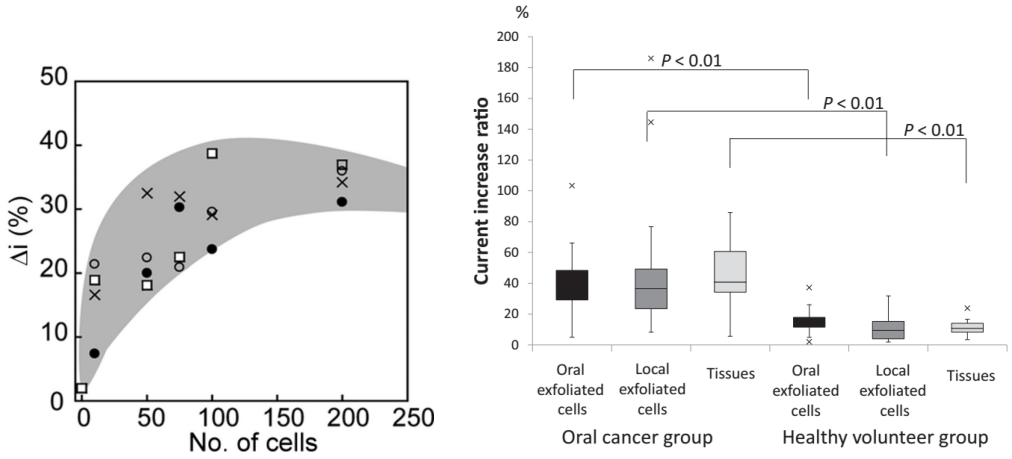

(a) ECTA results correlate the measured current variation with the number of 4 different tumor cells, from Mori et al. [15].

(b) Current variations obtained in a pilot study made to estabilish a screening system for oral cancer with ECTA, from Hayakawa et al. [16].

Figure 2.9 – Current variations obtained with ECTA in [15] and [16].

sufficiently negative to enforce a diffusion-limited current. Cottrell equation

$$i(t) = I_d(t) = \frac{nFAD^{1/2}C^b}{\pi^{1/2}t^{1/2}} \tag{2.3}$$

describes the chronoamperometric response of the system, and its integral

$$Q_d = \frac{2nFAD^{1/2}C^b t^{1/2}}{\pi^{1/2}} + Q_{dl} \tag{2.4}$$

gives the cumulative charge passed in reducing the diffusing reactant. In 2.4, n is the number of moles of electrons transferred per mole of reactant, F is the Faraday constant (96 487 $C/mole$), A is the working electrode area in square meters, D is the diffusion coefficient in m^2/s for the oxidized (reduced) species, C^b is the bulk concentration in $moles/m^3$ of the oxidized (reduced) species in the test solution and Q_{dl} the charge in the double layer. As shown in figure 2.10 Q_d rises with time, and a plot of its value with respect to $t^{1/2}$ is linear. Therefore, knowing one of n, A, D or C^b any one of the others value can be calculated using the slope extrapolated from this graph. In particular, this technique can be used to quantify the surface density of DNA molecules immobilized on the electrode surface. For example, Steel et al., [19] used a gold electrode together with 6-mercapto-1-hexanol (MCH) as a blocking agent for the gold surface

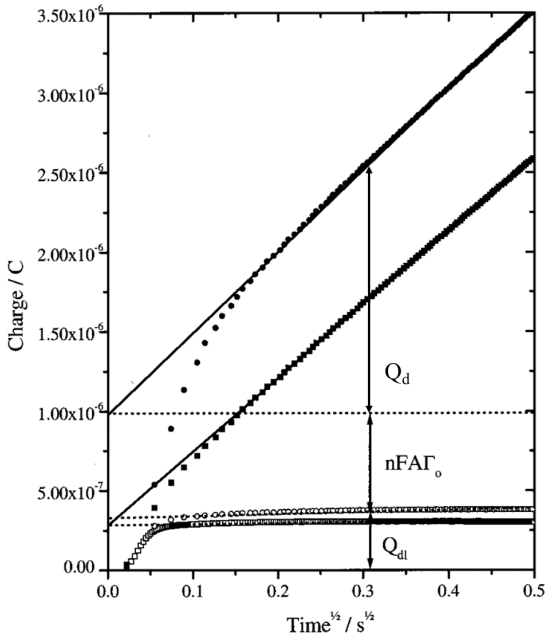

Figure 2.10 – Chronocoulometric response curves for MCH (squares) and P1/MCH (circles) modified electrodes in the absence (open) and presence (closed) of 50 μM RuHex. The lines represent the fit to the data used to determine the intercept at t) 0. The solid lines are the fits for the MCH curves, and the dashed lines are the fits for the P1/MCH curves. [19].

and hexaammineruthenium(III) chloride ($[Ru(NH_3)_6]^{3+}$) as a mediator for the process. Their results are reported in figure 2.10. Equation 2.4 states that diffusional component to the charge is zero at $t = 0$, yet the plot shown in 2.10 is not. The additional component of Q arise from double-layer charging and from the electroreduction of $[Ru(NH_3)_6]^{3+}$ molecules that might be adsorbed at E_i. These contribution can be included in the equation, adding two time independent terms in the integral form of Cottrel equation:

$$Q_d = \frac{2nFAD^{1/2}C^b t^{1/2}}{\pi^{1/2}} + Q_{dl} + nFA\Gamma_0 \tag{2.5}$$

where Q_{dl} is the capacitive charge, Γ_0 is the surface density of $[Ru(NH_3)_6]^{3+}$ and $nFA\Gamma_0$ quantifies the faradaic component associated to the reduction of the surface excess of adsorbed $[Ru(NH_3)_6]^{3+}$. Both $nFA\Gamma_0$ and Q_{dl} can be estimated through the intercept of the linear fit of the experimental data, as shown in 2.10. Therefore, the amount of DNA

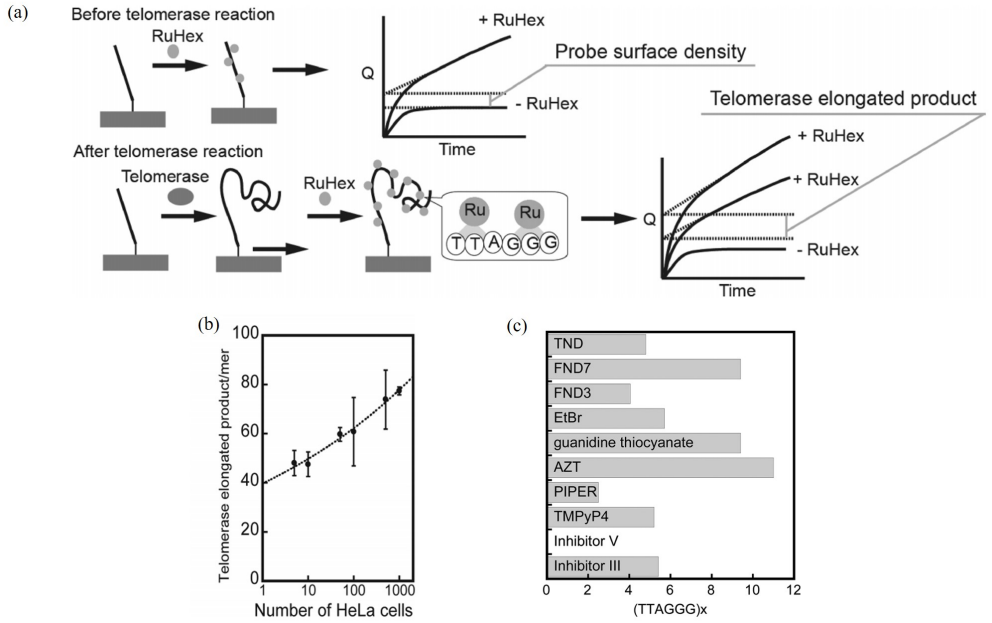

Figure 2.11 – (a) schematic representation of the working principle of the assay proposed by Sato et al. [18]; (b) number of oligonucleotides elongated, measured through chronocoulometric analysis, as a function of the number of cells used to prepare the cell extracts; (c) telomerase inhibitor evaluation [18].

molecules on the electrode given by

$$\Gamma_{DNA} = \Gamma_0 \frac{z}{m} N_A \tag{2.6}$$

where z is the charge of $[Ru(NH_3)_6]^{3+}$ and m the number of bases of DNA.

Sato and Takenaka [18] exploited this approach immobilizing a telomerase substrate DNA primer on a gold electrode and using chronocoulometry coupled with RuHex. Since RuHex binds to the phosphate backbone of the telomerase substrate (TS) oligonucleotide immobilized, it allows to quantify the amount of nucleotides added to the TS-primer by the action of the enzyme, as schematically represented in 2.11a. In particular, exploiting Cottrel equation (2.4), is possible to directly evaluate the amount of (TTAGGG) sequences added to the probes because of the elongation. Initially, the sensitivity of the assay was evaluated studying the elongation as a function of the number of cells used to prepare the cell extracts as shown in figure 2.11b. Telomerase inhibition was then assessed, using 10 drugs as shown in figure 2.11c.

It worth to note that evaluating $nFA\Gamma_0$ and Q_{dl} reliably usually requires other experiments to determine the double-layer properties of the system.

Electrochemical Impedence Spectroscopy

Voltammetry and Chronocoulometry apply a large perturbation on the system, such as a potential sweep or a step, in order to study reactions occurring at the interface with the working electrode. *Electrochemical Impedence Spectroscopy*, instead, employs a small signal sinusoidal voltage to study the electrical properties of the system. The application of such a signal to the cell and the study of the behavior of the system as a function of the applied frequency, allows to characterize the impedance of the system.

When a structure, such as an electrode, is exposed to a fluid environment, a so called *double-layer* appears on its surface. In electrochemistry, such a layer reflects the ionic zones formed in the solution as a consequence to the application of an electric potential to the surface of the considered structure. For example, a positively charged electrode attracts a layer of negative ions and vice versa. Since the interface must be neutral, the counterlayer is made of ions of opposite sign to that of the electrode. This structure was firstly studied by Hermann von Helmholtz [20], who first hypothesized the formation of electrical layers of ions as a consequence of the interaction between a charged metal and an electrolyte. This concept was then refined by Gouy[21] and Chapman [22], with the introduction of an additional *diffuse layer*, due to the Boltzmann distribution, in which the accumulated ions extend to some distance from the solid surface. In further studies, Stern proposed a model, including both the rigid Helmholtz layer and the diffuse layer of Gouy and Chapman.

Figure 2.12a depicts a simplified model of the electrical double-layer formed at the interface between a metal electrode and an electrolyte. The *compact layer* start close to the electrode surface, where water molecules are adsorbed at the interface with the metal surface. Assuming an excess of negative charge in the metal, hydrogen atoms of adsorbed water molecules are oriented towards the metal surface, thus leading to the water dipole orientation. The first layer, that is the *Inner Helmholz Plane* (IHP), passes through the centers of specifically adsorbed ions, or is simply located just behind the layer of adsorbed water. Possible adsorption of large neutral molecules should change the

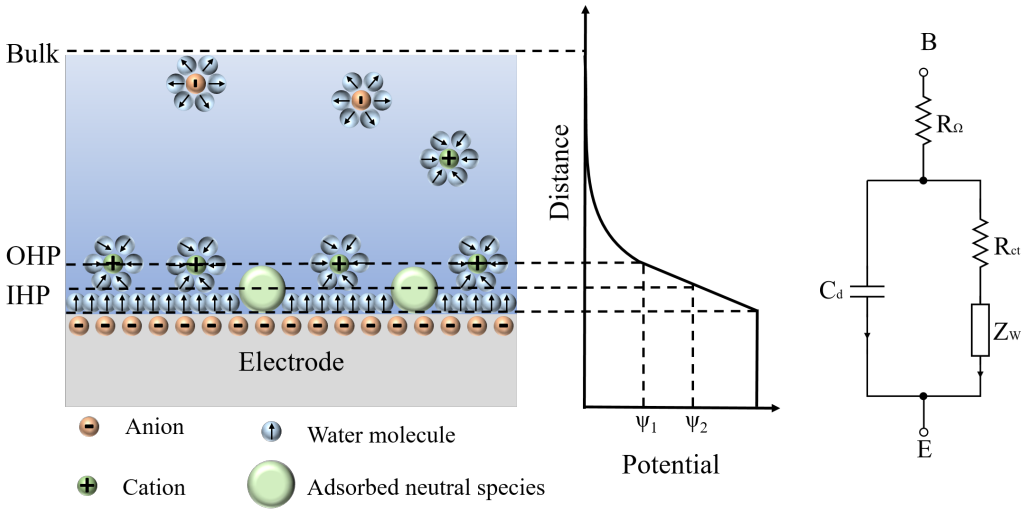

(a) Schematic representation of electrical double layer

(b) Randles equivalent circuit

Figure 2.12 – Double layer structure analysis.

properties of the layer replacing water molecules at the interface with the metal electrode. The subsequent layer, called *Outer Helmholz Plane* (OHP), passes through the centres of solvated ions at the distance of their closest approach to the electrode. The electric potentials linked to the IHP and OHP are usually written as Ψ_2 and Ψ_1, respectively. The outer layer, beyond the OHP, is the diffuse layer and extends until the bulk of solution. It contains scattered ions which concentration decreases exponentially vs the distance from the electrode surface.

Analyzing this structure and modifications of its components, it is possible to study various biological reactions [23, 24] such as DNA hybridization [25, 26], protein detection [27] or other parameters which are, or could be, related to clinical application such as glucose sensing [28] or pH variations [29].

From an electrical viewpoint, the electrochemical cell is frequently represented with the equivalent circuit showed in figure 2.12b, called *Randles equivalent circuit*. Here, both the process related to the double-layer charging and the faradaic current flow discussed in the previous section are considered. The double-layer contribution could be considered as purely capacitive, thus be represented by the capacitance C_{dl}. The faradaic process, on the contrary, is a frequency-dependent process which, in this model, is represented by the other branch: R_{ct} represent the charge-transfer process, while the impedance Z_W

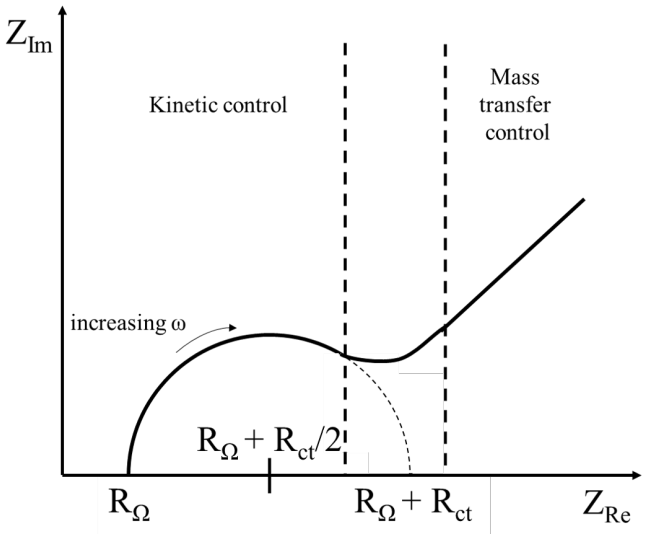

Figure 2.13 – Impedance plot for an electrochemical system.

represent a resistance element related to diffusion process and is the so called *Warburg impedance*. Eventually, since all of the current must flow through the bulk solution, R_Ω is inserted to model this effect in the equivalent circuit. At a given frequency ω, the equivalent circuit shown in figure 2.12b allows to measure the impedance of the whole system, which is given by:

$$Z_e = Z_{Re} - jZ_{Im} = R_B - j/(\omega C_B) \tag{2.7}$$

and therefore:

$$Z_{Re} = R_B = R_\Omega + \frac{R_{ct} + \Re(Z_W)}{A^2 + B^2} \tag{2.8a}$$

$$Z_{Im} = \frac{1}{\omega C_B} = \frac{B^2/\omega C_{dl} + A/\omega\Im(Z_W)}{A^2 + B^2} \tag{2.8b}$$

where $A = (C_{dl}/\Im(Z_W)) + 1$ and $B = \omega\Re(Z_W)C_{dl}$. Measuring these parameters and plotting Z_{Im} *vs.* Z_{Re} for different values of ω, a plot similar to that shown in figure 2.13 is obtained. A basic understanding of this method for impedance characterization, can be achieved studying separately the system behavior and characterizing Randles' circuit approaching very low and very high frequencies. Starting the circuit analysis as $\omega \to 0$, the diffusion process has to be taken into account. Assuming for simplicity that the

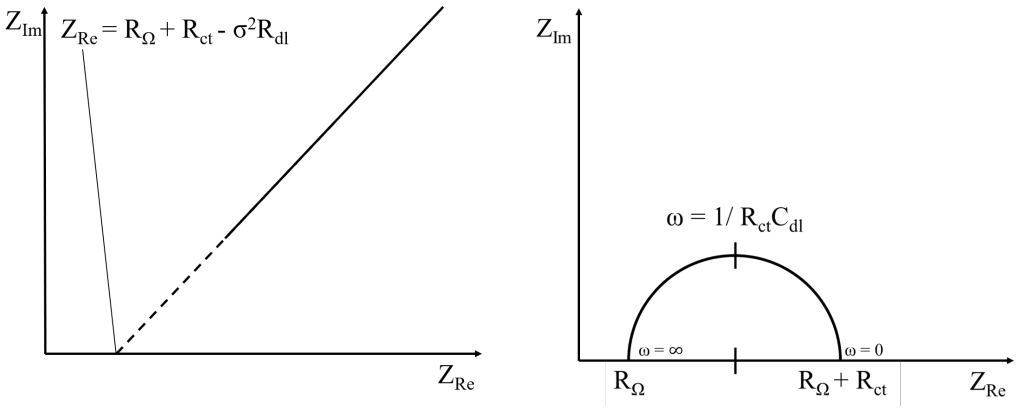

(a) Impedance plane plot for low frequency.

(b) Impedance plane plot for high frequency, obtained neglecting the Warburg element.

Figure 2.14 – Electrochemical Impedance Spectroscopy plot analysis.

diffusion thickness is infinite, the Warburg impedance can be written as

$$Z_W = \frac{\sigma}{\sqrt{\omega}}(1-j) \tag{2.9}$$

where σ is a parameter which depends on the concentration and the diffusion coefficient of the diffusing species, and the area of the electrode. Substituting 2.9 in 2.8a and 2.8b these last functions approach the limiting forms:

$$Z_{Re} = R_\Omega + R_{ct} + \sigma\sqrt{\omega} \tag{2.10a}$$

$$Z_{Im} = \sigma\sqrt{\omega} + 2\sigma^2 C_{dl} \tag{2.10b}$$

Subtracting 2.10a from 2.10b leads to the elimination of ω and gives

$$Z_{Im} = Z_{Re} - R_\Omega - R_{ct} + 2\sigma^2 C_{dl} \tag{2.11}$$

Thus, the corresponding Nyquist plot should be linear and have unit slope, as shown in figure 2.14a. Clearly, the frequency dependence in this regime come only from the diffusive component of the cell (i.e., the Warburg element), thus the linear correlation between Z_{Re} and Z_{Im} is a characteristic of diffusion-controlled process. As the frequency increases, the charge-transfer process and the double-layer capacitance assumes gradually a decisive role. On the other hand, as reported in the previous section, at very high frequency the concentration gradient increases and, thus, the Warburg impedance

becomes negligible. Therefore, the circuit analysis can be conducted neglecting the Warburg impedance. As a consequence, equations 2.8a and 2.8b can be rewritten as

$$Z_{Re} = R_\Omega + \frac{R_{ct}}{1+\omega^2 C_d^2 R_{ct}^2} \tag{2.12a}$$

$$Z_{Im} = \frac{\omega C_d R_{ct}^2}{1+\omega^2 C_d^2 R_{ct}^2} \tag{2.12b}$$

Elimination of ω from this pair of equations gives to

$$\left(Z_{Re} - R_\Omega - \frac{R_{ct}}{2}\right)^2 + Z_{Im} = \left(\frac{R_{ct}}{2}\right)^2 \tag{2.13}$$

which should give, in a Nyquist plot, a circular plot centered at $Z_{Re} = R_\Omega + R_{ct}/2$ and $Z_{Im} = 0$, with a radius of $R_{ct}/2$, as shown in figure 2.14b. The interpretation to equation 2.13 can be obtained looking at figure 2.12b, remembering that in this study the Warburg impedance has been neglected. Therefore, while at high frequency the C_{dl} component offers a low-impedance path for the current, when the frequency approach to zero its impedance strongly increases. In this case, R_{ct} provides the lower impedance path for the current flow. However, as long as the frequency decreases, the Warburg impedance is no longer negligible, so in general a departure from this plot should be expected, as shown in figure 2.13.

Electrochemical Impedance Spectroscopy has been successfully employed to detect DNA hybridization [30, 31, 32], as well as telomerase activity [33]. A gold electrode was functionalized with telomeres-line thiolated DNA probes, then characterized in presence of $Fe(CN)_6^{3-}/Fe(CN)_6^{4-}$, which acts as a redox probe in the supporting electrolyte solution. Figure 2.15 shows a schematic representation of the proposed approach. DNA immobilization decreases the area available for redox processes, blocking $Fe(CN)_6^{3-}/Fe(CN)_6^{4-}$ electrons transfer to the electrode surface, resulting in an increase of the R_{ct} component of Randles equivalent circuit, or rather in the radius of the semicircle in the kinetic controlled process of Nyquist plot. Incubation of the functionalized electrode with telomerase and dNTPs introduction results in the elongation of DNA probes. Their lengthening produce a gradudal increase in the measured impedance as a function of time, as shown in figure 2.15. In order to quantify telomerase activity, the recorded impedance was evaluated with respect to the number of cell. Telomerase activity was

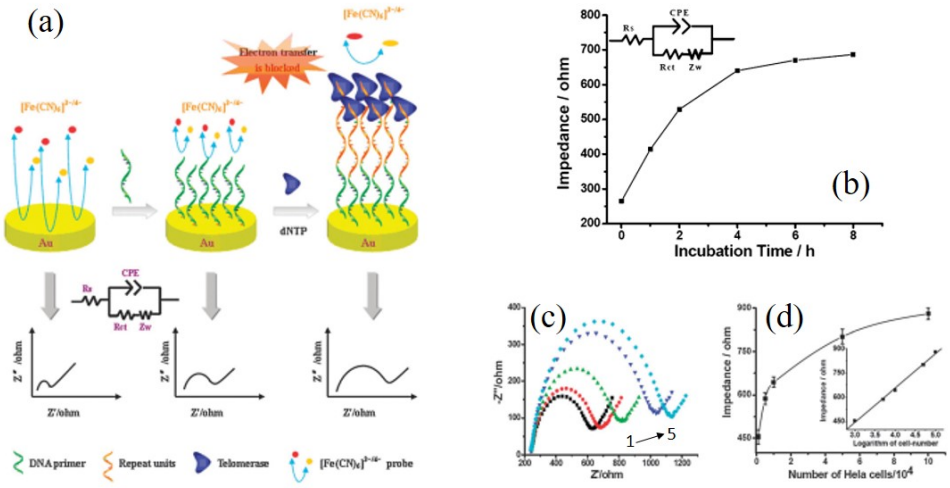

Figure 2.15 – Electrochemical impedance spectroscopy for telomerase activity detection, proposed by Yang *et al.* [33]: (a) schematic representation of detection working principle; (b) equivalent circuit used to model impedance data and impedance variation as a function of the incubation time; (c) Nyquist plot of electrodes incubated with different numbers of HeLa cells: 1) 1000, 2) 5000, 3) 10000 4) 50000, 5) 100000 incubated for 4 h at 37 °C; (d) calibration curve of the sensor.

detected in a sample extracted from 1000 HeLa cells, which is comparable with the previously reported examples.

According to the previously presented techniques, electrochemical detection systems provide an interesting way to perform direct, label-free detection of DNA and, more generally, of biological processes occurring in a liquid environment. Their capability to transduce the occurrence of a reaction under investigation, such as DNA hybridization or telomeres elongation, or the presence of an analyte in an electrical signal opened the possibilities of portable analysis, integrating several laboratory functions on a single integrated circuit. Such devices, namely *Lab-On-Chip*, offer several advantages in terms of required amount of analytes, processing time and area consumption.

Integration of electrochemical measurement systems in a single chip fabricated in a CMOS process was proposed by several research groups in different works [12][34][35][36]. The main limitation of this particular approach is the implementation of the reference electrode. Required materials for their fabrication are not standard in commercial CMOS process, and post-processing modifications are typically not trivial. In order to overcome such limitations, the employment of different configuration or materials and the

implementation of novel techniques are needed.

2.4 Electronic biosensors

Despite the interesting results obtained with the previously presented techniques, they suffer for severe limitations which impede their broad application and the delivery of a suitable biosensing platform. Electrochemical methods provide an interesting alternative to optical analysis, overcoming the requirement for a complex labeling step in order to bind a convenient fluorescent marker to a probe, or the employment of costly and bulky instrumentation. Their employment, however, is not trivial and important effort must be spent in order to reduce their complexity, cost and possibly allow the integration with standard CMOS technology. Furthermore, as thoroughly explained in 2.3, the output signal of such an assay is a current flow between the counter and the working electrode of the cell. Readout circuitry design for such current must face several issues, mainly related to the high signal-to-noise ratio required to effectively measure very small current variations related to biological effects. Several circuital solution have been proposed, such as current integration on a capacitance, or current-to-voltage converter with very high resolution. However, a significant increase in the complexity of the readout circuitry has to be taken into consideration.

In this perspective, Field Effect Transistors (FETs) are surely a promising alternative, which obviously improve scalability prospect and, moreover, reduce both issues related to the fabrication process and to signal processing. Such an approach, exploits the possibility to directly convert the signal coming from receptors to an electrical one. The broad diffusion of FET-based biosensors for biological applications (bioFETs) lie in the opportunity to exploit several transduction mechanisms, since the output current of a transistor depends on different contributions:

$$I_{DS} = \mu C_{ins} \frac{W}{L} \left((V_{GS} - V_{th}) V_{DS} - \frac{V_{DS}^2}{2} \right) \tag{2.14}$$

where μ represent carriers mobility, C_{ins} the insulator capacitance, W and L respectively channel width and length, V_{DS} and V_{GS} operating voltages, whereas V_{th} is the threshold voltage. Exploiting a proper functionalization strategy, or structure, in principle should be

possible to use each one of them for biochemical transduction. Just as for electrochemical sensors, direct biosensing is generally preferable in terms of easiness of biochemical processes and interpretation of the results. For this reason, a big effort is expended to the design and developing of bioFETs for the transduction of characteristic properties of biomolecules, such as their inner charge.

So far, two main technologies and their evolutions have been employed for bioFETs fabrication:

- **Metal-Insulator-Semiconductor Field-Effect Transistors** (MISFETs), Electrolyte-Insulator-Semiconductor FETs (EISFETs), and Thin-Film Transistors (TFTs) offers different possibilities in terms of sensing possibilities. In fact, while in MISFETs structures only the source, drain and gate contacts are directly accessible and can be conveniently modified, EISFETs enable the possibility to functionalize the insulator/semiconductor interface, thus exploiting the possibility to directly influence the flat band voltage ($V_{FB} = f(Q_t)$) through the trapped charge at the insulator-semiconductor interface Q_t. Consequently, the threshold voltage of the transistor ($V_{th} = f(V_{FB})$) is directly related to the presence of a target analyte.
- **Nanowires** (NWs) are configured as FETs device which exhibit a conductivity change in response to variations in the electric field or potential at the surface. In this case, a general sensing device can be obtained by linking NWs receptor groups that recognize specific molecules to the surface of the NW. The main reasons for the attention attained in the last years is related to their one-dimensional structure which allows the overcoming of short channel effects, and the subsequent high surface-to-volume ratio, which obviously leads to an increase of sensitivity with respect to different structures.

Such technologies allows both a direct and an indirect measurement of biological reactions occurring in liquids and in the past decade have been successfully employed for several kind of bio-related reactions such as pH sensors [37][38], direct [39] and indirect [40] nucleic acid detection.

In this scenario, an increased number of electronics sensors based on organic materials has been observed. The reasons behind Organic Thin-Film Transistors (OTFTs) broad

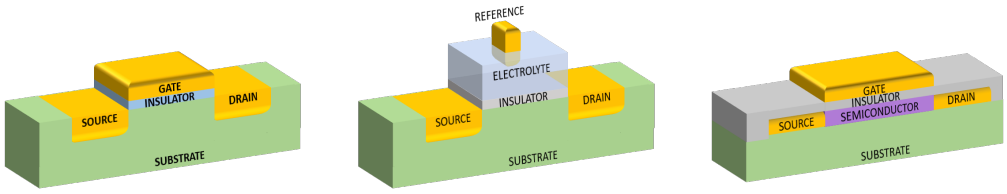

(a) (b) (c)

Figure 2.16 – Various bioFET structures: (a) Metal-Insulator-Semiconductor Field-Effect Transistors (MISFET), (b) Electrolyte-Insulator-Semiconductor FET (EISFET), (c) Thin-Film Transistor in top-gate top-contact configuration.

diffusion is related to the low-cost and large area processes which can be employed for the fabrication of devices on flexible, transparent plastic substrates, thus being particularly interesting in the field of disposable sensors for field kits. Moreover, the interaction between biological molecules and organic materials is typically stronger and easier to set up with respect to the inorganic counterpart. As different chemical and physical techniques can be employed in the fabrication process, several transduction mechanisms can be used to exploited the multi-parametric sensing abilities of such devices.

- **Charge injection modulation** relies on the change of the source and drain metal work function, by means of a functionalization procedure. As the variations in the electrical performances of OTFTs can be quantified and directly related to the characteristics of the considered molecules, the modulation of charge injection/extraction can be employed as transducing mechanism for DNA hybridization sensing [41].

- **Morphology variation** takes advantage of the correlation between the characteristics of the organic semiconductor film and the charge carrier mobility. Using semiconductor morphological changes as transducing element can be very effective not only for mechanical sensing, but can be employed to detect other variety of analytes such as protein [42].

- **Field-Effect modulation** represents the standard transduction mechanism as well as for the other bioFET structures previously mentioned. As well as for MISFETs developments, exposing the semiconductor interface to an electrolyte allows to exploit a variation in the threshold voltage of the device, as it happens in ISFET-based structures and Electrolyte-Gated OFETs (EGOFETs) [43]. As an alternative,

a device in a bottom gate configuration can be employed, exploiting the metallic surface as sensing area.

Limitations of bioFET-based detection

A strong limitation to direct sensing of electrically-charged molecules with field-effect devices is related to the ionic strength of the electrolyte: the higher is the ionic strength, the larger is the screening effect on the intrinsic charge of the molecules by the free ions in solution. The screening effect is generally described introducing the *Debye length*:

$$\lambda_D = \sqrt{\frac{\varepsilon_R \varepsilon_0 k_B T}{e^2 N_a 2C}} \tag{2.15}$$

where ε_R and ε_0 are the relative dielectric constant of the solution and electrical permittivity of the vacuum, respectively, k_B the Boltzmann constant, T the absolute temperature of the solution, e the electric charge, N_a the Avogadro number adn C the ionic strength of the solution.

According to the definition, only the molecular charge located within the Debye length from the sensing surface of the device can contribute to the field-effect modulation, while the charge that lies beyond the Debye length is completely screened. As a consequence, the charge associated with large macromolecules, such as oligonucleotides and antibodies, can be electrically detected only in solutions with a very low ionic strength, i.e. in conditions that are very different from those of reactions occurring in vivo. This is therefore considered as a strong limitation to the potential of these devices for a reliable detection [44].

Electronic biosensors for Telomerase activity detection

Among the various different techniques presented so far, electronic devices are the best candidates for the development of a sensor able to directly detect telomerase activity, in real-time. As previously mentioned, several transduction mechanisms can be exploited

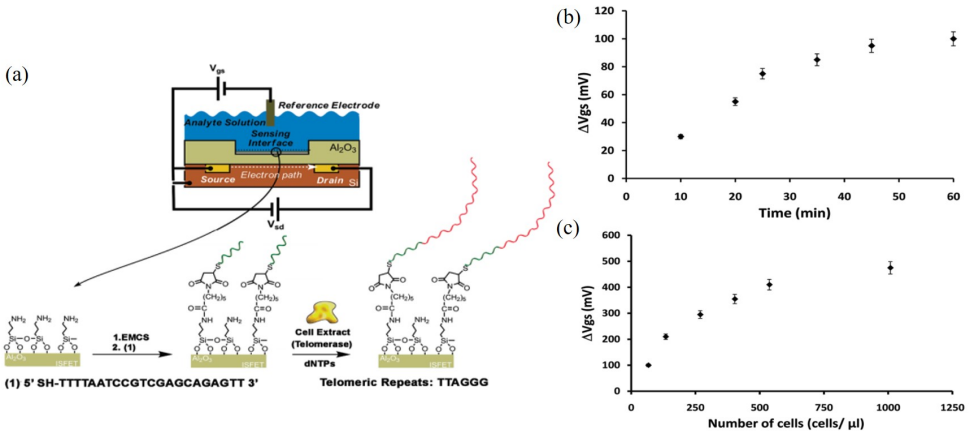

Figure 2.17 – The ISFET-based bioFET for telomerase activity detection in [45]: (a) ISFET configuration and gate modification for the proposed analysis; (b) time-dependent variations of gate potential upon elongation of telomeres; (c) gate potential changes as a function of different concentration of cells.

in order to detect a biological reaction. Despite of the innovation of these approaches, however, some drawbacks have so far limited the employment of such a transduction mechanisms. As an example, characterization of devices modified to exploit charge injection mechanism, have to be performed in dry state, which is an unlikely condition for a lot of biological molecules. On the other hand, a direct exposure of the semiconductor to an aqueous media and to analytes, can strongly affect the stability and performances of the results. Consequently, only few examples have been employed to the detection of telomerase activity [45][46].

Figure 2.17a shows an ISFET structure, modified in order to detect telomerase activity. Structure's sensitivity is related to chemical groups that natively cover the surface of many insulating materials employed in silicon processes, as silicon dioxide (SiO_2), alumina (Al_2O_3), titanium oxide (TiO_2) and tantalium pentoxide (Ta_2O_5). In particular, the primary modification of the Al_2O_3 gate of the ISFET device was achieved by the treatment of the ISFET with an aminosilane molecule (3-aminopropyltriethoxysilane) at room temperature for 12 h. After a thorough rinse of the silylated chip, nucleic acids were covalently linked to the aminosiloxane-functionalized gate interface by treatment of the gate with a protein crosslinking reagent (N-[e-Maleimidocaproyloxy]succinimide ester) at room temperature for 30 min. The chip was rinsed with water, then with an organic buffering agent (HEPES), and then treated with 0.2 mL of probes for 2 h. For an

ISFET structure, the flat band voltage is given by

$$V_{FB} = (E_{REF} + \phi_{ij}) - (\phi_{eo} - \chi_e) - \frac{\varphi_{Si}}{q} - \frac{Q_0}{C_{INS}} \tag{2.16}$$

where E_{REF} is the potential of the reference electrode with respect to the vacuum level, ϕ_{ij} is the voltage drop between solution and electrode, ϕ_{eo} is the voltage drop between solution and insulator, χ_e is the voltage related to surface dipoles, φ_{Si} is the silicon working function, while Q_0 and C_{INS} are charge and capacitance per area unit of the insulating layer. As a consequence, according to 2.16, the threshold voltage of ISFET can be simplified and related to the threshold voltage of a MOSFET as in [47]:

$$V_T = V_{th(MOS)} + V_{chem} \tag{2.17}$$

where V_{chem} depends both on chemical potentials and temperature. According to [48], the variation of charge, Q_s, at the oxide/electrolyte interface produces, by field effect, a reorganization of the charge in the near surface region of the semiconductor/oxide interface. The problem is then reduced to calculating the relationship between Q_s and such potential, within the semiconductor at the Si/SiO_2 interface. The telomerase-induced elongation of a telomerase primer linked to the gate of the ISFET device (figure 2.17a) could then alter the charge on the gate, thus enabling the sensing of telomerase activity. Therefore, telomeres-like probes were immobilized on top of the gate surface, acting as a primer for telomearase. The functionalized device was then exposed to telomerase extracts and to a mixture of dNTPs that stimulated the elongation process on the gate. As the time-dependent telomerization proceeds on the ISFET device, it stimulates a potential change that enables the analysis of telomerase activity. Figure 2.17b shows the gate voltage variation observed upon the telomerase-induced elongation. The saturation effect is attributed to the deactivation of telomerase as elongation is prolonged. Figure 2.17c shows the resulting calibration curve that corresponds to the analysis of a different number of $293T$ cells by the FET device. The method enabled the detection of telomerase originating from 65 ± 10 293T cells/μL.

The main drawbacks of such approach, are related to the readout circuitry employed to

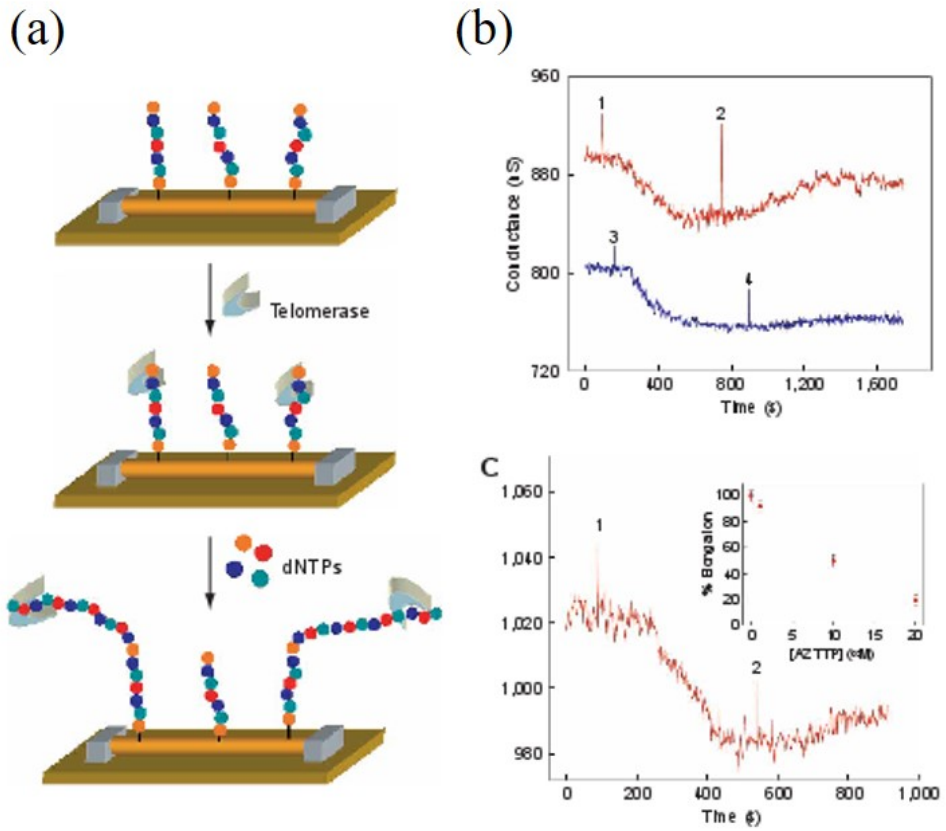

Figure 2.18 – The SiNWTFT-based system for real-time monitoring of telomerase activity in [46]: working principle of the proposed method (a); (b) conductance variation for two different p-type SiNWTFTs (red and blue curves) to the introduction of telomerase ((1) and (3)) and to its activity when all the four kind of nucleotides (2) and just cytosine (4) are inserted and (c) conductance-versus-time variation after the introduction of a solution containing extract of telomerase, dNTPs and a telomerase inhibitor agent (AZTTP).

measure the gate potential, and the fabrication process. In fact, as well as for electrochemical detection methods, ISFET functionality require a reference electrode immersed in solution. Moreover, because of non-ideal behaviors such as threshold voltage variations due to trapped charge and loss of transconductance efficiency which degrade sensors performances, existing ISFET front-end circuits suffer of several issues as well. Such a random variations can be difficult to compensate, as they arise as a consequence of random and inconsistent phenomena.

An alternative approach, based on silicon nanowire TFT (SiNWTFT), was employed by Zheng *et al.* in [46]. In figure 2.18a, the employment of the device for the detection

of telomerase activity is shown. Figure 2.18b shows SiNWTFT conductance variations of different p-type SiNWTFTs modified with DNA probes, after the introduction of (1) a solution containing extract from 100,000 normal human fibroblast cells and 0.4 mM dCTP, (2) a mixture of all four dNTPs each at 0.1 mM, (3) a solution containing extract from 10,000 HeLa cells, 0.4 mM dCTP, and 5 mM oligonucleotide (sequence: 5-TTTTTTAATCCGTCGAGCAGAGTT-3), (4) a mixture of all four dNTPs each at 0.1 mM, (5) a solution containing extract from 10,000 heat-deactivated HeLa cells (90 deg, 10 min) and 0.4 mM dCTP and (6) a mixture of all four dNTPs each at 0.1 mM. A first reduction of the conductance was recorded for both SiNWTFTs as a consequence of the positively-charged telomerase, which, binding to the DNA probes, reduce the total negative charge anchored onto the nanowire. Telomerase can elongate the DNA probes only if all kind of nucleotides are in the solution: consequently, an increase of the conductance of the first sensor was recorded as a consequence of the DNA probes elongation, while no further significant variation were obtained from the second one.

2.5 Conclusions, aim and motivations

In the previous section, several examples of biosensors and sensing technologies have been examined, focusing particular attention to their application in telomerase activity detection. Optical methods, which are considered the gold standard for biochemical analysis, require expensive and bulky instrumentation, as well as a highly specialized operator to be performed. Electrochemical detection methods offer several advantages with respect to such approach, however integration of materials and systems needed for their operation in LoCs in not a trivial task.

Detection of biomolecules and biological reaction with an electronic device represent an interesting alternative to the above mentioned methods: direct detection of the analyte through their intrinsic properties, such as electrical charge, can be exploited through several transduction mechanisms; moreover, their integration with an electronic readout system is simplified not only because of their inherent nature, but also because of the amplification of the electrical signal coming out from the receptor.

Despite their potentiality, some drawbacks hinder bioFETs broad diffusion and their application to clinical screening: ISFET-based devices still require a reference electrode,

which largely limit device integration in LoCs, while nanowire-based detection methods require complex and costly techniques, which can not be easily integrated with a standard CMOS fabrication process. Therefore, in order to overcome such limitations, alternative transduction mechanisms or detection strategies have to be explored.

Bibliography

[1] J. W. Shay and S. Bacchetti, "A survey of telomerase activity in human cancer," *European Journal of Cancer*, vol. 33, no. 5, pp. 787–791, 1997.

[2] M. Meyerson, "Role of telomerase in normal and cancer cells," *Journal of Clinical Oncology*, vol. 18, no. 13, pp. 2626–2634, 2000.

[3] C. B. Harley, "Telomerase and cancer therapeutics," *Nature Reviews Cancer*, vol. 8, no. 3, pp. 167–179, 2008.

[4] IUPAC, *Compendium of Chemical Terminology*. 2014.

[5] L. C. Clark Jr. and C. Lyons, "Electrode systems for continuous monitoring in cardiovascular surgery.," *Ann. N. Y. Acad. Sci.*, vol. 102, no. Art. 1, pp. 29–45, 1962.

[6] D. G. M. Rebecca L. Rich, "An efficient two step purification and molecular characterization of beta-galactosidases from Aspergillus oryzae.," *Journal of molecular recognition : JMR*, vol. 20, pp. 300–366, 2007.

[7] S. P. Rad'Ko, S. A. Voronina, A. V. Gromov, O. V. Gnedenko, N. V. Bodoev, A. S. Ivanov, and K. N. Yarygin, "Use of oligonucleotides conjugated to gold nanoparticles and streptavidin for amplification of optical biosensor signal during detection of telomeric repeats," *Bulletin of Experimental Biology and Medicine*, vol. 147, no. 6, pp. 746–749, 2009.

[8] C. Maesawa, T. Inaba, H. Sato, S. Iijima, K. Ishida, M. Terashima, R. Sato, M. Suzuki, A. Yashima, S. Ogasawara, H. Oikawa, N. Sato, K. Saito, and T. Masuda, "A rapid biosensor chip assay for measuring of telomerase activity using surface plasmon resonance.," *Nucleic acids research*, vol. 31, no. 2, pp. E4–4, 2003.

[9] X. T. Zheng and C. M. Li, "Single living cell detection of telomerase overexpression for cancer detection by an optical fiber nanobiosensor.," *Biosensors & bioelectronics*, vol. 25, no. 6, pp. 1548–52, 2010.

[10] V. Brabec, "433 - Nucleic acid analysis by voltammetry at carbon electrodes," *Journal of Electroanalytical Chemistry and Interfacial Electrochemistry*, vol. 8, no. 4, pp. 437–449, 1981.

[11] T. Aiyejorun, J. Kowalik, J. Janata, and M. Josowicz, "Label-free detection of dna hybridization by cyclic voltammetry. an advanced undergraduate analytical chemistry laboratory experiment," *Journal of Chemical Education*, vol. 83, no. 8, p. 1208, 2006.

[12] "Active CMOS sensor array for electrochemical biomolecular detection," vol. 43, no. 8, pp. 1859–1871, 2008.

[13] Z. Bagheryan, J. B. Raoof, and R. Ojani, "Voltammetric characterization of human telomeric G-quadruplex: A label free method for anticancer drug detection," *Bioelectrochemistry*, vol. 107, pp. 25–29, 2016.

[14] L. Wu, J. Wang, J. Ren, and X. Qu, "Ultrasensitive telomerase activity detection in circulating tumor cells based on dna metallization and sharp solid-state electrochemical techniques," *Advanced Functional Materials*, vol. 24, no. 18, pp. 2727–2733, 2014.

[15] K. Mori, S. Sato, M. Kodama, M. Habu, O. Takahashi, T. Nishihara, K. Tominaga, and S. Takenaka, "Oral cancer diagnosis via a ferrocenylnaphthalene diimide-based electrochemical telomerase assay," *Clinical Chemistry*, vol. 59, no. 1, pp. 289–295, 2013.

[16] M. Hayakawa, M. Kodama, S. Sato, K. Tomoeda-Mori, K. Haraguchi, M. Habu, S. Takenaka, and K. Tominaga, "Electrochemical telomerase assay for screening for oral cancer," *British Journal of Oral and Maxillofacial Surgery*, vol. 54, no. 3, pp. 301–305, 2016.

[17] U. Eskiocak, D. Ozkan-Ariksoysal, M. Ozsoz, and H. A. Öktem, "Label-free detection of telomerase activity using guanine electrochemical oxidation signal," *Analytical Chemistry*, vol. 79, no. 22, pp. 8807–8811, 2007.

[18] S. Sato and S. Takenaka, "PCR-free telomerase assay using chronocoulometry coupled with hexaammineruthenium(III) chloride," *Analytical Chemistry*, vol. 84, no. 3, pp. 1772–1775, 2012.

[19] A. B. Steel, T. M. Herne, and M. J. Tarlov, "Electrochemical quantitation of DNA immobilized on gold," *Analytical Chemistry*, vol. 70, no. 22, pp. 4670–4677, 1998.

[20] H. Helmholtz, "Ueber einige Gesetze der Vertheilung elektrischer Ströme in körperlichen Leitern mit Anwendung auf die thierischâĂŘelektrischen Versuche," *Annalen der Physik*, vol. 165, no. 6, pp. 211–233, 1853.

[21] G. Gouy, "Sur la Constitution de la Charge Electrique a la Surface d'un Electrolyte," *Compt. Rend.*, vol. 149, p. 654, 1910.

[22] D. L. Chapman, "LI. A contribution to the theory of electrocapillarity," *Philosophical Magazine Series 6*, vol. 25, no. 148, pp. 475–481, 1913.

[23] A. Manickam, A. Chevalier, M. McDermott, A. D. Ellington, and A. Hassibi, "A CMOS electrochemical impedance spectroscopy (EIS) biosensor array," *IEEE Transactions on Biomedical Circuits and Systems*, vol. 4, no. 6 PART 1, pp. 379–390, 2010.

[24] Y. Hu, P. Zuo, and B.-C. Ye, "Label-free electrochemical impedance spectroscopy biosensor for direct detection of cancer cells based on the interaction between carbohydrate and lectin," *Biosensors and Bioelectronics*, vol. 43, no. Supplement C, pp. 79 – 83, 2013.

[25] Y. Hu, F. Li, X. Bai, D. Li, S. Hua, K. Wang, and L. Niu, "Label-free electrochemical impedance sensing of DNA hybridization based on functionalized graphene sheets.," *Chemical communications (Cambridge, England)*, vol. 47, pp. 1743–1745, 2011.

[26] A. Li, F. Yang, Y. Ma, and X. Yang, "Electrochemical impedance detection of dna hybridization based on dendrimer modified electrode," *Biosensors and Bioelectronics*, vol. 22, no. 8, pp. 1716 – 1722, 2007.

[27] J. A. Lee, S. Hwang, J. Kwak, S. I. Park, S. S. Lee, and K. C. Lee, "An electrochemical impedance biosensor with aptamer-modified pyrolyzed carbon electrode for label-free protein detection," *Sensors and Actuators, B: Chemical*, vol. 129, no. 1, pp. 372–379, 2008.

[28] R. K. Shervedani, A. H. Mehrjardi, and N. Zamiri, "A novel method for glucose determination based on electrochemical impedance spectroscopy using glucose oxidase self-assembled biosensor," *Bioelectrochemistry*, vol. 69, no. 2, pp. 201–208, 2006.

[29] E. Scavetta, A. G. Solito, M. Demelas, P. Cosseddu, and A. Bonfiglio, "Electrochemical characterization of self assembled monolayers on flexible electrodes," *Electrochimica Acta*, vol. 65, pp. 159–164, 2012.

[30] C. Ruan, L. Yang, and Y. Li, "Immunobiosensor chips for detection of escherichia coli o157:h7 using electrochemical impedance spectroscopy," *Analytical Chemistry*, vol. 74, no. 18, pp. 4814–4820, 2002. PMID: 12349988.

[31] F. Yan and O. A. Sadik, "Enzyme-modulated cleavage of dsdna for supramolecular design of biosensors," *Analytical Chemistry*, vol. 73, no. 21, pp. 5272–5280, 2001. PMID: 11721929.

[32] F. Patolsky, A. Lichtenstein, and I. Willner, "Electronic transduction of dna sensing processes on surfaces:âĂL' amplification of dna detection and analysis of single-base mismatches by tagged liposomes," *Journal of the American Chemical Society*, vol. 123, no. 22, pp. 5194–5205, 2001. PMID: 11457381.

[33] W. Yang, X. Zhu, Q. Liu, Z. Lin, B. Qiu, and G. Chen, "Label-free detection of telomerase activity in HeLa cells using electrochemical impedance spectroscopy," *Chemical Communications*, vol. 47, no. 11, p. 3129, 2011.

[34] "CMOS Capacitive Sensors With Sub-um Microelectrodes for Biosensing Applications," *IEEE Sensors Journal*, vol. 10, no. 5, pp. 991–996, 2010.

[35] "An electrochemical array sensor with CMOS signal processing circuits integrated on a single chip," pp. 138–141, 2010.

[36] J. F. Yang, C. L. Wei, J. F. Wu, and B. D. Liu, "Design of a dual-mode electrochemical measurement and analysis system," *Conference proceedings : ... Annual International Conference of the IEEE Engineering in Medicine and Biology Society. IEEE Engineering in Medicine and Biology Society. Annual Conference*, vol. 2013, pp. 3265–3268, 2013.

[37] Y. Cui, "Nanowire Nanosensors for Highly Sensitive and Selective Detection of Biological and Chemical Species," *Science*, vol. 293, no. 5533, pp. 1289–1292, 2001.

[38] "A novel pH sensitive ISFET with on chip temperature sensing using CMOS standard process," vol. 76, no. 1-3, pp. 582–593, 2001.

[39] J. Hahm and C. M. Lieber, "Direct ultrasensitive electrical detection of dna and dna sequence variations using nanowire nanosensors," *Nano Lett.*, vol. 4, no. C, pp. 51–54, 2004.

[40] "Real-Time Monitoring of DNA Polymerase Reactions by a Micro ISFET pH Sensor," *Analytical Chemistry*, vol. 64, no. 17, pp. 1996–1997, 1992.

[41] F. Yan, S. M. Mok, J. Yu, H. L. W. Chan, and M. Yang, "Label-free DNA sensor based on organic thin film transistors," *Biosensors and Bioelectronics*, vol. 24, no. 5, pp. 1241–1245, 2009.

[42] M. D. Angione, S. Cotrone, M. Magliulo, A. Mallardi, D. Altamura, C. Giannini, N. Cioffi, L. Sabbatini, E. Fratini, P. Baglioni, G. Scamarcio, G. Palazzo, and L. Torsi, "Interfacial electronic effects in functional biolayers integrated into organic field-effect transistors," *Proceedings of the National Academy of Sciences*, vol. 109, no. 17, pp. 6429–6434, 2012.

[43] L. Kergoat, B. Piro, M. Berggren, M. C. Pham, A. Yassar, and G. Horowitz, "DNA detection with a water-gated organic field-effect transistor," *Organic Electronics*, vol. 13, no. 1, pp. 1–6, 2012.

[44] A. Poghossian, A. Cherstvy, S. Ingebrandt, A. Offenhäusser, and M. J. Schöning, "Possibilities and limitations of label-free detection of DNA hybridization with field-effect-based devices," in *Sensors and Actuators, B: Chemical*, vol. 111-112, pp. 470–480, 2005.

[45] E. Sharon, R. Freeman, M. Riskin, N. Gil, Y. Tzfati, and I. Willner, "Optical, electrical and surface plasmon resonance methods for detecting telomerase activity," *Analytical Chemistry*, vol. 82, no. 20, pp. 8390–8397, 2010.

[46] G. Zheng, F. Patolsky, Y. Cui, W. U. Wang, and C. M. Lieber, "Multiplexed electrical detection of cancer markers with nanowire sensor arrays," *Nature Biotechnology*, vol. 23, no. 10, pp. 1294–1301, 2005.

[47] L. M. Shepherd and C. Toumazou, "A biochemical translinear principle with weak inversion ISFETs," *IEEE Transactions on Circuits and Systems I: Regular Papers*, vol. 52, no. 12, pp. 2614–2619, 2005.

[48] E. Souteyrand, J. P. Cloarec, J. R. Martin, C. Wilson, I. Lawrence, S. Mikkelsen, and M. F. Lawrence, "Direct Detection of the Hybridization of Synthetic Homo-Oligomer DNA Sequences by Field Effect," *The Journal of Physical Chemistry B*, vol. 101, no. 15, pp. 2980–2985, 1997.

3 Charge Modulated FET for the detection of biological processes

In this chapter, a reference-less bioFET structure, namely Charge-Modulated Field-Effect Transistor (CMFET), will be presented. The working principle and the results so far reported in literature will be presented, specially focusing on biosensing applications and to the results whose are particularly interesting in the context of telomerase activity detection.

Contents

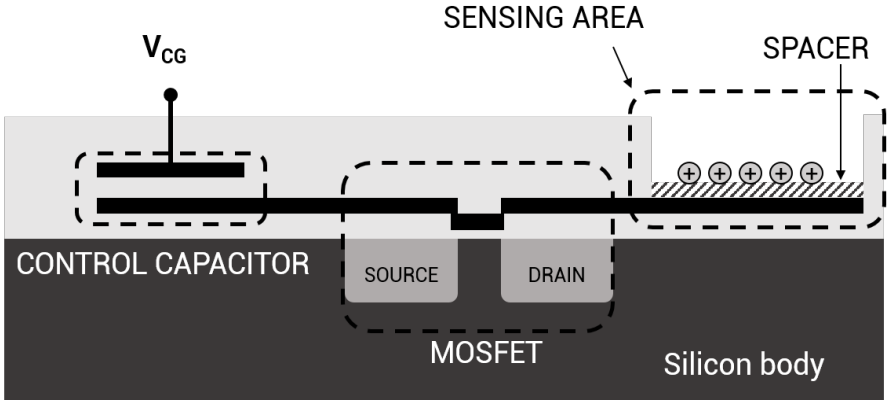

Figure 3.1 – Basic structure of the Charge-Modulated Field-Effect Transistor.

3.1 The Charge Modulated FET working principle

An interesting alternative approach to those previously introduced was proposed in 2005 by Barbaro *et al.* [1]. The device, namely *Charge-Modulated Field-Effect Transistor* (CMFET), was patented by the National Council for Condensed Matter Physics and was conceived to overcome some of the main issues of the bioFETs. The device structure is based on a modification of a floating-gate MOSFET, as depicted in figure 3.1. The layout is modified in order to expose a part of the floating gate to the external environment. This exposed part acts as *active*, or *sensing area*, while a *control capacitor* is used to set the voltage of the floating gate. The sensing area makes the voltage of the floating gate reliant on charge modulation in its near proximity. In the proposed model, this charge Q_S interacts with the floating gate in an electrostatic way, through an insulating spacer which is supposed thinner than other insulating layer in the structure and thus determine a capacitive structure on the sensing area.

A relationship between the actual charge immobilized on top of the sensing area and the potential applied to the control gate (V_{CG}) arises from the charge conservation principle. In fact, the total charge into the insulated floating-gate must remain constant:

$$Q_{F0} = Q_i(Q_S) + Q_{CFB} + Q_{CG} \tag{3.1}$$

where Q_{F0} is the total charge trapped inside the floating gate, Q_i is the charge induced by the surface charge Q_S, Q_{CFB} the charge related to the parasitic capacitor determined by floating gate and bulk and Q_{CG} the charge induced by the control capacitor. Writing

all charges in terms of capacitance, if the dependence on the voltages is make explicit, we can rewrite 3.1 as:

$$Q_{F0} = Q_i(Q_S) + C_{FB}V_{FB} + C_{CG}(V_{FB} - V_{CG}) \tag{3.2}$$

Therefore, we can make explicit the dependence of the floating gate voltage on the actual charge immobilized on the sensing area:

$$V_{FG} = \frac{C_{CG}}{C_{CG} + C_{FB}} V_{CG} + \frac{Q_i(Q_S) - Q_{F0}}{C_{CG} + C_{FB}} \tag{3.3}$$

As usually done for floating gate transistors, the effect of different sources is modeled as a change in the effective threshold voltage (V_{THF}) of the transistor, simply subtracting V_{TH} on both member of 3.3:

$$\begin{aligned} V_{FG} - V_{TH} &= \frac{C_{CG}}{C_{CG} + C_{FB}} V_{CG} + \frac{Q_i(Q_S) - Q_{F0}}{C_{CG} + C_{FB}} - V_{TH} \\ &\approx V_{CG} - \left(V_{TH} - \frac{Q_i(Q_S) - Q_{F0}}{C_{CG} + C_{FB}} \right) \\ &= V_{CG} - V_{THF} \end{aligned} \tag{3.4}$$

where

$$V_{THF} \approx V_{TH} - \frac{Q_i(Q_S) - Q_{F0}}{C_{CG} + C_{FB}} \tag{3.5}$$

As clearly stated during the derivation of eq. 3.4, the last equation lies on the hypothesis that the parasitic capacitances are negligible with respect to the control capacitor. Moreover, if the spacer thickness is far lower than the other insulating layer in the layout, a perfect charge induction on the sensing area can be considered ($Q_i = -Q_S$); in this case, the last equation can be rewritten as:

$$V_{THF} \approx V_{TH} + \frac{Q_S + Q_{F0}}{C_{CG} + C_{FB}} \tag{3.6}$$

The effectiveness of the linear model was demonstrated both in two and three dimensions: in the 2D-model, the section shown in 3.1 was considered, as the electric field in the structure can be considered essentially vertical. The 3D-model was then calculated in order to include possible secondary effects. In figure 3.2 the results of these simulations

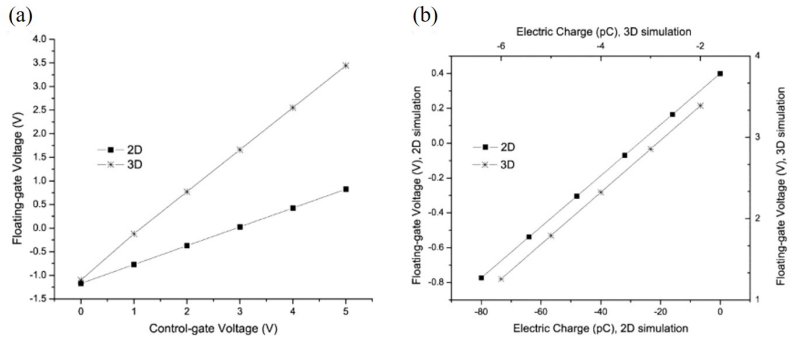

Figure 3.2 – (a) 2D (V_{CG} = 1 V, oxide thickness = 5 μm) and 3D (V_{CG} = 5 V, oxide thickness = 0.02 μm) simulations of the dependence of the floating gate voltage to the electric charge density. (b) 2D (Q_S = -1 pC) and 3D (Q_S = -20 pC) simulations of the dependence of the floating gate voltage to the control gate voltage [1].

are shown.

According to equation 3.4, the device is a charge sensor and its floating gate voltage linearly depends on both the charge immobilized on the sensing area and the voltage applied to the control gate. Therefore, it is possible to use the control gate to set the operating point of the device, eventually zeroing the contribution of the unknown charge trapped inside the floating gate Q_{F0}, while monitoring the charge present on the sensing area through the variation of the effective threshold voltage of the FET structure.

According to the presented working principle, this structure proves interesting features in applications requiring the detection of charged species in liquids. The lack of a sensing electrode is one of the main advantages, largely facilitating its employment and miniaturization. Moreover, the integration of a reference electrode such as required for the employment of ISFET based device or electrochemical impedance spectroscopy, in fact, is usually a limiting factor from the fabrication point of view. Such electrodes must have a well-known potential in order to determine the voltage drop between the reference electrode itself against counter and working electrodes potential; specific materials, such as platinum, silver and silver chloride compound is usually employed at this purpose. Clearly, the integration of this material with a standard CMOS process is not trivial, thus preventing the fabrication of a low-cost, disposable devices. Interestingly, CMFET working principle is independent from the technology employed for its fabrication, thus enabling the employment of novel material and techniques for its implementation.

3.2 CMFET-sensors: state of the art

Complementary to the CMOS implementation, a research activity on an Organic implementation was conducted. Organic CMFET (OCMFET) research activity especially focused on the development of disposable device on plastic substrates for field measurement kits. In addition to the already introduced advantages of the CMFET working principle over the basic bioFET approach, the separation between the sensing area and the transistor area results particularly interesting in the organic implementation, as damages of the organic semiconductor introduced in the previous chapter, are here prevented. So far, three applications were investigated: temperature sensing, pH sensing and metabolic cell activity monitoring.

CMFET sensors for chemo-physical sensing

In 2009 Caboni *et al.* firstly proposed a pH sensor based on OCMFET, later improved by Spanu *et al.* in 2017 [2]. The former implementation he device, shown in Figure 2.9(a), consisted on two OCMFETs, biased through the same control capacitor, measured in a differential mode. The device was fabricated in a bottom contact-bottom gate free standing configuration, as the employed plastic substrate (DuPont Mylar , 1.4 μm-thick) acted also as gate insulating layer. The sensitivity to pH was obtained by functionalizing the gold sensing areas with an amino-terminated ($-NH_2$) Self-Assembled Monolayer (SAM). In 3.3a, the threshold voltage of sensor (square) and reference (circles) are reported as a function of the pH at the sensor. As expected, the output current of the

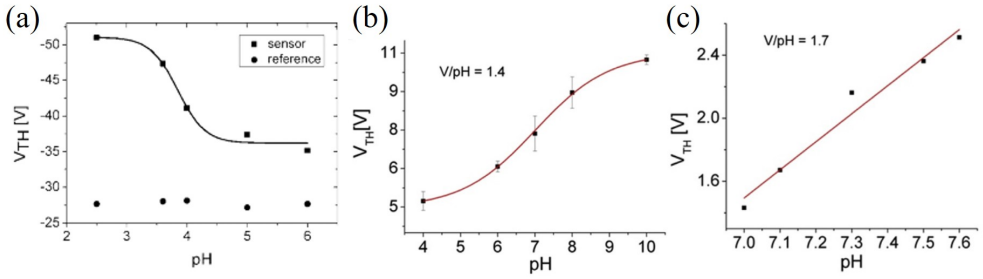

Figure 3.3 – Organic CMFET (OCMFET) as pH sensor: (a) variation in the threshold voltage of sensor and reference with pH as in [3]; (b) calibration curve of the sensor in [2] and (c) fine characterization of an OCMFET pH sensor in the range 7 - 7.6.

sensor progressively decreased with pH, as the threshold voltage increased in response to the protonated aminic groups at the surfaces; on the contrary, no significant variation in the reference were obtained, as it was maintained at pH = 6. The improvements proposed in [2] regard the employment of a bottom-gate bottom-contact structure, operating at low-voltages and a novel sensing layer, namely a thin film of O_2 plasma-activated Parylene C. Figure 3.3a the threshold voltage of sensor (square) and reference (circles) are reported as a function of the pH at the sensor.

In 2013, Lai *et al.* proposed a pressure-modulated sensor based on the exploitation of the Organic implementation of the CMFET structure. The employment of a compressible polydimethylsiloxane capacitor integrated with the core structure of the CMFET was fabricated on a flexible substrate (figure 3.4a), using the same structure and fabrication methods employed for the pH sensor in [2]. The main novelty of the working principle consists in the physical separation between the pressure-sensitive area and the active area of the OFET. The complete characterization of the device, in response to the application of different pressures, is shown in figure 3.4b.

In 2015, Viola *et al.* integrated a pyroelectric polymeric element, namely polyvinylidene fluoride (PVDF), with the OCMFET structure, to realize a temperature sensor. In order to perform such a measurement, a PVDF-based capacitor was transferred onto the sensing area of the floating gate (figure 3.4a). The pyroelectric properties of the PVDF capacitor produce a charge separation in the PVDF film, thus leading to a charge perturbation in the device floating gate. Figure 3.4d shows the characterization of the temperature sensor as presented in [5].

CMFET sensors for DNA hybridization detection

Beyond the previously presented applications, in the last decade various implementations have exploited this structure both in CMOS [6][7] and organic [3] [8]technologies, in order to perform DNA hybridization detection.

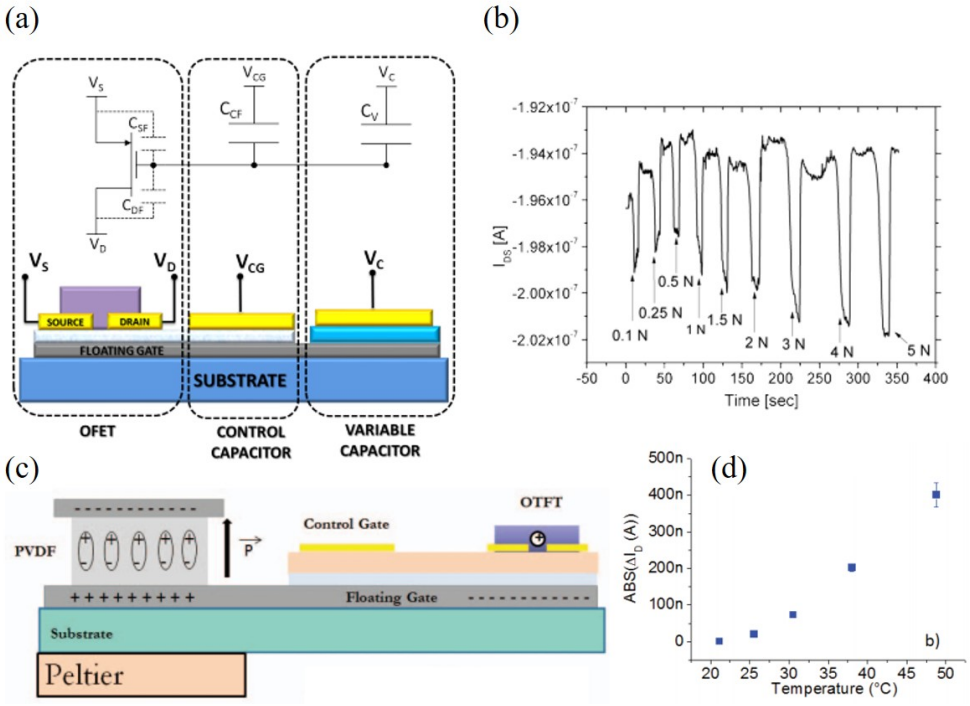

Figure 3.4 – Electrical model and basic structure (a) and output current versus time (b) for the Pressure modulated OFET as different forces were applied to the variable capacitor[4]; schematic representation of the OCMFET integrated with a pyroelectric capacitor (c) and calibration curve of the sensor [5].

CMFET-based Lab-on-Chip

In order to verify the performances of the implementation of CMFET structures in LoCs sensing unit, a complete LoC hosting the sensing elements, a basic readout scheme and interface electronics was designed and fabricated in 0.35 μm CMOS process [6]. The main innovation introduced in such implementation, with respect to the previous ones [9], regards the sensing unit were a PMOS-NMOS pair employed to increase the range of detectable charges. Three different sensing areas and control capacitors dimensions have been employed, together with the introduction of a pair of electrodes for electrically promote and step-up the hybridization process (figure 3.5b). Two programmable read-out schemes were employed [7] and are shown, for the PMOS transistor, in figure 3.6 The circuit shown in figure 3.6a is biased with two programmable currents I_1 and I_2 and a programmable input voltage (V_{DAC}). The output V_{outP} is the drain voltage of a diode-connected PMOS transistor, which is paired (and matched) to the PMOS transistor of the sensor selected from the array. The two currents I_1 and I_2 are generated by means

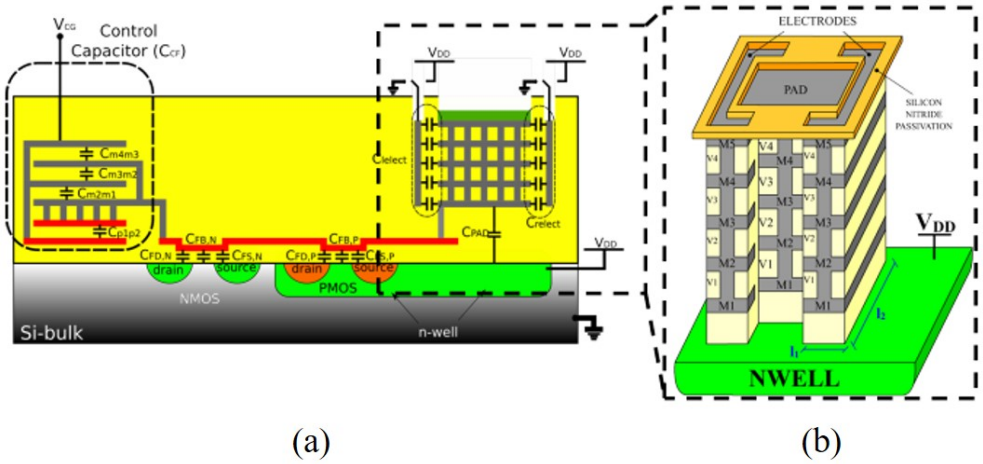

Figure 3.5 – (a) Cross section of the sensing area in the LoC; (b) particular of the sensing area in [6].

of two programmable current generators, whereas the control gate of the sensor is driven by a D/A converter. The output voltage linearly depends on the threshold voltage of the PMOS transistor of the sensors selected from the array:

$$V_{outP} = V_{DAC} + \Delta|V_{TH}| + k\left(\sqrt{(I_1)} - \sqrt{(I_2)} - \sqrt{(I_2)}\right) \tag{3.7}$$

The second read-out circuit is shown in figure 3.6b for the PMOS transistor sensor. It is an I-V converter where the drain terminal of the sensor is connected to the negative terminal of an amplifier with a variable feedback resistor. Both the control-gate voltage of the CMFET sensing unit (V_{DAC1}) and the voltage applied to the non-inverting terminal of the amplifier (V_{DAC2}) are configured in order to make the sensor work in linear region,

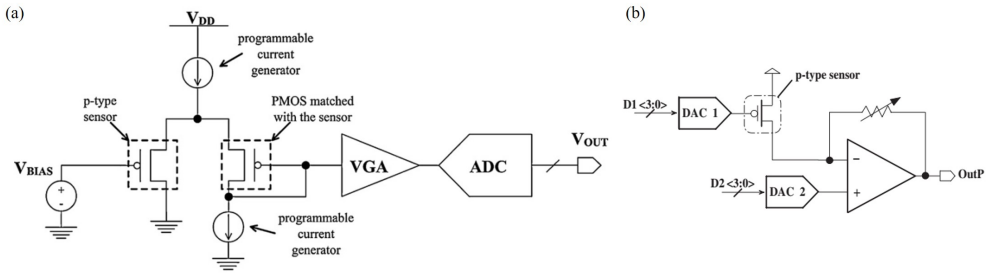

Figure 3.6 – Readout and conditioning systems: (a) level-shifter; (b) I-V converter.[7]

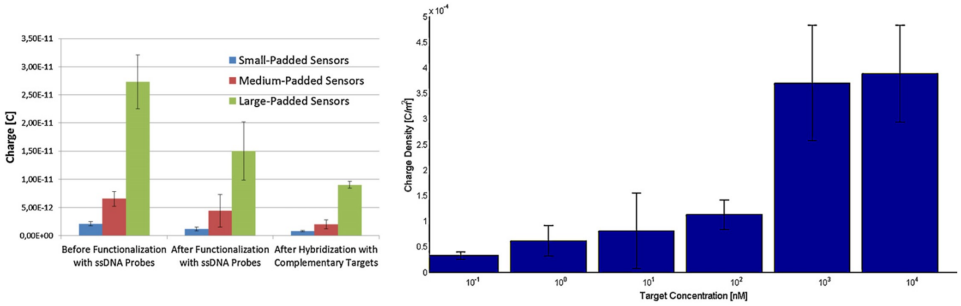

(a) (b)

Figure 3.7 – [6]

thus obtaining:

$$V_{TH} = V_{DD} - V_{DAC1} - \frac{V_{DAC2} - V_{outP}}{k_{sens}\,(V_{DD} - V_{DAC2})} \cdot \frac{1}{R} \tag{3.8}$$

where the value of the feedback resistor (R) can be digitally set. The output signal coming from the readout circuitry is then digitally converted with a 10 bit A/D converter. Figure 3.7a reports the average charge associated to the oligonucleotides in the different phases of the process for the different typologies of sensors. It is possible to observe how the amount of the sensed charge correctly depends on the area of the pads; besides, the negative charge increases after the functionalization and the hybridization processes making the overall charge decreases. Results of a calibration of the sensor with respect to the target concentration is shown in figure 3.7b. A linear dependence of the detected charge to target concentration is obtained until 100 nM dilution. For higher concentrations, the detected charge rapidly increases and saturates.

Organic CMFET-based DNA hybridization sensor

In 2012 Demelas *et al.* proposed to employ the CMFET working principle to the detection of DNA hybridization [10]. Immobilization of DNA probes were on self-assembled-monolayer (SAM) was employed to functionalize the sensing area. As for the pH sensor previously presented, a differential configuration was adopted, in order to evaluate the threshold voltage variation of the sensor with respect to the one of a reference device. The net threshold voltage variation of such implementation is showed in figure 3.8. Accordingly with the device working principle, the occurring hybridization process and, then, the increase of DNA phosphate-backbone negative charge leads to a

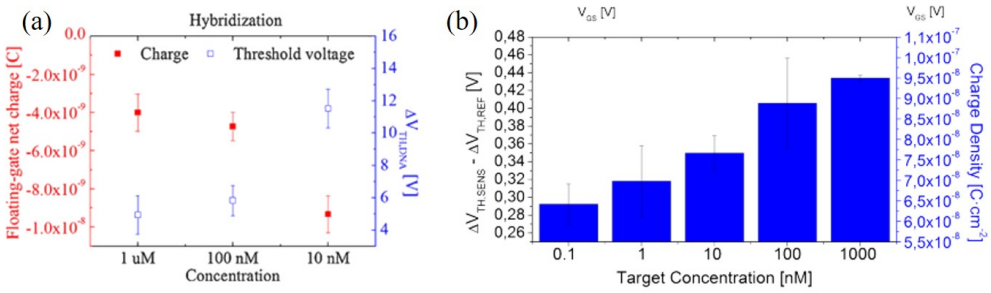

Figure 3.8 – Sensitivity of the OCMFET employed as DNA sensor, as reported in (a) [10] and (b) [8].

shift of the threshold voltage and to an increase of the output current of the device, as a p-type semiconductor (TIPS pentacene) was employed. In 2013 Lai *et al.* proposed a novel implementation of this approach. The introduction of a novel hybrid-dielectric technology [11] allows to operate the device at low-voltages and thus improving sensor's overall performances. Figure 3.8 shows a comparison between the results obtained with the former and the latter implementation, respectively. Clearly, the reduction of the operating voltages played a crucial role in enhancing the reliability of the OCMFET behaviour, allowing to reduce capacitance values at the denominator of equation 3.6.

A further increase of OCMFET sensitivity was obtained through the employment of a self-alignment procedure [12], which allows to detect single nucleotide polymorphism and measure a concentration as low as 1 pM and extrapolate an even lower detection limit of 100 fM (figure 3.9a) [13]. Noteworthy, such a device demonstrated to be able to operate in particular measurement conditions, i.e. with a relatively high salt concentration, which is particularly interesting since overcome one of the most important limitation of bioFET [14], as previously discussed in section 2.4.1. In particular, several tests have been carried out using different probes length, as shown in figure 3.9. Interestingly, the hybridization signal is almost completely lost only with a probe 42 nucleotide long. The explanation proposed by Lai and coworkers [15] is schematically depicted in figure 3.9c: as the Debye length screening is not affecting the proposed measurement, they suggest that the dsDNA molecules are not lying perpendicularly to the surface but are tilted to a certain extent such that, at least for probes long 24 and 31 nucleotides, a certain portion of the molecule is included within the Debye length.

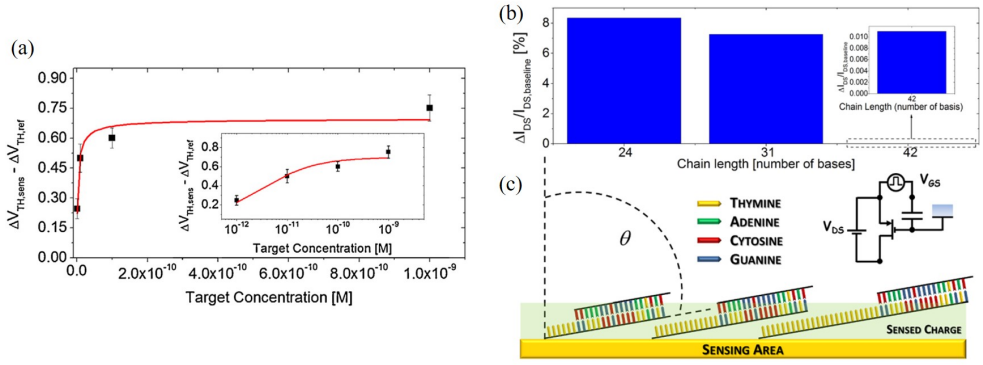

Figure 3.9 – (a) OCMFET improved sensitivity, demonstrated in [13]; (b) percentage variation of the output current as a response of the device to hybridization process when chains with different spacers are considered; in the inset, the variation for a probes 42 42 nucleotides long is reported with a different scale to result visible in the plot; (b) supposed characteristics of the DNA monolayer during the measurements[15]

Bibliography

[1] M. Barbaro, A. Bonfiglio, and L. Raffo, "A charge-modulated fet for detection of biomolecular processes: Conception, modeling, and simulation.," *IEEE Trans. Electron Devices*, vol. 53, no. 1, pp. 158–166, 2005.

[2] A. Spanu, F. Viola, S. Lai, P. Cosseddu, P. Ricci, and A. Bonfiglio, "A reference-less pH sensor based on an organic field effect transistor with tunable sensitivity," *Organic Electronics*, vol. 48, pp. 188–193, 2017.

[3] A. Caboni, E. Orgiu, E. Scavetta, M. Barbaro, and A. Bonfiglio, "Organic-based sensor for chemical detection in aqueous solution," *Applied Physics Letters*, vol. 95, no. 12, 2009.

[4] S. Lai, P. Cosseddu, A. Bonfiglio, and M. Barbaro, "Ultralow voltage pressure sensors based on organic FETs and compressible capacitors," *IEEE Electron Device Letters*, vol. 34, no. 6, pp. 801–803, 2013.

[5] F. A. Viola, P. Cosseddu, S. Lai, A. Spanu, and A. Bonfiglio, "Flexible temperature sensors based on charge modulated organic thin film transistors," in *2015 11th Conference on Ph.D. Research in Microelectronics and Electronics, PRIME 2015*, pp. 278–281, 2015.

[6] M. Barbaro, A. Caboni, D. Loi, S. Lai, A. Homsy, P. D. Van Der Wal, and N. F. De Rooij, "Label-free, direct DNA detection by means of a standard CMOS electronic chip," *Sensors and Actuators, B: Chemical*, vol. 171-172, pp. 148–154, 2012.

[7] A. Caboni, "A CMOS integrated circuit for DNA hybridization detection with digital output and temperature control," *Electronic Engineering*, pp. 137–140, 2007.

[8] "Ultralow voltage, OTFT-based sensor for label-free DNA detection," *Advanced Materials*, vol. 25, no. 1, pp. 103–107, 2013.

[9] M. Barbaro, A. Caboni, and D. Loi, "A CMOS integrated DNA-chip for hybridization detection with digital output," in *Proceedings of the 2nd IEEE International Workshop on Advances in Sensors and Interfaces, IWASI*, 2007.

[10] M. Demelas, S. Lai, G. Casula, E. Scavetta, M. Barbaro, and A. Bonfiglio, "An organic, charge-modulated field effect transistor for DNA detection," *Sensors and Actuators, B: Chemical*, vol. 171-172, pp. 198–203, 2012.

[11] P. Cosseddu, S. Lai, M. Barbaro, and A. Bonfiglio, "Ultra-low voltage, organic thin film transistors fabricated on plastic substrates by a highly reproducible process," *Applied Physics Letters*, vol. 100, no. 9, 2012.

[12] S. Lai, P. Cosseddu, G. C. Gazzadi, M. Barbaro, and A. Bonfiglio, "Towards high frequency performances of ultra-low voltage OTFTs: Combining self-alignment and hybrid, nanosized dielectrics," *Organic Electronics: physics, materials, applications*, vol. 14, no. 3, pp. 754–761, 2013.

[13] S. Lai, M. Barbaro, and A. Bonfiglio, "Tailoring the sensing performances of an OFET-based biosensor," *Sensors and Actuators, B: Chemical*, vol. 233, pp. 314–319, 2016.

[14] A. Poghossian, A. Cherstvy, S. Ingebrandt, A. Offenhäusser, and M. J. Schöning, "Possibilities and limitations of label-free detection of DNA hybridization with field-effect-based devices," in *Sensors and Actuators, B: Chemical*, vol. 111-112, pp. 470–480, 2005.

[15] S. Lai, M. Barbaro, and A. Bonfiglio, "The role of polarization-induced reorientation of DNA strands on organic field-effect transistor-based biosensors sensitivity at high ionic strength," *Applied Physics Letters*, vol. 107, no. 10, 2015.

4 Organic CMFET-based sensor for telomerase activity detection

In this chapter, the design, fabrication and characterization of the sensor will be presented. A thorough examination of preliminary experiments will be discussed, as well as experimental results on the direct detection of telomerase activity.

Contents

Previously mentioned works demonstrated the effectiveness of CMFET-based sensor for biosensing applications. According to the working principle of such a device, thoroughly derived and demonstrated in the previous chapter (3.1), DNA hybridization can be directly detected as a consequence of its intrinsic negative charge of the phosphate groups in the backbone. Therefore, the possibility to directly detect the telomerase activity related to telomeres elongation was investigated: being the actual DNA charge Q_{DNA} immobilized onto the sensing area directly related to the number of nucleotides whereof the molecule is composed, anchoring telomeres-like probes the sensing area should enable the direct detection of telomerase activity, monitoring their elongation. Indeed, telomeres lengthening should determine a variation of the negative charge anchored onto the sensing area A_{SENS} and, thus, a shift in the threshold voltage:

$$\Delta V_{TH} = \frac{Q_{DNA}}{C_{TOT}} = \frac{q \cdot l \cdot A_{SENS} \cdot \sigma_{probes}}{C_{TOT}} \tag{4.1}$$

where C_{TOT} is the sum of all the capacitances ($C_{TOT} = C_{SF} + C_{DF} + C_{FG} + C_{CG}$), σ_{probes} represent the surface density of the immobilized probes and l is the length, namely the number of nucleotides, of which the DNA strand is made of.
Figure 4.1 shows a pictorial representation of the proposed working principle. Oligonucleotides having one or more repetitions of telomeres base sequence ($[TTAGGG]_{n+1}$) at the 3'-end are immobilized on top of the sensing area at their 5'-end. Such sequences, having a structure complementary to the telomerase active site, act as probes, allowing the enzyme to promote their elongation. It is interesting to note that, since telomerase is positively charged at physiological pH, not only the elongation of probes terminal parts but also the enzyme presence can be directly transduced.

Even if the OCMFET working principle has been thoroughly demonstrated, several challenges have to be faced for the specific application:

- telomerase activity requires relatively high ionic concentration in the measurement solution, but this condition is generally accepted as limiting factor for detection of charged biomolecules [1], as the free ions in the solution could screen their intrinsic charge. Furthermore, its activity promotes the elongation of the distal part of the oligonucleotides probes, further limiting such detection;
- as telomerase activity determine small elongation of the DNA molecules (if com-

pared to the primer initial length), an high charge sensitivity is required. In order to fulfill this requirement, precise design rules should be derived and, consequently, layout and technological processes should be optimized to this aim;

- flushing operations needed to deliver the reagents on the sensing area, determining the noise that could mask the specific response due to the telomerase activity; noise rejection must be taken into account both in the sensor design and in the definition of the chemistry for the primer anchoring onto the sensing area.

4.1 Sensing unit design

Telomerase activity promotes the elongation of a small portions of telomeres structure, catalyzing the synthesis of the sequence of six nucleotides (TTAGGG). According to the proposed working principle (cfr. par 3.1), sensor's sensitivity is related to the variation of the threshold voltage of the device, which is inversely proportional to the capacitive contribution of the overall structure. In particular, equation 3.1, can be rewritten in a more general form. In particular, being Q_{F0} the charge initially present in the floating gate, the continuity equation for charge can be stated as a function of the overall capacitance of the structure, and of the voltages applied at each terminal of the device:

$$\begin{aligned} &\epsilon_{ins} E_{FG} (A_{SENS} + A_S + A_D + A_{CG}) \\ &- \epsilon_{ins} E_S A_S - \epsilon_{ins} E_D A_D - \epsilon_{ins} E_{CG} A_{CG} - \epsilon_{spacer} E_{SP} A_{SENS} = Q_{F0} \end{aligned} \tag{4.2}$$

where ϵ_{ins} is the dielectric constant of the insulating layer; E_{SF} and E_{DF} the electric fields in the parasitic capacitors C_{SF} and C_{DF} of the MOS structure, while E_{FG} and C_{FG}, are the electric field and the capacitance between floating gate and body of the sensing unit.

If the spacer thickness is several orders of magnitude smaller than the size of active area, the electric field in the spacer is perpendicular to the metal layer and constant since, for every point of the spacer, the surface molecules are seen as an infinite sheet of charge. Similarly, if the insulating layer between metal plates of capacitors is sufficiently small,

the relationship between the electric field and applied potential can be written as:

$$E_{SF} = \frac{V_S - V_{FG}}{t_{ins}} \qquad E_{DF} = \frac{V_D - V_{FG}}{t_{ins}} \qquad E_{FG} = \frac{V_{FG}}{t_{ins}} \qquad E_{CG} = \frac{V_{CG} - V_{FG}}{t_{ins}} \tag{4.3a}$$

$$C_{SF} = \epsilon_{ins}\frac{A_{SF}}{t_{ins}} \qquad C_{DF} = \epsilon_{ins}\frac{A_{DF}}{t_{ins}} \qquad C_{FG} = \epsilon_{ins}\frac{A_{CG} + A_{SF} + A_{DF} + A_{SENS}}{t_{ins}}$$

$$C_{CG} = \epsilon_{ins}\frac{A_{CG}}{t_{ins}} \tag{4.3b}$$

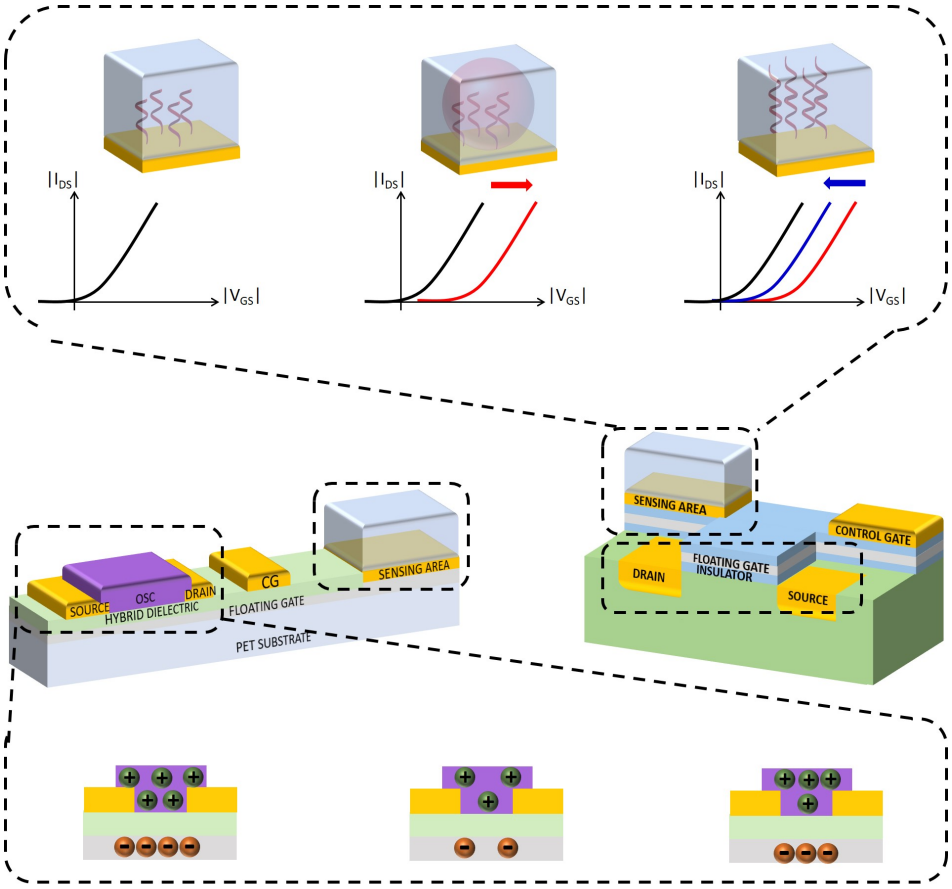

Figure 4.1 – Pictorial representation of organic (left) and CMOS implementation of CMFET sensor for telomerase activity detection: oligonucleotides having a sequence complementary to telomerase active site are immobilized on top of the sensing area and act as a probe for the enzyme. Telomerase introduction on the incubation chamber produce a shift of the threshold voltage because of its net positive charge at physiological pH. So, its activity produce the elongation of the immobilized probes and, therefore, of the total amount of negative charge immobilized on top of the sensing area, thus leading to an opposite shift of the threshold voltage, with respect to the one induced from telomerase injection.

where t_{ins} is the thickness of the insulating layer.
The charge induced on the floating gate by the surface immobilized on the sensing area can be expressed as:

$$Q_i\,(Q_{SENS}) = \epsilon_{spacer} E_{SP} A_{SENS} \tag{4.4}$$

Combining 4.2 with 4.3a, 4.3b and 4.4, the relationship between the floating gate voltage, the charge immobilized on the sensing area and others voltages is obtained:

$$C_{FG}V_{FG} - C_{SF}\,(V_S - V_{FG}) - C_{DF}\,(V_D - V_{FG}) - C_{CG}\,(V_{CG} - V_{FG}) - Q_{DNA} = Q_{F0} \tag{4.5}$$

Finally, solving for V_{FG}:

$$V_{FG} = \frac{C_{CG}}{C_{TOT}} V_{CG} + \frac{C_{DG}}{C_{TOT}} V_D + \frac{C_{SG}}{C_{TOT}} V_S + \frac{Q_i(Q_S) + Q_{F0}}{C_{TOT}} \tag{4.6}$$

where C_{TOT} is the sum of all the capacitances ($C_{TOT} = C_{SF} + C_{DF} + C_{FG} + C_{CG}$). As previously showed in 3.1, the relationship between the effective threshold voltage (V_{THF}) of the transistor, and other contributions can be calculated subtracting V_{TH} on both member of 4.6:

$$\begin{aligned} V_{FG} - V_{TH} &= \frac{C_{CG}}{C_{TOT}} V_{CG} + \frac{C_{DG}}{C_{TOT}} V_D + \frac{C_{SG}}{C_{TOT}} V_S + \frac{Q_i(Q_S) + Q_{F0}}{C_{TOT}} - V_{TH} \\ &= V_{CG} - V_{THF} \end{aligned} \tag{4.7}$$

Thus:

$$V_{THF} = V_{CG} - \left(\frac{C_{DG}}{C_{TOT}} V_D + \frac{C_{SG}}{C_{TOT}} V_S + \frac{Q_i(Q_S) + Q_{F0}}{C_{TOT}} - V_{TH} \right) \tag{4.8}$$

A rapid inspection of equation 4.8 suggests that sensor's sensitivity can be expressed in term of threshold voltage variations. A first-order model simplification suggests that, if the spacer thickness is much thinner than other dimensions, a perfect induction can be hypothesized and the induced charge Q_i would be opposite to the sensing charge Q_S. Assuming constant all the potentials applied to the FET structure, sensor's sensitivity can be expressed in term of threshold voltage variation and can be expressed as follows:

$$\Delta V_{THF} \approx -\frac{\Delta Q_{SENS}}{C_{TOT}} \tag{4.9}$$

Table 4.1 – Parasitic capacitances estimation.

	C_{FG}	C_{GS}	C_{GD}
OTFT	0	$\frac{1}{2}C_{ins} \cdot W \cdot L_{ov}$	$\frac{1}{2}C_{ins} \cdot W \cdot L_{ov}$
CMOS	$\propto A_{SENS}$	$C_{ov}W$	$\frac{2}{3}C_{ins} \cdot W \cdot L + C_{ov}W$

Equations 4.8 and 4.9 dictate a rationale behind the tradeoff between control gate size and device design: parasitic capacitances can be adequately reduced carefully designing the layout, thus increasing sensor' sensitivity. Control capacitor dimension, instead, must be sized in order to be able to precisely set the device operating point.

Parasitic capacitances size strictly depends on the technology employed and on the specific implementation preferred for the fabrication. Clearly, not only equations vary considerably from the two realizations, but also technology-dependent parameters influence their actual value. As an example, in CMOS technology, parasitic capacitances arise as a consequence of the creation of the depletion regions between source/drain diffusions, or the overlap between such areas and the gate contact. As a consequence, an appropriate design strictly depends on the chosen implementation.

4.2 Design and conception

Employment of novel materials proved to possess various interesting features, specially in bio-related applications. Low-cost and large-area fabrication make this approach particularly interesting for the development of disposable sensors for biological applications. Organic electronics technologies were therefore employed in the sensor's first implementation, in order to exploit such features.

Probes immobilization

According to the previous discussion, sensor design requires to carefully consider several technological elements. In particular, immobilization of oligonucleotides on solid surfaces represents a crucial procedure for the correct functionality of optical, electrochemical and electronic DNA sensors. Functionalization of conductors and semiconductors, in fact, plays a crucial role in the development of novel organic/inorganic heterostructures

suitable as materials in sensors, biosensors and clinical diagnostics. In this context, to obtaining a stable and durable bond with the surface with a controllable process, is essential in the development of biological sensing platforms and portable analytical devices such as DNA and protein sensors. In fact, in order to ensure the device stability in aqueous media, obtaining a durable functionalization layer on the sensing area is a central issue in sensor's engineering, since a long time immersion in buffer solution [2] or a mechanical stress such as a flow of a buffer solution [3] could produce a variation in the output signal of the sensor which could be misinterpreted if, at the same time, an analyte is added to the sensing environment. So far, several procedures and studies have been proposed for different materials. In particular, thiol-modified single-stranded DNA (HS-ssDNA) probes have been thoroughly examined. The thiol group (HS) is well known to form a strong chemical bond with several metal surfaces [4][5]; among metals, gold represents the standard case study, as it is biocompatible, stable in liquids and easy to be deposited in thin films. The electroreduction of aryldiazonium salts is a promising alternative to conventional techniques such as Self Assembled Monolayer. This approach was firstly proposed in 1992 [6] and has been used to promote covalent bonds between aryl groups with different substituents and several substrates such as glassy carbon, silicon and gold [7].

Electrochemical procedure

The functionalization of gold electrodes which constitute the sensor's sensing area was performed through the electroreduction of 4-nitrobenzenediazonium (NBD) salts and was conducted in collaboration with the Department of Mechanical, Chemical and Materials Engineering of the University of Cagliari[1]. Such procedure was firstly tested on gold electrodes fabricated on a PET substrate. Since the electrochemical steps required for the electrodeposition of diazonium salts, and their subsequent reduction, produced the delamination of the gold layer from the substrate, a 2 μm-thick Parylene C layer was employed in order to improve the adhesion of the metal to the substrate. All electrochemical experiments were performed at room temperature using an AUTOLAB PGSTAT302N (Metrohm, Switzerland) potentiostat/galvanostat equipped with a frequency response

[1]The author gratefully acknowledges Prof. Michele Mascia, Prof. Annalisa Vacca and Dr. Simone Rizzardini for the precious support in setting-up the instrumentation to fulfill the procedure described in the following section.

analyzer controlled with the NOVA software. Electrodes modification was performed as follows (figure 4.2):

- each electrode undergone to 5 voltammetric cycles (scan rate 100 mV/s) in 0.2 M phosphate buffer (PBS) at pH 7 and then rinsed with double-distilled water;
- electrodeposition of diazonium salts was performed by cyclic voltammetries performed at a scan rate of 100 mV/s in acetonitrile (ACN) solution containing 0.1 M tetrabutylammonium hexafluorophosfate (TBAPF6) and 2 mM NBD, then rinsed in ACN;
- electrochemical reduction of nitro group to amino group was performed by cyclic voltammetry in water/ethanol solutions (90/10 %V) containing 0.1 M of KCl using a scan rate of 100 mV/s;
- immersion in PBS solution containing 0.1 M of N-Hydroxysuccinimide (NHS) and 0.1 M of N-(3-Dimethylaminopropyl)-N'-ethylcarbodiimide (EDC) for 12 hours at 4 °C was employed to bind adipic acid to the amino phenyl group;
- single-strands oligonucleotides (ssDNA) were immobilized on the electrode surface using PBS solution containing 0.1 M of N-Hydroxysuccinimide (NHS) and 0.1 M of N-(3-Dimethylaminopropyl)-N'-ethylcarbodiimide (EDC), following the procedure described by Hai *et al.* [8]; electrodes were immersed in such solution for for 12 hours at 4 °C.

Figure 4.3a shows the cyclic voltammetry of the electrode in the presence of NBD in ACN. The voltammogram presents an irreversible reduction wave at $E_p = 0.2V$. Upon the second scan the cathodic peak is totally suppressed, indicating the progressive blocking of the electroactive surface due to the formation of the nitrophenyl layer onto gold electrode. In figure 4.3b the same electrode was submitted to 5 cyclic voltammetries at scan rate 100 mV/s in water/ethanol solutions (90/10 %V) containing 0.1 M KCl. It is well known that the reduction of nitrophenyl moieties in protic medium occurs through an intermediate reversible step which involves the nitrous/hydroxylamine (NO/NHOH) redox couple, followed by the irreversible amination of the hydroxylamine group [9][10]. According to this mechanism, data presented in figure 4.3b show the anodic peak related

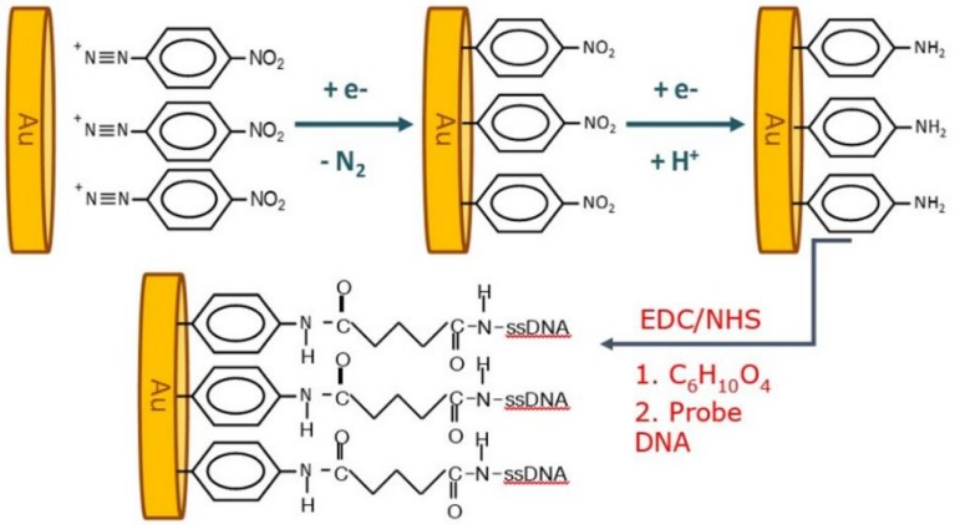

Figure 4.2 – Steps involved in ssDNA immobilization on gold electrodes:

to the intermediate process at about -0.35 V : just a knee is observable in the direct scan, assessing the corresponding reduction, due to its partial overlapping with the irreversible reduction wave, which has its maximum at around -0.9 V. The presence of this signal indicates that nitro-phenyls are immobilized on the electrode.

After an accurate rinse with PBS, electrodes characterization was performed by electrochemical impedance spectroscopy at the open circuit potential (OCP) in solutions containing $Fe(CN)_6^{3-}$ / $Fe(CN)_6^{4-}$ 1 mM in phosphate buffer 0.2 M pH 7: the frequency was varied from 100 kHz down to 0.01 Hz. Figure 4.3d represents the equivalent circuit used to model the impedance spectra.
Figure 4.3c shows the Nyquist plots of the modified electrodes immediately after NBD deposition (black circles), and before and after ssDNA immobilization (red and blue, respectively). According to the mechanism introduced in 2.3.1, binding of adipic acid to amino group and subsequent DNA immobilization decreases the area available for redox processes, thus blocking $Fe(CN)_6^{3-}$/$Fe(CN)_6^{4-}$ electrons transfer to the electrode surface, resulting in an increase of the R_{ct} component of Randles equivalent circuit (figure 4.3d), or rather in the radius of the semicircle in the kinetic controlled process of Nyquist plot.

Sensor fabrication

Sensors were fabricated on a 175μm thick Polyethylene terephthalate (PET) substrate. No particular preparation of the substrate was necessary before the actual fabrication steps, apart from a basic cleaning step performed by a subsequently rinsing with acetone, isopropyl alcohol and deionized water. The floating gate was obtained by photolithograhic patterning of an unique aluminium film, deposited in vacuum ($\sim 10^{-4} Torr$) by thermal evaporation. An hybrid organic/inorganic dielectric was employed, in order to obtain low-voltage operation, which is crucial in biological analysis of samples in

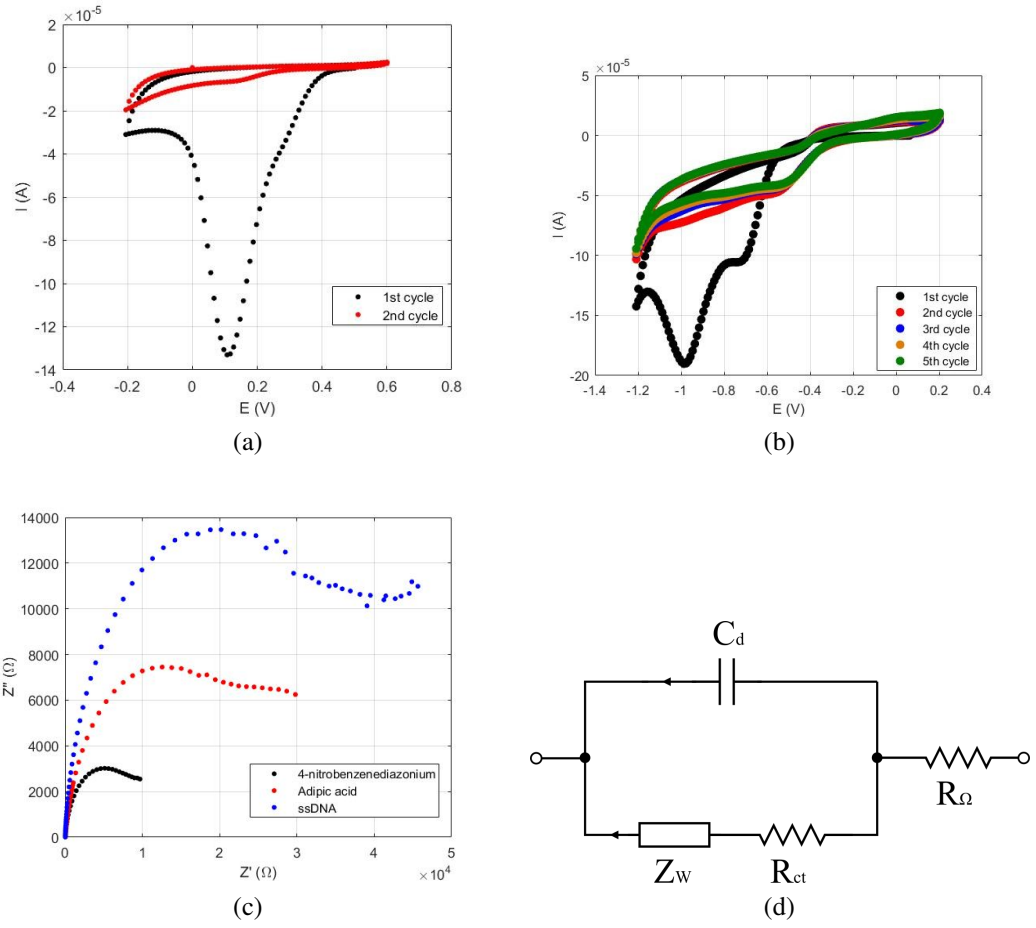

Figure 4.3 – (a) cyclic voltammograms of gold electrode in 2 mM NBD recorded at 100 mV/s in acetonitrile and 0.1 M (TBAPF6); (b) cyclic voltammetric response of gold electrode modified recorded in water/ethanol solutions (90/10%V) containing 0.1 M KCl at a scan rate of 100 mV/s; (c) Nyquist plots for the Faradaic impedance measurements in 1 mM $Fe(CN)_6^{3-}$ / $Fe(CN)_6^{4-}$ and 1 mM in phosphate buffer 0.2 M pH 7; (d) equivalent circuit used for measurements shown in (c).

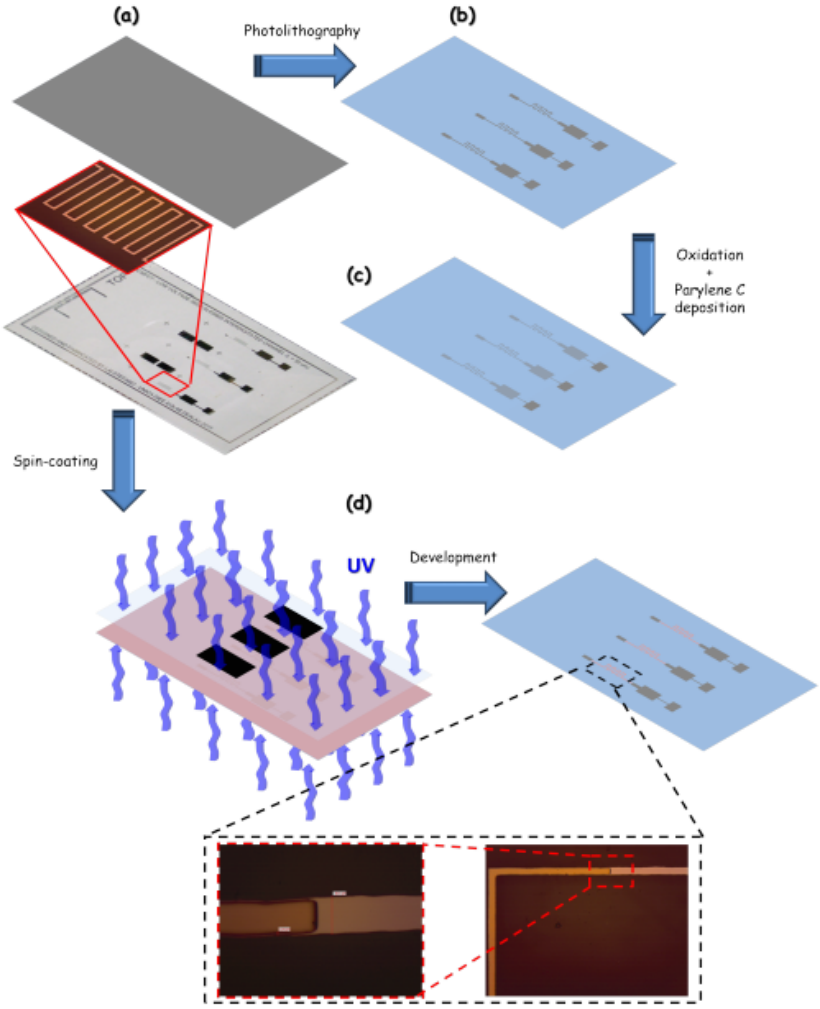

Figure 4.4 – (a)-(b) Definition of the floating gates of the low-voltage, self-aligned OCMFET by means of photolithography; (c) fabrication of the hybrid gate dielectric; in the insert, a detail of the channel area is shown; (d) modified self-alignment process; in the insert, the transition area for the photoresist-covered channel area is shown.

aqueous media [11]. A combination of two ultra-thin insulating films, namely a 6 nm Al_2O_3 film, was grown on the aluminium surface by baking the substrate in an oven for at least twelve hours at 50 °C. Then, a 40 nm thick Parylene C film was deposited by means of chemical vapor deposition process.

The last step for the layout definition is the definition of the source and drain contacts in the transistors' area, of the control capacitor and of the sensing areas. Gold was employed for all these components, as it forms a good interface with p-type organic

semiconductors. In order to considerably reduce parasitic capacitance of the device and improve sensor's sensitivity, as shown in figure 4.4, a self alignment process[12] was employed at this step. A micrometrical, uniform photoresist film was deposited onto the whole substrate by means of spin-coating onto a rotating plate, and then dried into an oven at 45 °C for 45 minutes. In this case, the device was exposed to UV radiation contemporary from both the bottom and top sides, using the floating gate as mask for the radiation coming from the bottom side and a second mask for the one coming from the top side. This mask is simply represented by rectangles covering the channel area in the floating gates. As final result, the residual photoresist was located only in the area of the channel, while the rest of the floating gate remains uncovered. A gold film was then deposited in vacuum ($\sim 10^{-4} Torr$) by thermal evaporation on the whole substrate, comprising the area covered with photoresist. The excess of gold was removed by lift-off, rinsing the surface with acetone to remove the photoresist and the gold layer lying on it. After the lift-off procedure, source and drain electrodes were patterned with a standard photolithographic technique. The device was finally completed by drop-casting the p-type organic semiconductor (TIPS pentacene, 1 wt% in anisole) onto the channels of the OCMFET.

Layout definition

Equation 4.9 highlights sensor sensitivity's dependence on structure capacitance so that, for a fixed charge, the lower the sum of the capacitances, the higher the obtained sensitivity. As a consequence, preliminary considerations have concerned channel area and control capacitor sizing, since their dimensions directly affect the above mentioned capacitances. In particular, since the overlap between drain/source and gate electrodes, L_{ov}, is defined by the employed technology, the control gate capacitor should be minimized in order to increase the sensitivity. Since its role is to properly bias the device, the actual dimensions of such capacitor must be related to the previously mentioned parasitic capacitances. In order to obtain a rough estimation of their amount, the equations in table 4.1 were used. According to morphological and physical characterization of the self-alignment technique, an overlap in the range of $1\mu m$, reproducible along the whole gate border, was considered. A preliminary test inspects the electrical caracteristics of the sensor, considering two different values of the ratio $\alpha = C_{CG}/C_{TOT}$. Such devices

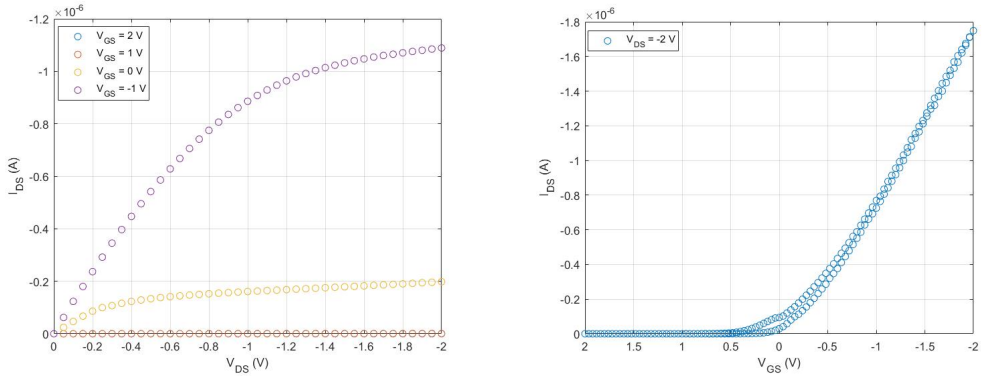

(a) (b)

Figure 4.5 – An example of output (a) and transfer (b) characteristic curves of the OCMFET.

were fabricated defining an interdigitated channel ($W/L = 900$), with a nominal channel length of $L = 20\mu m$.

Electrical characterization of the fabricated devices, was performed by a Keithley 2636 SourceMeter, controlled by means of custom Matlab scripts. Figure 4.5 shows an example of the output and transfer characteristic curves of the device. Data reported in table 4.2 clearly show that a substantial reduction of the control gate's size, with respect to stray capacitances, does not cause a remarkable deterioration in electrical performances. Variations in the mobility values can be ascribed to the deposition of the semiconductor, performed by drop casting, which obviously leads to morphological non-regularity between different transistors.

The diameter of the sensing area was then defined, according to equation 4.1, in order to obtain a nominal sensitivity of 0.3 mV/6 bases, considering a nominal surface coverage for the DNA probes immobilized on the gold surface with the previously described procedure, of $\sim 3 \cdot 10^9$ molecules/cm^2. Aforementioned value was estimated through chronocoulometry measurement conducted by the Department of Mechanical, Chemical and Materials Engineering of the University of Cagliari. The conceived layout, shown in figure 4.6a, allows to perform electrochemical modification of the four sensors at one time, electrically connecting the floating gates through the pad on the right to the potentiostat. In order to disconnect them once the procedure is completed, the substrate must be cut at the specified length. Table 4.3 summarizes the discussed layout

Table 4.2 – Control gate sizing, electrical characterization

α	$V_{TH}[V]$	$\mu[cm^2/Vs]$	$I_{GS}(A)$	$I_{DS,on}(A)$	$I_{DS,off}(A)$
0.93	0.1 ± 0.2	$(3.2 \pm 1) \cdot 10^{-2}$	$(2.3 \pm 2) \cdot 10^{-12}$	$(-1.0 \pm 0.3) \cdot 10^{-6}$	$(-100 \pm 1) \cdot 10^{-12}$
0.83	0.1 ± 0.2	$(2.1 \pm 0.3) \cdot 10^{-2}$	$(11 \pm 8) \cdot 10^{-12}$	$(-1.2 \pm 0.2) \cdot 10^{-6}$	$(-14 \pm 1) \cdot 10^{-9}$

Table 4.3 – Sensor layout

Charge density	Channel Length	Channel width	C_{par}	Control gate area	C_{CG}	Sensing area	Sensitivity
$3 \cdot 10^{9}$ molecules/cm^2	30 μm	2.7 cm	0.3 nF	0.04 cm^2	1.52 nF	0.18 cm^2	290 mV

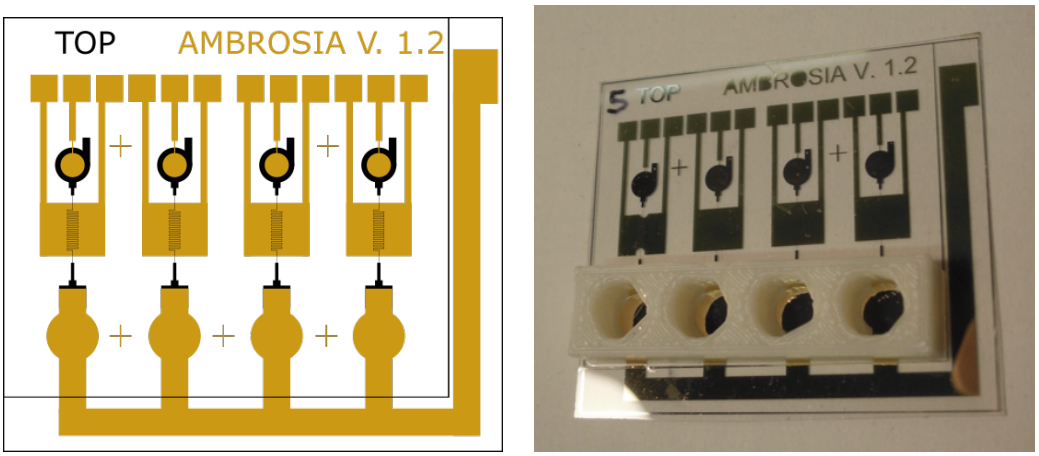

(a) (b)

Figure 4.6 – Implemented layout and sensors' realization.

dimensions.

Finally, incubation chambers necessary to contain the liquid environment for the telomerase reaction, were realized in polylactic acid (PLA) using a Makerbot Replicator 2X 3d printer, and glued to the surface using polydimethylsiloxane (PDMS). PDMS was prepared by mixing the elastomer and the curing agent in a 10:1 proportion, then strewed on the incubation chambers, arranged on the substrate and let dry in oven at 40 ° for 2 hours.

4.3 Device characterization: electrical performances and stability

Previous analyses deeply investigate the relationship between the threshold voltage of the device and the amount of charge immobilized on top of the sensing area. In particular, sensor's sensitivity is related to the threshold voltage of the device, which can be evaluated from the transfer characteristic curves in saturation regime, given by the relationship:

$$I_{DS} = \frac{1}{2}\mu C_{INS}\frac{W}{L}(V_{FG} - V_{TH})^2 \tag{4.10}$$

According to the CMFET working principle, being the source contact connected to the reference voltage, the floating gate voltage can be expressed as follows

$$\begin{aligned} V_{FG} &= \frac{C_{CG}}{C_{TOT}} V_{CG} + \frac{C_{DG}}{C_{TOT}} V_D + \frac{Q_{SENS}}{C_{TOT}} \\ &= \alpha V_{CG} + \beta V_D + \gamma Q_{SENS} \end{aligned} \tag{4.11}$$

Therefore, the square root of equation 4.10 can be rewritten as:

$$\begin{aligned} \sqrt{I_{DS}} &= \sqrt{\frac{1}{2}\mu C_{INS}\frac{W}{L}}\left[\alpha V_{CG} - \left(V_{TH} - \beta V_D - \gamma Q_{SENS}\right)\right] \\ &= k\left(\alpha V_{CG} - V_{THF}\right) \end{aligned} \tag{4.12}$$

where the effective threshold voltage of the transistor was introduced. This last equation is linear in V_{CG} with slope $m = k\alpha$ and intercept $q = kV_{THF}$. Consequently,threshold voltage and mobility can be obtained as:

$$V_{TH} = -\alpha\frac{q}{m} \tag{4.13}$$

$$\mu = \frac{2 \cdot L \cdot m^2}{W \cdot C_{INS} \cdot \alpha^2} \tag{4.14}$$

Packaging and connections

Since the sensing areas have to be completely immersed in an electrochemical cell (figure 4.8a), in order to allow probes immobilization to the gold substrate, and the information about the sensed reaction is stored as charge distribution in the floating gate, a proper protection of the devices against improper handling, accidental squirt during the modification, or environmental interference is mandatory. In order to limit as much as possible these problems, a packaging procedure was determined: sensing areas were firsly covered with a glass slide, in order to guarantee that their surface remain shielded from the insulating procedure, thus leaving the gold surface untouched. Then, the device was covered with a 2 μm thick Parylene C layer in order to passivate the whole device. Finally, the device was capped using CYTOP^{TM}, deposited by spin coating. Measurements performed on a set of 9 devices, shown that the interaction of Parylene C layer with the semiconductor produces several effects, (4.7a), such as a decrease of

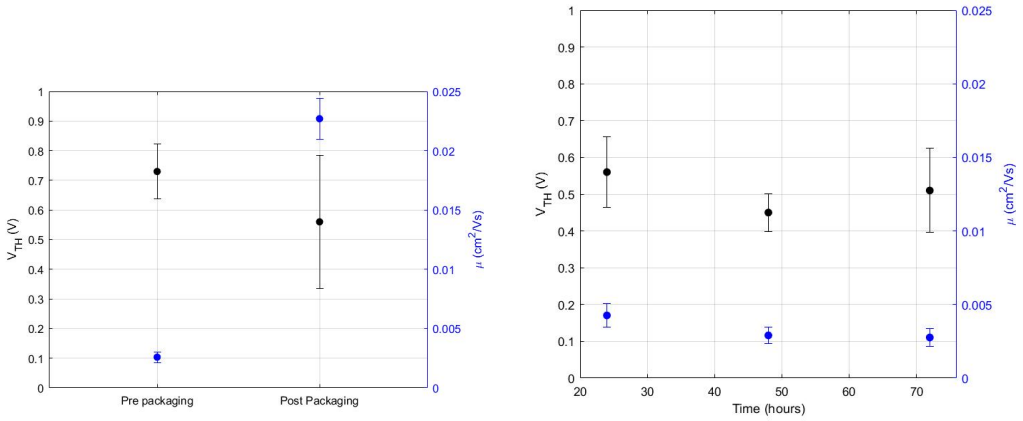

(a) (b)

Figure 4.7 – Threshold voltage and mobility variations (a) before and after the packaging procedure and (b) over time, after packaging.

the threshold voltage and semiconductor's mobility. Nevertheless, figure 4.7b shows that such variations were progressively and partially absorbed in a few days, as regards mobility, while remain constant with regards to the threshold voltage. Consequently, the device would not be employed for sensing during this period.

Finally, the packaging was completed by sticking a black tape onto the area of the transistor in order to prevent the photogeneration of charge carriers, that could determine a threshold voltage shift if the light condition changed during measurements. Devices were then measured on a custom support fabricated in Acrylonitrile butadiene styrene (ABS) using a Makerbot Replicator 2X 3d printer, and electrically contacted through contact spring connectors (figure 4.8b).

Probes immobilization: electrical tests

After the packaging procedure and the relaxation time necessary to let be the effect of such procedure absorbed, the device underwent to the electrochemical functionalization procedure previously described. Gold sensing areas were electrically connected to the potentiostat using the pad showed in figure 4.6a. Then, the substrate was cut at the location specified in the same picture. As the electrochemical modification apply a voltage to the floating gate, devices were compared. Figure 4.9a shows an example of the

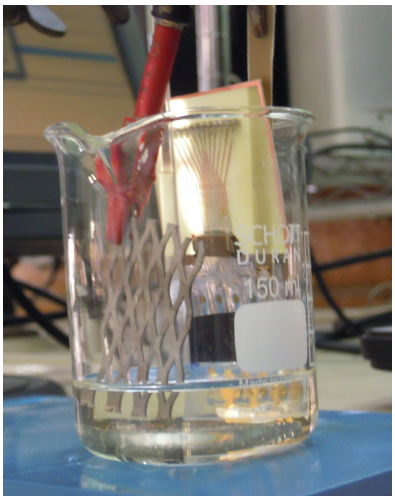

(a) A device immersed in an electrochemical cell.

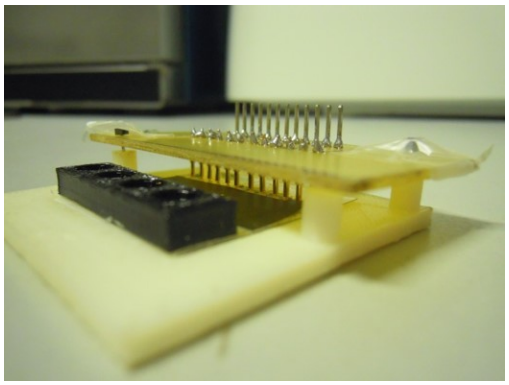

(b) A completed device.

Figure 4.8

transfer curve of a device, before the procedure and after the bind of adipic acid. Since the floating gate was electrically connected to the potentiostat and the voltage needed to perform cyclic voltammetries was directly applied to it, such variation can not be directly ascribed to the functionalization with the adipic acid.

Finally, sensor's response was evaluated in terms of output current stability with respect to reagents delivery, in real-time measurement. In fact, beyond others non-ideal effects which may occur during relatively long time operation of OTFTs, the delivery of liquid in the incubation chamber, could produce artifacts difficult to discriminate from the reaction under investigation. The experiment was led on two different sensors configuration: a device functionalized with the same procedure described in previous implementation of the sensor [13] was employed as a reference for the evaluation of the device functionalized as described in section 4.2.1. The former immobilization procedure require a preliminary accurate cleaning of the surface with sodium hypochlorite ($NaClO$): a 5% Cl active solution of $NaClO$ in water was spotted onto the sensing area and let acting for ten minutes. The sensing areas were then rinsed with measurement solution (50 mM phosphate buffer solution, 50 mM sodium chloride). A solution containing 100 nM of HS-ssDNA probes, diluted in a 1 M KH_2PO_4 buffer solution, were spotted onto the sensing areas. After 90 minutes, a small volume of 1 mM solution of 6-mercapto-1-hexanol was spotted onto the sensing areas, in order to avoid a too dense packing of the

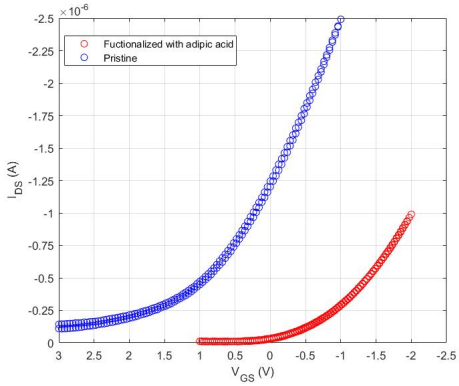

(a) Example of transfer characteristic of a device recorded before (blue circles) and after (red circles) surface modifications.

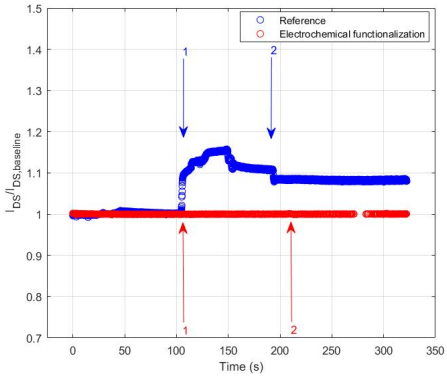

(b) Output current measurements of a sensor with DNA molecules immobilized on top, through a SAM as described in [13] (blue circles) and the electrochemical procedure described in section 4.2.1 (red circles).

Figure 4.9

probes on the surface and prevent their folding. The device was finally stored for 15 hours in order to allow a complete ordering of the probes.

After probes immobilization, sensing areas were accurately rinsed and finally filled with 60 μL of measurement buffer solution. Since the organic semiconductor is sensitive to temperature variations, devices modified with the electrochemical procedure were allowed to stand for 2 hours at room temperature. Measurement were performed applying a pulsed gate signal ($V_{CG,OFF}$ = 0 V, $V_{CG,ON}$ = 1.5 V, f = 50 Hz, duty cycle = 20 %) and a constant drain-source voltage (V_{DS} = - 2V). In this way, the transistor was alternatively set in underthreshold and overthreshold conditions, thus reducing the actual time in which the device is turned on. Such measurement setup is particularly beneficial in order to reduce the progressive charge trapping at the insulator/semiconductor interface (bias stress), due to the continuous operation of the transistor, which consequently determine a threshold voltage shift and a reduction of the OTFT output current. Measurement results are shown in figure 4.9b. Output current was normalized with respect to its baseline value ($I_{DS,baseline}$), and each sensor underwent to the delivery of 2 μL of measurement buffer solution. The reference sensor exhibited a significant variation of the output current, which is only partially reabsorbed over time and could mask the current variations related to the reaction under investigation.

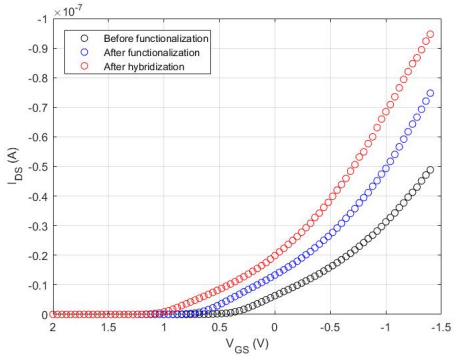

(a) OCMFET transfer curves shift related to the functionalization and hybridization process.

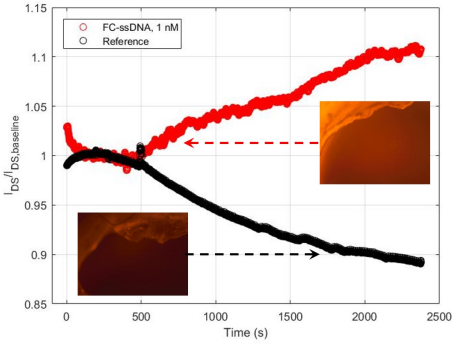

(b) Real-time measurement of the output current of a sensor, and the related reference, during the hybridization process.

Figure 4.10 – Preliminary DNA hybridization tests.

4.4 Sensor validation: DNA hybridization detection

The proper operation of the device was validated by means of DNA hybridization detection. Sensor's response was therefore evaluated before and after functionalization and hybridization. As previously discussed, since the electrochemical procedure requires a direct connection to the floating gate of the device, thus impeding to evaluate a variation of the immobilized charge before and after the whole procedure, the threshold voltage of the device was firstly measured after the grafting of adipic-acid to the amino-groups. Since the semiconductor is sensitive to temperature variations, the device was let stabilize for 2 hours at room temperature. After an accurate rinse with measurement buffer solution, was then characterized as described in section 4.3, then single-stranded DNA probes (ssDNA) $[NH_2 - 5' - (A)_{18}TTAGGGTTAGGG - 3']$ (P0), were immobilized on top of the sensing area. After functionalization, the device was subsequently characterized and then a first hybridization test was carried out: 2 μL of hybridization buffer (TE 1 M NaCl buffer) containing 1 nM of fully-complementary ssDNA (FC-ssDNA) were spotted on the sensing area. After 1 hour at ambient temperature, the sensing area was then accurately rinsed with measurement buffer and a third transfer characteristic was acquired. According to the discussed working principle, as shown in figure 4.10a, a shift of the transfer characteristic curves was measured both after functionalization and hybridization, with two subsequent increases of the output current of the device.

Usually, direct readout of the output current is more attractive than the transfer curve shift, as it allows to precisely evaluate the reaction time, which is not possible in static measurements. Therefore, a real-time measurement of the hybridization process was carried out. The device was biased with a pulsed gate potential as previously discussed and, after current stabilization, 2 μL of hybridization buffer containing 1 nM of FC-ssDNA target sequences was spotted on the sensing area. Figure 4.10b shows the recorded output current of two OCMFET: sensor's output current was compared to the response of an another identical device in which 2 μL of hybridization buffer were delivered. Clearly, such a device does not show a response to the hybridization and the decrease of the output current was ascribed to non-specific interaction of free-ions present in solution, combined with residual bias-stress effect in the organic semiconductor. The actual hybridization was also verified by means of fluorescence analysis, by employing FC-ssDNA marked with Cy-3 fluorescent dyes. As reported in the inserts of 4.10b, the immobilization of the target sequences after hybridization is distinguishable from the back-scattering light coming from the bare gold surface.

4.5 Towards telomerase activity detection: DNA length measurement

In order to verify the effective ability of the sensor to discriminate among DNA strands of different length, and thus be able to directly measure telomerase activity in terms of telomeres elongation, a further preliminary test was carried out. In fact, since the surface potential generated from the immobilized charges is not a linear function of their actual distance from the metal, even if the capability of the CMFET to operate beyond the Debye length was already demonstrated, the actual possibility to perform such a measurement must be verified. Theoretically, the length between two adjacent bases in double-strand DNA (dsDNA) is about 0.34 nm; since telomerase can add multiple of a six nucleotides-repeating sequence, the distances between the surface and the charge is estimated to increase as a multiple of 2.04 nm. Furthermore, the telomerase usually require relatively high ionic concentration in the measurement solution, which leads to an estimated Debye length of few nm. Providing an analytical explanation of the phenomena which take place at the surface of such a structure is beyond the aim of this

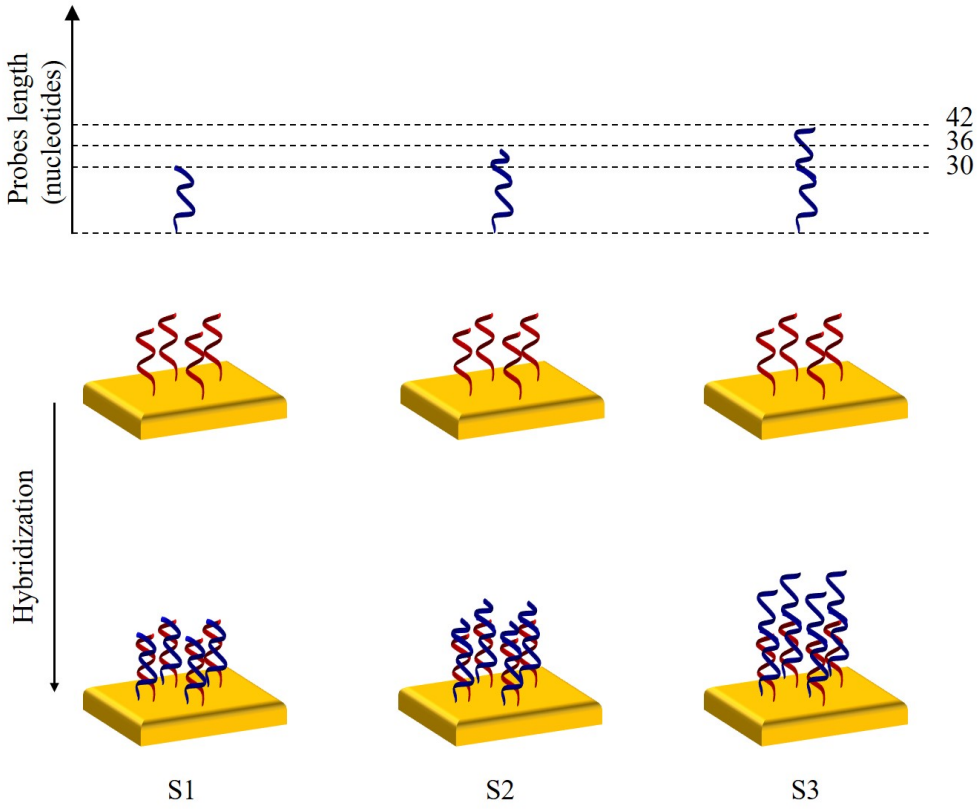

Figure 4.11 – Schematic representation of the setup employed to perform DNA length measurement: after probes immobilization, their hybridization with complementary nucleotides with an overhang of 0 (S1), 6 (S2) and 12 (S3) oligonucleotides was evaluated.

thesis and, furthermore, a precise study of this last point is actually hindered by the working principle of the structure, which would be perturbed from the presence of an external monitoring system such as an external electrode immersed in solution.

Therefore, in order to evaluate the feasibility of the approach, the setup schematically depicted in 4.11 was employed: after probes (P_0) immobilization ($NH_2 - 5' - (A)_{18}TTAGGGTTAGGG - 3'$), their response to different dsDNA lengths was evaluated by means of three different ssDNA target oligonucleotides, having different length. In particular, target sequences having a complementary structure ($5' - [CCCTAA]_{n+2}(T)_{18} - 3'$) ($T_{30}$) with an overhang of 6 (T_{36}) or 12 (T_{42}) nucleotides were employed. After functionalization, each device was characterized accordingly to the procedure described for the DNA hybridization test, and then 2 μL of hybridization buffer (TE 1 M NaCl buffer) containing 1 nM of one of the target sequences reported in table 4.4 were spotted on the

Table 4.4 – DNA sequences employed in DNA length measurement.

Label	Sequence
P_0	$NH_2 - 5' - (A)_{18}TTAGGGTTAGGG - 3'$
T_{30}	$5' - CCCTAACCCTAA(T)_{18} - 3'$
T_{36}	$5' - CCCTAACCCTAACCCTAA(T)_{18} - 3'$
T_{42}	$5' - CCCTAACCCTAACCCTAACCCTAA(T)_{18} - 3'$

sensing area. Each device was let stabilize for 1 hour, then accurately rinsed before a subsequent transfer curve acquisition.

Threshold voltage shift subsequent to functionalization and hybridization process, were then evaluated using 3 sensors for each target sequence employed and shown in table 4.4. The charge related to the probes ($NH_2 - 5' - (A)_{18}TTAGGGTTAGGG - 3'$) anchored in the functionalization process can be obtained subtracting the threshold voltage measured after adipic-acid grafting ($V_{TH,before-func}$) from the same parameter evaluated after probes immobilization ($V_{TH,after-func}$):

$$\begin{aligned}\Delta V_{TH,func} &= V_{TH,after-func} - V_{TH,before-func} \\ &= \left[V_{TH} - \beta V_D - \gamma\left(Q_{DNA,func} + Q_0\right)\right] - \left(V_{TH} - \beta V_D - \gamma Q_0\right) \\ &= -\gamma Q_{DNA,func}\end{aligned} \tag{4.15}$$

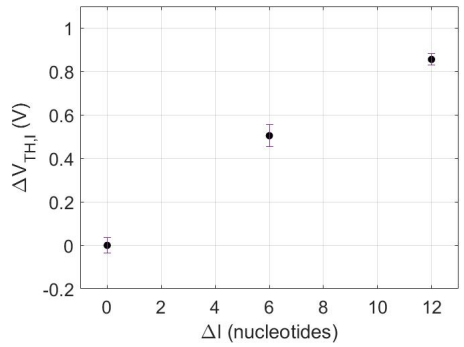

Figure 4.12 – OCMFET response to DNA length variation.

Similarly, the charge immobilized during the hybridization process can be obtained as:

$$\begin{aligned}\Delta V_{TH,hyb} &= V_{TH,after-hyb} - V_{TH,after-func} \\ &= \left[V_{TH} - \beta V_D - \gamma\left(Q_{DNA,hyb} + Q_{DNA,func} + Q_0\right)\right] \\ &- \left[V_{TH} - \beta V_D - \gamma\left(Q_{DNA,func} - Q_0\right)\right] \\ &= -\gamma Q_{DNA,hyb}\end{aligned} \tag{4.16}$$

As a consequence, the contribution of DNA length variations to the threshold voltage shift can be evaluated combining equation 4.16 and 4.1:

$$\begin{aligned}\Delta V_{TH,l} &= \Delta V_{TH,n} - \Delta V_{TH,30} \\ &= -\gamma\left(Q_{DNA,hyb\_n} - Q_{DNA,hyb\_30}\right)\end{aligned} \tag{4.17}$$

where Q_{DNA,hyb_n} represent the charge immobilized after the hybridization of the generic target sequence having length n and Q_{DNA,hyb_30} the one related to the hybridization of sequence T_{30}. Figure 4.12 shows the results of the aforementioned experiment. Each point has been calculated as the average threshold voltage of at least three independent OCMFET. A clear dependence of the threshold voltage shift respect to the oligonucleotides length, which should allow to directly monitor telomerase activity detection.

4.6 Telomerase activity detection

The device was finally tested for telomerase activity detection. In particular, as previously shown for DNA hybridization tests, the investigation was carried out monitoring the output current of the transistor, since such operating condition allows for a precise observation of the occurring reaction. Experiments have been carried out using DNA probes complementary to the active site of the enzyme (*TTAGGG*), immobilized to the gold surface through the previously discussed procedure, at their $5'-$end. As telomerase is a relatively large protein, steric hindrance of the molecules could impede its binding to the immobilized probes. In fact, it has been demonstrated that a 3'- overhang smaller than 6 nucleotides inactivate telomerase, while an overhang of 8 nucleotides or longer is a preferred substrate for telomerase with improved activity and processivity [14]. To avoid

this issue, a sequence of 18 adenines is used to distance the telomeres sequence from the gold surface, preventing the formation of tertiary structures typical in nucleic acids sequences that are rich in guanine, and a telomeric substrate made of 2 repetitions of telomere base sequence was employed: $5'-(A)_{18}(TTAGGG)_2-3'$. A peltier module was installed under the sensing area of devices, in order to maintain a temperature of 37 °C, as it was demonstrated that the catalytic activity of human telomeratse significantly increases in this condition [15]. Incubation chamber were filled with 60 μL of solution (10 mM Tris-HCl buffer, pH 8.3, 10 mM $MgCl_2$, 1.5 mM KCl, 1 mM $EGTA$). Telomerase extracts from 10000 cells were employed from the experiments [2]. Figure 4.13a shows the output current measured as a function of time of an OCMFET (red curve), after the delivery of 1μL of solution containing 1500 ng of telomerase extracts and 1μL containing a 1 mM mixture all four dNTPs (dATP, dGTP, dUTP and dCTP). As a p-type semiconductor was employed, the output current increase is consistent with the substrate primer elongation. In order to validate such an hypothesis, two different references were employed: a telomerase extract containing 1500 ng of telomerase was used to estimate sensor's response to the enzyme. As the net charge on a protein is zero at the isoelectric point (pI), positive at pHs below the pI, and negative at pHs above the pI, since telomerase is positively charged at physiological pH (pI $\sim$ 10)[16], its binding with immobilized probes produce a decrease in the device's output current, according to the previously described model. In addition, in order to evaluate possible non-specific contribution of dNTPs, a heat-denatured (100 °C for 10 min) telomerase extract, was used. The actual sensor's response was then estimated comparing sensor output current variations with such a reference.

Finally, in order to further discriminate various contribution to the output current variation, each component required for telomerase activity was delivered at different time. Figure 4.13b shows an example of such an experiment: according to the previous discussion, the output current decreases after the introduction of 1μL of solution containing 1500 ng of telomerase extracts (1). On the contrary, after the introduction of 1μL containing a 1 mM mixture all four dNTPs (2), an output current increase related to telomeres elongation was recorded.

[2]The author gratefully acknowledge Dr. Sofia Francia (Istituto di Genetica Molecolare, Consiglio Nazionale delle Ricerche) for telomerase extract preparation and helpful discussion regarding the biological component of the experimental setup

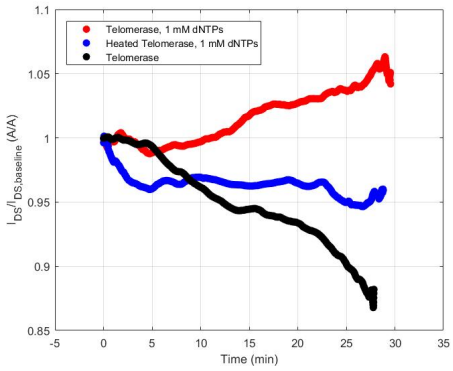

(a) OCMFET output current variations after the introduction of 1500 ng of telomerase (black curve), heat-denatured telomerase with 1 mM dNTPs (blue curve) and 1500 ng of telomerase with 1 mM dNTPs (red curve).

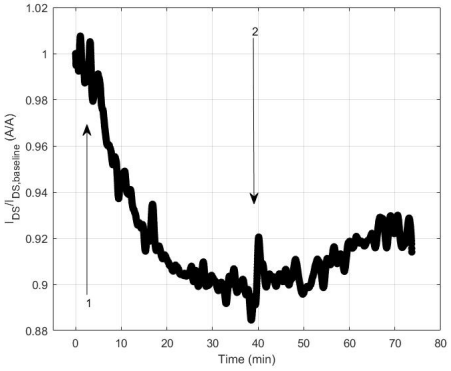

(b) Recorded output current of an OCMFET after the introduction of telomerase (1) and 1 mM of a mixture of all four dNTPs (2).

Figure 4.13

Figure 4.14 shows the obtained results in terms of percentage variation of the baseline current, with respect to the introduction of the enzyme and to the enzyme and dNTPs. Three devices per experiment were measured waiting 30 minutes after samples delivery. A behaviour coherent with the proposed model was obtained, with a good reproducibility, allowing to correctly follow the enzyme reaction over time using a cell extract without the need for sample purification, nor filtration.

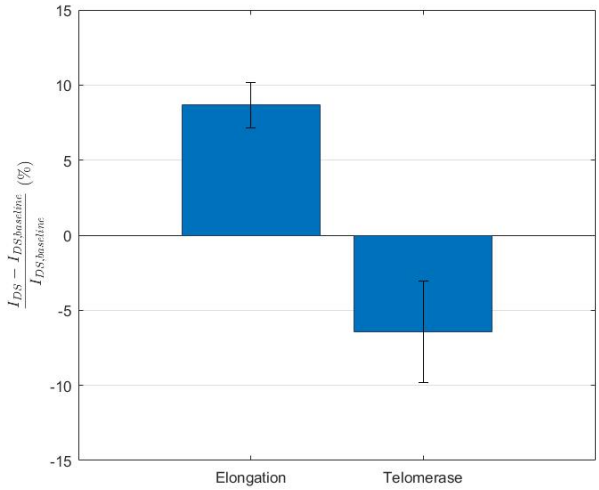

Figure 4.14 – Percentage of output current variation, measured after the delivery of 1500 ng of telomerase extracts and of 1500 ng of telomerase extracts and 1 mM of a mixture of dNTPs.

Bibliography

[1] A. Poghossian, A. Cherstvy, S. Ingebrandt, A. Offenhäusser, and M. J. Schöning, "Possibilities and limitations of label-free detection of DNA hybridization with field-effect-based devices," in *Sensors and Actuators, B: Chemical*, vol. 111-112, pp. 470–480, 2005.

[2] N. T. Flynn, T. N. T. Tran, M. J. Cima, and R. Langer, "Long-term stability of self-assembled monolayers in biological media," *Langmuir*, vol. 19, no. 26, pp. 10909–10915, 2003.

[3] O. Seitz, P. G. Fernandes, R. Tian, N. Karnik, H.-C. Wen, H. Stiegler, R. a. Chapman, E. M. Vogel, and Y. J. Chabal, "Control and stability of self-assembled monolayers under biosensing conditions," *Journal of Materials Chemistry*, vol. 21, no. 12, p. 4384, 2011.

[4] E. Delamarche and B. Michel, "Structure and stability of self-assembled monolayers," *Thin Solid Films*, vol. 273, no. 1-2, pp. 54–60, 1996.

[5] J. C. Love, L. A. Estroff, J. K. Kriebel, R. G. Nuzzo, and G. M. Whitesides, "Self-assembled monolayers of thiolates on metals as a form of nanotechnology," 2005.

[6] M. Delamar, R. Hitmi, J. Pinson, and J. Savéant, "Covalent Modification of Carbon Surfaces by Grafting of Functionalized Aryl Radicals Produced from Electrochemical Reduction of Diazonium Salts," *Journal of the American Chemical Society*, vol. 114, no. 14, pp. 5883–5884, 1992.

[7] A. Vacca, M. Mascia, S. Rizzardini, S. Palmas, and L. Mais, "Coating of gold substrates with polyaniline through electrografting of aryl diazonium salts," *Electrochimica Acta*, vol. 126, pp. 81–89, 2014.

[8] L. V. Hai, S. Reisberg, A. Chevillot-Biraud, V. Noel, M. C. Pham, and B. Piro, "Simultaneous electroreduction of different diazonium salts for direct electrochemical DNA biosensor development," *Electrochimica Acta*, vol. 140, pp. 49–58, 2014.

[9] B. Ortiz, C. Saby, G. Y. Champagne, and D. Bélanger, "Electrochemical modification of a carbon electrode using aromatic diazonium salts. 2. Electrochemistry

of 4-nitrophenyl modified glassy carbon electrodes in aqueous media," *Journal of Electroanalytical Chemistry*, vol. 455, no. 1âĂŞ2, pp. 75–81, 1998.

[10] W. Richard, D. Evrard, and P. Gros, "New insight into 4-nitrobenzene diazonium reduction process: Evidence for a grafting step distinct from NO2 electrochemical reactivity," *Journal of Electroanalytical Chemistry*, vol. 685, pp. 109–115, 2012.

[11] H. U. Khan, M. E. Roberts, O. Johnson, R. Förch, W. Knoll, and Z. Bao, "In situ, label-free DNA detection using organic transistor sensors," *Advanced Materials*, vol. 22, no. 40, pp. 4452–4456, 2010.

[12] S. Lai, P. Cosseddu, G. C. Gazzadi, M. Barbaro, and A. Bonfiglio, "Towards high frequency performances of ultra-low voltage OTFTs: Combining self-alignment and hybrid, nanosized dielectrics," *Organic Electronics: physics, materials, applications*, vol. 14, no. 3, pp. 754–761, 2013.

[13] "Ultralow voltage, OTFT-based sensor for label-free DNA detection," *Advanced Materials*, vol. 25, no. 1, pp. 103–107, 2013.

[14] M. Lei, A. J. Zaug, E. R. Podell, and T. R. Cech, "Switching human telomerase on and off with hPOT1 protein in vitro," *Journal of Biological Chemistry*, vol. 280, no. 21, pp. 20449–20456, 2005.

[15] D. Sun, C. C. Lopez-Guajardo, J. Quada, L. H. Hurley, and D. D. Von Hoff, "Regulation of catalytic activity and processivity of human telomerase," *Biochemistry*, vol. 38, no. 13, pp. 4037–4044, 1999.

[16] N. Kim, M. Piatyszek, K. Prowse, C. Harley, M. West, P. Ho, G. Coviello, W. Wright, S. Weinrich, and J. Shay, "Specific association of human telomerase activity with immortal cells and cancer," *Science*, vol. 266, no. 5193, pp. 10114–10118, 1994.

5 A CMOS Lab-on-Chip for telomerase activity detection

In this chapter, a CMFET-based Lab-on-Chip for telomerase activity detection is presented. Either sensing unit design and readout circuitry issues will be addressed, as well as accessory functionalities. Electrical post-layout simulations, using a custom model of the sensor, will be presented.

Contents

In the previous chapter, the employment of CMFET sensors for telomerase activity detection was profusely discussed. In particular, the organic implementation was examined, in order to fabricate a cost-effectiveness disposable sensors. The obtained results allow both to precisely detect DNA strands of different length, and to accurately detect either the presence of the enzyme and its activity. Apart from technological aspects, which offer different interesting features in bio-related applications, organic electronics allows a widespread and capillary diffusion because of the low-cost fabrication process. However, cost-effectiveness of organic electronics is actually achieved for technological processes avoiding large scale of integration, which is a peculiar feature for the development of high-parallel sensing platforms conceived for laboratory environment. Taking advantage of the possibility of exploiting the CMFET approach in CMOS technology, and taking into consideration the outcomes of the experimental results achieved with the organic implementation of the sensor, as a conclusion of this work a fully CMOS Lab-on-Chip for telomerase activity detection in a 0.18 μ m standard CMOS process was developed [1]. The block diagram in figure 5.1 summarizes the implemented functionality.

The exploitation of the CMFET approach into a solid-state Lab-on-a-Chip would pave the way to several additional or complementary advantages with respect to the organic implementation, in terms of functionality and sensing performances. In particular, in order to improve the signal-to-noise ratio and extend the sensitivity range, each sensing element was designed using a floating gate NMOS-PMOS pair. Readout circuitry for signal conditioning, amplification and A/D conversion was directly integrated on the chip in order to realize a standalone device, capable to perform a whole measure without the need for any external instrumentation. In this perspective, a control over temperature was achieved by temperature sensors and heating elements embedded in the chip.

5.1 Sensing unit

As already pointed out, the reduction of parasitic capacitances plays a crucial role in enhancing the sensitivity of the CMFET sensor. In fact, as already profusely discussed,

[1] Such activity was carried out in collaboration with S. Sonedda, who particularly worked at the layout of functional blocks and to the design of the level shifter schematic.

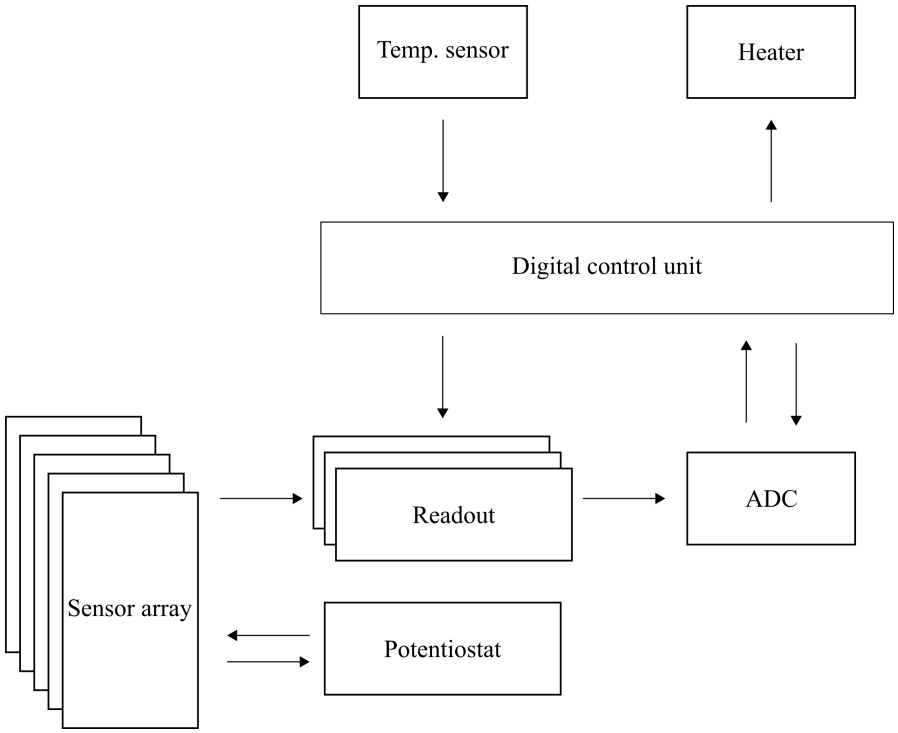

Figure 5.1 – Schematic representation of LoC functional blocks.

the basic sensitivity of the device is related to the capacitors in the layout:

$$\Delta V_{THF} \approx V_{TH} - \frac{Q_0 + Q_{DNA}}{C_{TOT}} \tag{5.1}$$

In contrast to the previously discussed implementation (cfr. section 4.2.3), in order to estimate the parasitic capacitances of the device the capacitive coupling between the floating gate and the silicon body (C_{FG}) has to be considered. In fact, the sum of the whole capacitance of the device is depicted in figure 5.2 and can be expressed as follows:

$$C_{TOT} = C_{SF} + C_{DF} + C_{FG} + C_{CG} \tag{5.2}$$

where the parasitic capacitor between the floating gate and body was explicitly divided in three terms: $C_{FB,P}$, $C_{FB,N}$ are stray contributions related to the coupling of the NMOS-PMOS pair with the silicon body, whereas C_{PAD} is the parasitic capacitance due to the coupling of the sensing pad and body, and represents the most important contribution to

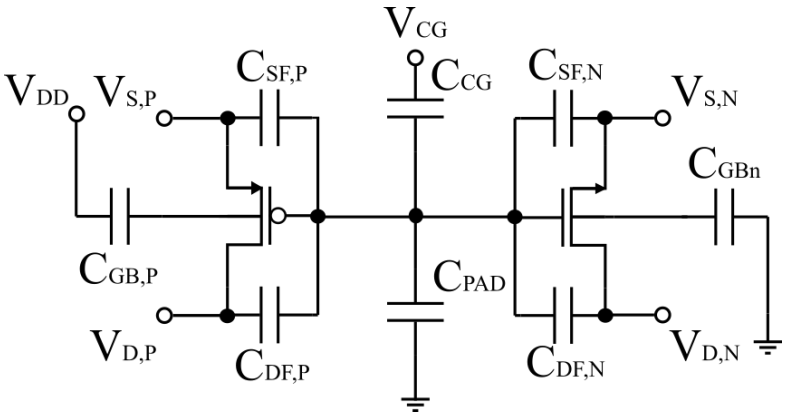

Figure 5.2 – Equivalent circuit of the CMFET sensor's capacitances.

C_{FB}.

Figure 5.3a depicts a cross section of the first CMFET structure implemented. Such a layout was originally reported in [1], and in the following will be referred to as "*planar*". Sensor's aspect ratio (W/L) was defined in order to minimize both the mismatch between sensors and the stray capacitances related to the MOS structure. Finally, the size of the control gate was accordingly defined. In order to further improve sensor's performances, according to layout design considerations thoroughly addressed in the previous chapter, a novel implementation of the sensing unit was considered. Figure 5.3b shows a schematic cross section of the proposed structure *Circuit Under Pad* (CUP) structure: such an implementation exploits the possibility to overlap part of the circuitry with the sensing area, thus leading to a reduction of the capacitive coupling of the floating gate with body. Such a possibility, not only reduce the main contribution to C_{TOT}, which is related to C_{PAD}, but achieve a significant reduction of the area consumption as well.

Figure 5.4a shows the schematic of a pixel of the array, containing an NMOS-PMOS pair: custom-built components, modeling a transistor with a charge-modulated threshold voltage, were employed. The layout design was performed with the Virtuoso Analog Environment, and schematically depicted in figure 5.3, for both structures. Because of its higher capacitive coupling for a given area, the control capacitor (C_{CG}) was realized with a double sandwich capacitor, which make use of three different levels of metal. Finally, the sensing area was designed with a pad opening in the SiO_2 passivation, that allows to access a 3 μm metal.

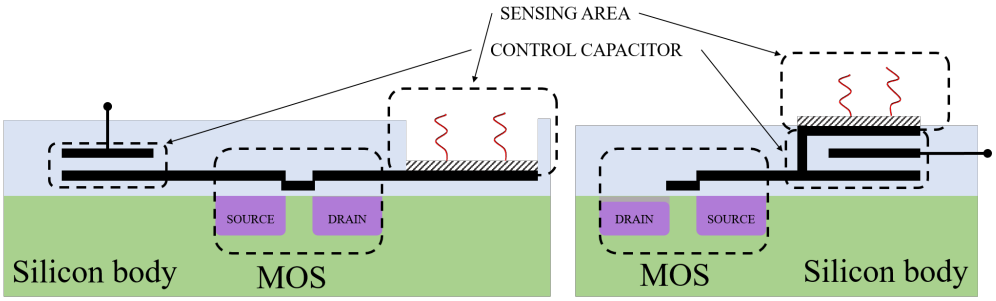

(a) (b)

Figure 5.3 – Schematic cross section of the employed layout: (a) planar implementation, as originally reported in Barbaro *et al* [1] and (b) new layout employing a circuit under pad structure.

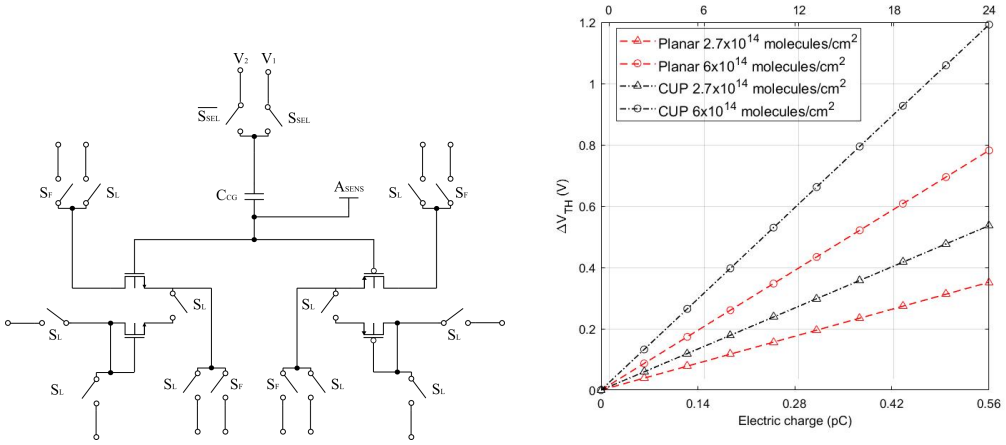

(a) (b)

Figure 5.4 – (a): electrical scheme of the sensing unit and (b) electrical simulation of the sensing unit threshold voltage variation, performed employing a custom-built component implementing 5.3.

As the sensing unit is highly sensitive to parasitics, such values were quantified by means of post-layout simulations using Spectre Circuit Simulator, and are summarized in table 5.1.

In order to perform electrical simulation shown in figure 5.4b, the charge which induces a threshold voltage shift on the device was expressed as follows:

$$Q = \sigma_{DNA} \cdot n_{bases} \cdot q \cdot A_{SENS} \tag{5.3}$$

Table 5.1 – CMFET parasitic capacitances summary.

	C_{MOS}	C_{PAD}	C_{CG}	α
Planar	0.24 pf	70 fF	3.96 pF	0.92
CUP	0.24 pf	1 fF	2.76 pF	0.92

where, σ_{DNA} is the probes density per unit area, n_{bases} is the length of the DNA strand expressed in number of nucleotides, q the electron charge, and A_{SENS} is the sensing area surface. According with the results obtained in previous implementation of CMFET chip [2], a surface density of $\sim 10^{14}$ molecules/m^2 was considered.

According to the results reported in figure 5.4b, the CUP structure achieves an increased sensitivity of 30% with respect to its planar counterpart. Furthermore, sensor's sensitivity is obviously greatly affected by surface density variations: a threshold voltage variation of 137 mV/6 nucleotides in a worst case scenario of 10^{14} molecules/m^2 was achieved with the CUP structure. On the other hand, a threshold voltage variation of more than 1 V should be expected, as a consequence of the functionalization procedure.

5.2 Readout and interfacing circuitry

The large threshold voltage variation related to the functionalization of the sensing unit, should largely affect the device operating point and, therefore, the operation of the readout circuitries. To mitigate such an issue, both the aforementioned were implemented in the chip, in order to achieve different sensitivity values. Furthermore, several conditioning and readout scheme were designed, in order to face such a problem. In fact, the on-chip addressing circuitry allows to independently select a DNA sensor from the array, selecting one of three different readout schemes.

Readout circuit: level-shifter

The first readout circuit implemented is depicted in figure 5.5 for an NMOS sensor. A complementary configuration was employed for the PMOS transistor.

The circuit is biased with two currents I_1 and I_2 and a programmable input voltage

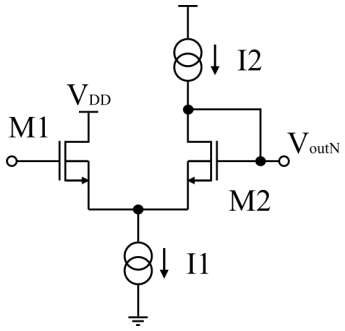

Figure 5.5 – Readout circuit: level shifter.

applied to the gate of the NMOS transistor of the sensing unit, M1. The output V_{outN} is the drain voltage of a diode-connected NMOS transistor, M2, which is paired (and matched) to the NMOS transistor of the sensor selected from the array. The two currents I_1 and I_2 are generated by means of two current mirrors, whereas the control gate of the sensor is driven by an external voltage. The output voltage V_{outN} can be written as:

$$V_{outN} = V_{FG} - \Delta V_{TH} + k\left(\sqrt{(I_2)} - \sqrt{(I_1 - I_2)}\right) \tag{5.4}$$

where $k = \sqrt{\frac{2}{\mu_n C_{OX} W/L}}$ is a constant, dependent on process and design parameters, while V_{FG} is the floating gate voltage, which can be estimated using the relationship:

$$V_{FG} = \frac{C_{CG}}{C_{TOT}} V_{CG} \tag{5.5}$$

Equivalent calculations, made for the PMOS complementary circuit, lead to the relationship:

$$V_{outP} = V_{FG} + \Delta|V_{TH}| + k\left(\sqrt{(I_2)} - \sqrt{(I_1 - I_2)}\right) \tag{5.6}$$

Finally, as the two current mirrors are designed so that $I_1/I_2 = 2$, both V_{out} expressions can be simplified as follows:

$$V_{outN} = V_{FG} + (|V_{THF}| - |V_{TH}|) \tag{5.7}$$

$$V_{outP} = V_{FG} - (V_{THF} - V_{TH}) \tag{5.8}$$

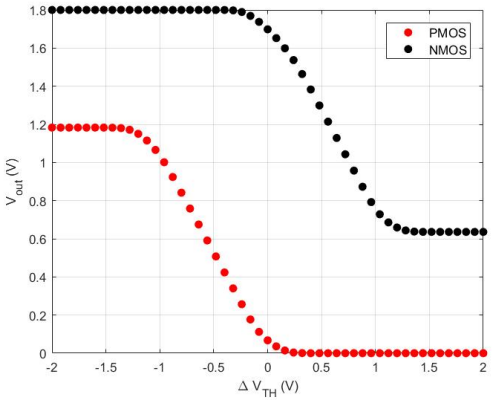

Figure 5.6 – Level shifter output voltage for both NMOS and PMOS transistor.

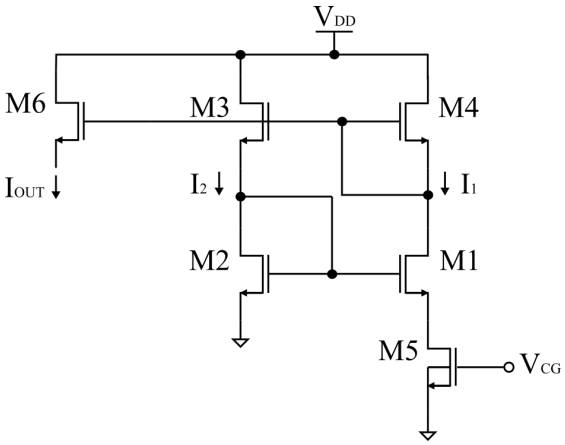

Figure 5.7 – Electrical scheme of the readout circuit with current output.

thus allowing to directly measure the threshold voltage variation of the sensor.

Figure 5.6 shows the simulations results of the proposed circuit, for a PMOS and an NMOS transistors, both belonging to a CMFET sensing unit designed as previously discussed.

Readout circuit: current output

An alternative readout circuit is shown in figure 5.7 for the NMOS transistor of the sensor pair. Obviously, the complementary circuit can be employed for the PMOS transistor.

In such a scheme the NMOS transistor of the sensing unit, M5, is biased in its linear operating region and acts as a variable resistor, as well as in a β multiplier reference

circuit. The transistors M3 and M4 mirror the current in order to enforces equality of M1 and M2 drain currents.
From circuit inspection, follows:

$$V_{GS2} = V_{GS1} + \frac{I_1}{g_{m5}} \tag{5.9}$$

which can be valid if $V_{GS2} > V_{GS1}$. To ensure that this is the case, M2 must be larger than M1. In this particular design, $W_1 = 4W_2$.
Being $I_1 = I_{DS1} = I_{DS5}$, and since M5 is assumed to work in linear region, the output current flowing in M6 can be written as follows:

$$I_{OUT} = I_2 = I_1 = \frac{W_5}{L_5}\mu_n C_{OX}\,(V_{GS5} - V_{TH5}) \cdot V_{DS5} \tag{5.10}$$

Circuit sensitivity can, therefore, be expressed as follows:

$$\frac{\partial I_{OUT}}{\partial V_{TH}} = -\frac{W_5}{L_5}\mu_n C_{OX} V_{DS5} \tag{5.11}$$

While the voltage drop across drain and source of M5 can is:

$$\frac{I_1}{g_{m5}} = \frac{W_5}{L_5}\mu_n C_{OX}\,(V_{GS5} - V_{TH5}) \cdot V_{DS5} \cdot \left(\frac{W_5}{L_5}\mu_n C_{OX} V_{DS5}\right)^{-1} \tag{5.12}$$

Finally, substituting equation 5.12 in 5.11:

$$I_{OUT} = -\frac{W_5}{L_5}\mu_n C_{OX}\,(V_{GS5} - V_{TH5}) \tag{5.13}$$

Equation 5.13 is linear with respect to the sensor's threshold voltage, as long as M5 remains in linear region, that is:

$$\begin{cases} V_{DS5} \leq V_{GS5} - V_{TH5} \\ V_{GS5} \geq V_{TH5} \end{cases} \tag{5.14}$$

Assuming $V_{GS5} = V_{DD}$ in order to maximize the linear range:

$$V_{TH5} \leq V_{DD} - V_{DSAT1} - V_{DSAT4} \tag{5.15}$$

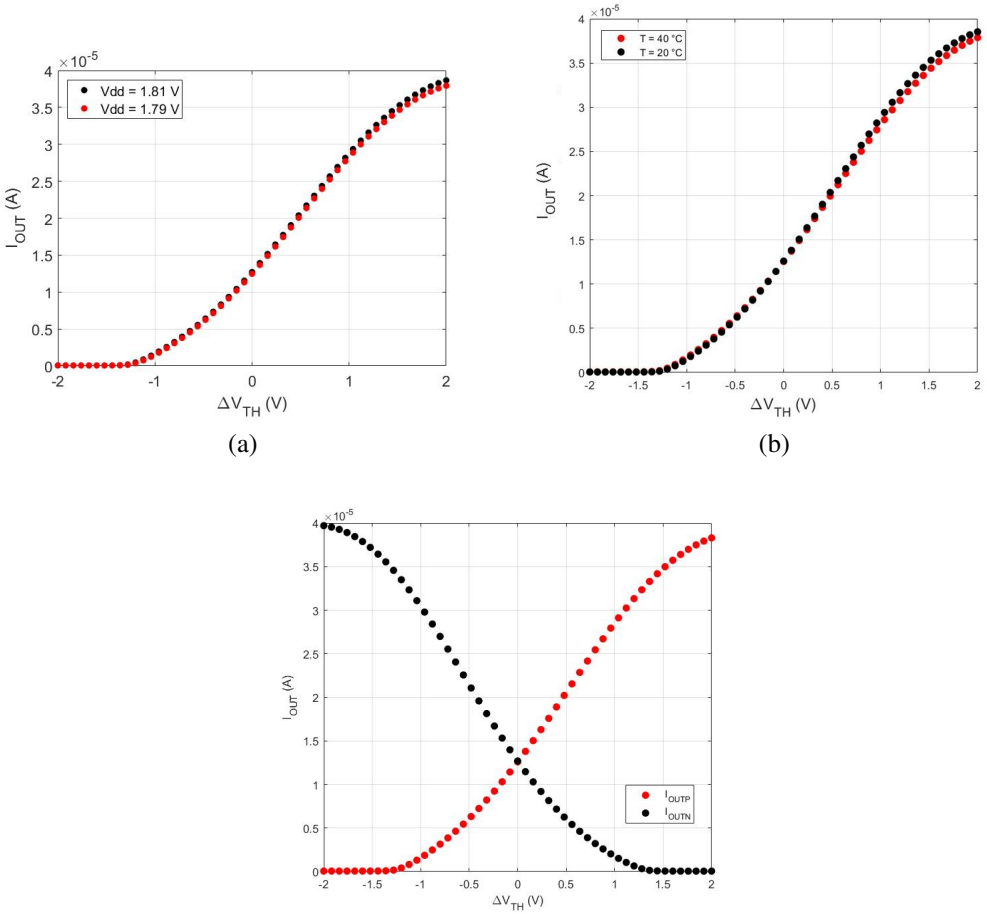

Figure 5.8 – (a) output current as a function of supply voltage variation; (b) Output current as a function of temperature variation; (c) output current as a function of threshold voltage variation.

Figure 5.8 shows electrical simulations of the aforementioned circuit, when connected to an NMOS transistor of a CMFET sensor: a sensitivity of $175nA$/100 mV was obtained in a linear range of 3.1 V (figure 5.8c). A current variation of 0.4%/°C (figure 5.8b) and 1.1%/10mV of suppply voltage variation (figure 5.8a) was achieved.

Readout circuit: current-starved ring oscillator

In order to extract threshold voltage variations, the output current can be directly measured or be used to bias a current-starved ring oscillator and then transduced into a

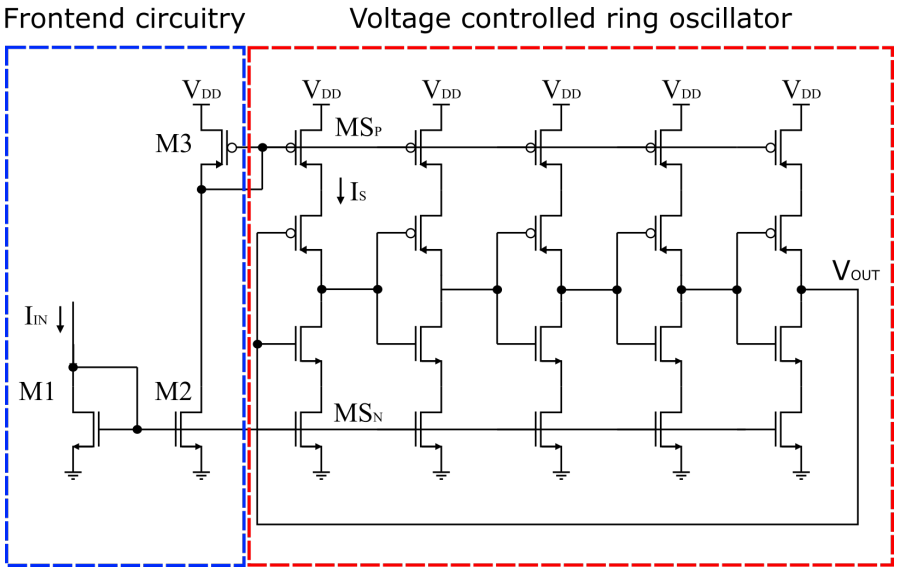

Figure 5.9 – Readout circuit: 5 stage current-starved ring oscillator architecture.

frequency (analog-to-time conversion). This latter prospect allows the employment of a simple counter for the final time-to-digital conversion. Therefore, a 5 stage current-starved ring voltage controlled ring oscillator (VCO) architecture was employed as an alternative readout circuit.

For a standard ring oscillator, the oscillating frequency depends on the current I_S which flows on the inverter and can be expressed as follows:

$$f_{OSC} = \frac{I_S}{NV_{DD}C_{TOT}} \tag{5.16}$$

where V_{DD} is the supply voltage, C_{TOT} the total output capacitor of the loop and N is the number of stage. As stated from equation 5.16, it is possible to conveniently tune the oscillator frequency through the current I_S. Figure 5.9 shows the schematic of the employed circuit. The input current I_{IN}, that is the output current of the previously described readout circuit, is mirrored from the frontend circuitry through the transistors M1 and M2. The drain currents of M2 and M3 are then mirrored in each current source stage of the VCO. The current sources MS_P and MS_N limit the current I_S available to the inverter, thus allowing the frequency control of the output (V_{OUT}). To make the

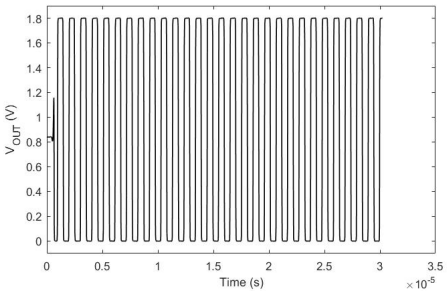

(a) Current-starved ring oscillator output voltage

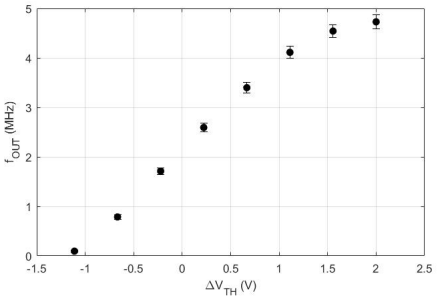

(b) Monte Carlo simulations of the current-starved ring oscillator, as a function of the threshold voltage variation of the sensing unit.

Figure 5.10

current linear with the input voltage at the gate of M1, the transistor width (W_1) is made wider than the one of M2 ($W_1 = 10W_2$) so that its V_{GS} is always approximately V_{THN} [3].

Figure 5.10a and 5.10b show respectively the output voltage of the voltage controlled oscillator and the results of Monte Carlo analysis with process and mismatch variations (200 points) of the proposed circuit. The output frequency is linear with the variation of the threshold voltage for a range of 2.2 V of each sensor, thus achieving an overall linearity range of 2.8 V. A sensitivity of 0.33 MHz/100 mV has been achieved.

5.3 Time-to-digital converter

A dual-slope time-to-digital converter (TDC) was chosen, in order to be able to perform the analog-to-digital conversion of both voltages (level-shifter) and currents.

The working principle of the circuit shown in figure 5.11 rely on the ratio of the time required to charge the two capacitances C1 and C2. During a reset stage, control signals S1 and S2 disconnect the respective switch and both capacitances, C1 and C2, are discharged by a reset signal. Subsequently, the switch S1 connects C1 to I_{SENS}. Assuming a perfect current source, the voltage V_+ increases linearly and reaches a final value given by $V_+ = \frac{I_{SENS}}{C_1}\Delta T_1$. The signal S1 finally disconnects C1 from the corresponding current, and the capacitance becomes floating. Then, C2 is connected to a

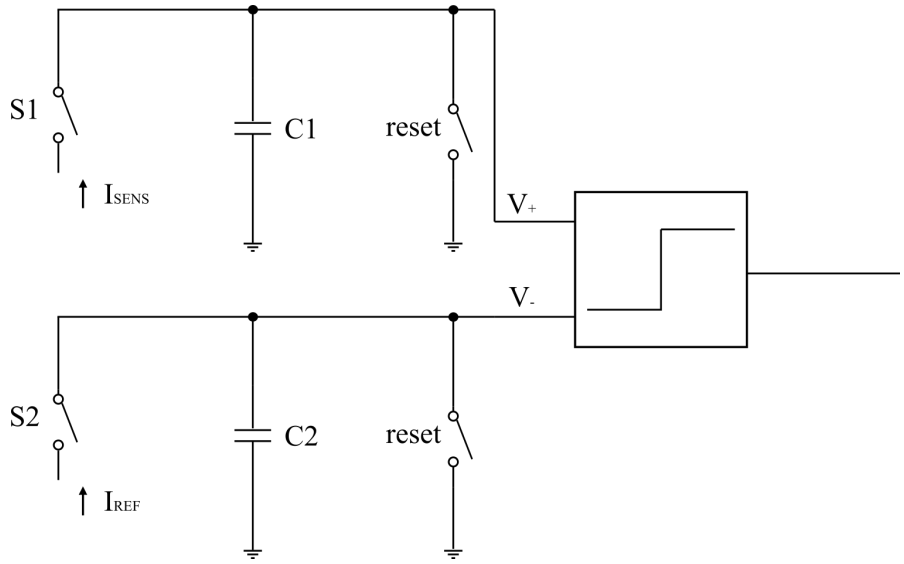

Figure 5.11 – Schematic circuit diagram of the employed dual slope time-to-digital converter.

second current source I_{REF} by S2. The voltage V_- across C2 is given by $V_+ = \frac{I_{REF}}{C_2}\Delta T_2$ where ΔT_2 is the time elapsed since the signal S2 connected C2 to I_{REF}. A comparator connected to both capacitors detects when the two voltages V_+ and V_- are equal, that is:

$$\Delta T_1 + \Delta T_2 = \left(1 + \frac{C_2}{C1}\frac{I_{SENS}}{I_{REF}}\right)\Delta T_1 \tag{5.17}$$

With a capacitance ratio $M = \frac{C_2}{C_1}$ and a current ratio $N = \frac{I_{SENS}}{I_{REF}}$ the initial time interval ΔT_1 is stretched by a factor $(1 + M \cdot N)$ which can be measured employing a simple counter for the final time-to-digital conversion. Furthermore, as both factors M and N are ratios of physical quantities, this approach turns out to be very robust against process variations. In particular, being interested in differential measurements, any systematic error would be uninfluential.

Figure 5.12a shows the simulation of the aformentioned circuit. Simulations were performed using a clock frequency of 10 MHz, M=100, a reference current I_{REF} of 500 nA and a sensing current I_{SENS} of 500 nA. Control signals acts as previously described: the conversion begins with a start signal, and the reset of both C1 and C2 to a programmable voltage. The conversion evolves as previously mentioned until the voltage V_- across the capacitance C2 is equal to V_+. Then, S2 disconnects C2 and the

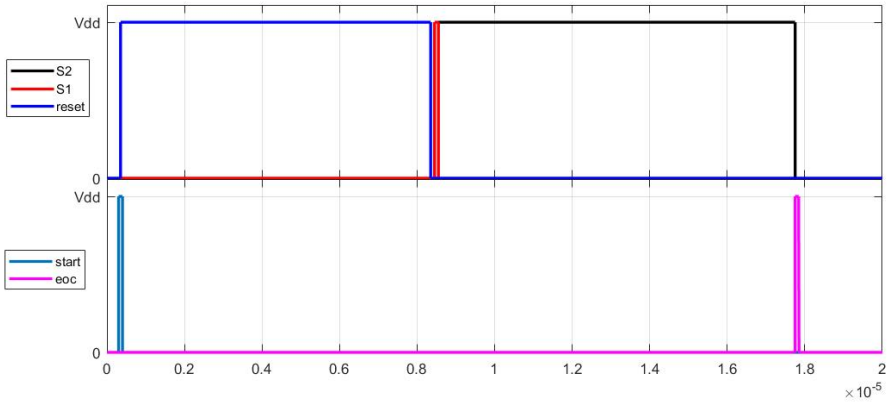

(a)

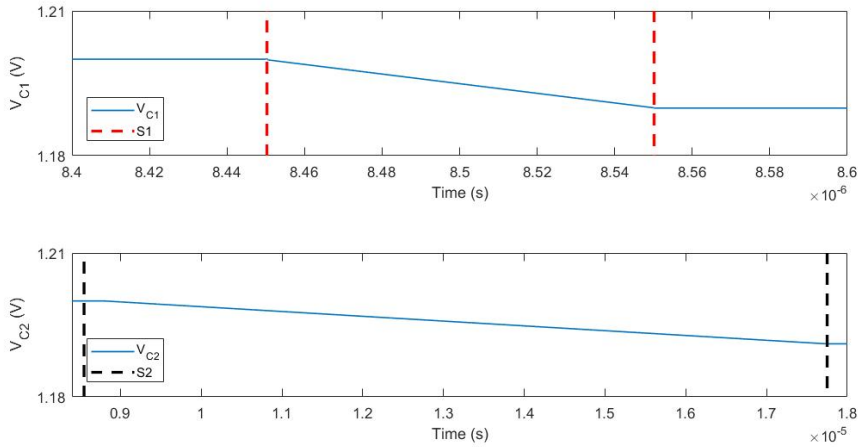

(b)

Figure 5.12 – Time-to-digital converter: (a) control signals and (b) voltage across C1 and C2.

end-of-conversion (eoc) signal notices for the completion of the conversion. Figure 5.12b shows the linear increase of the voltage across C1 and C2.

Such an implementation can be easily be employed to perform a voltage-to-time conversion, directly connecting the unknown voltage V_x to the capacitor C1 so that the comparator directly compare V_- and V_x.

Figure 5.13a shows the results of a complete simulation: the output current of the output

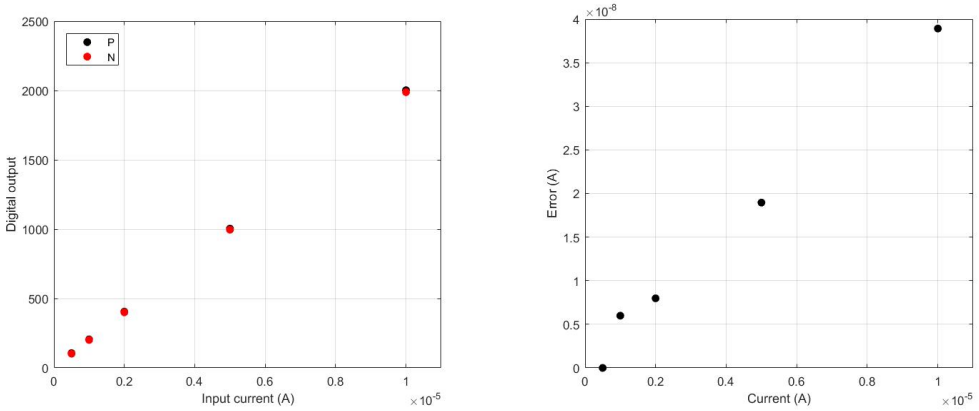

(a) (b)

Figure 5.13 – Time-to-digital converter: (a) digital output (b) error.

current of the readout circuit was directly read from the TDC. Figure 5.13b shows the dependency of the error on the input current, which determine a resolution of 38.9 nA. Such a behavior is related to the leakage current of C1, which gradually decreases the voltage V_+ thus affecting the converter performances. In the case of voltage conversion, as the leakage current of the capacitor C1 does not affect the measurement, a final resolution of 100 μV was achieved.

According to the previously presented simulations, such accuracy allows to precisely detect variations of the threshold voltage related to the addition of 6 nucleotides to immobilized probes, thus allowing to adequately measure the elongation process. In particular, considering both the immobilization procedure and its related surface density coverage, as well as the enzyme's activity, the presented circuitry allows to correctly employ the LoC for telomerase activity detection.

5.4 Accessory functionality

A complete Lab-on-Chip, in order to perform a complete analysis independently from other laboratory instrumentations, requires the introduction of some accessory functionality. In particular, a temperature control system was designed using a resistor as a heating element, and a temperature sensor. Finally, in order to enable the possibility to perform electrochemical modifications, a potentiostat was implemented as well.

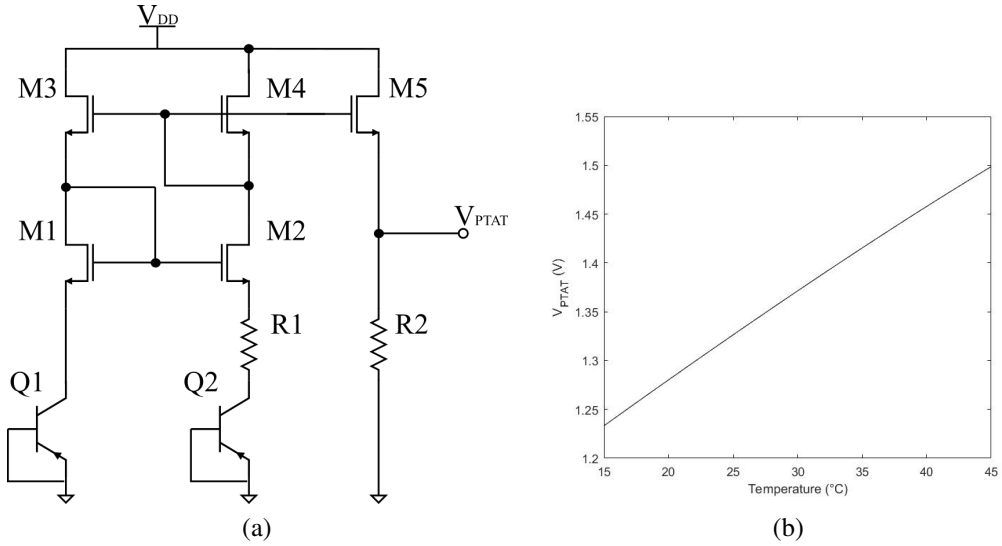

Figure 5.14 – (a) Schematic circuit of the employed PTAT temperature sensors and (b) the related output voltage variations as a function of temperature.

Temperature sensor

Temperature control is a critical factor in order to promote biological processes, as previously discussed in the case of telomerase activity. Therefore, a temperature sensor was implemented in order to monitor this parameter. In particular, a proportional to absolute temperature (PTAT) sensor was employed and it is shown in figure 5.14a.

The PTAT voltage is obtained biasing two bipolar transistors Q1 and Q2, having different areas ($A_2 = n \cdot A_1$), with the same current. This condition is guaranteed by the current mirrors M1, M2 and M3, M4. In such conditions, assuming V_1 and V_2 potentials at the same level, the drain currents of M1 and M2 are equal to:

$$I_{DS1} = I_{DS2} = \frac{k \cdot T}{q} \cdot \frac{ln(n)}{R_1} \tag{5.18}$$

where k is the Boltzmann's constant, q the electron charge, T the absolute temperature and n the ratio between A_2 and A_1.

Consequently, the output current can be expressed as follows:

$$V_{PTAT} = I_{DS5} \cdot R_2 = \frac{W_5}{W_4} \cdot I_{DS2} = \frac{W_5}{W_4} \cdot \frac{k \cdot T}{q} \cdot \frac{ln(n) \cdot R_2}{R_1} \tag{5.19}$$

Simulation results, reported in figure 5.14b, show the linear dependence of the PTAT output voltage with respect to the temperature. A resolution of 9.488 mV/°C was achieved, thus leading to a final resolution of the system of 0.1 °C.

Potentiostat

Finally, in order to enable the possibility to perform electrochemical modification on the electrodes, a two electrode potentiostat was implemented. The possibility to perform a surface modification, addressing each single each electrode independently, not only allows to employ specific electrochemical procedures to improve improve the surface properties in terms of binding with probes or selectivity, but also permit to modify each electrode in a different way. The possibility to implement different electrochemical modifications allows performing diverse measurements at the same time, or to implement different sensing strategies. In order to accomplish such a modification, however, not only the circuitry necessary to regulate the cell potential is needed, but also a method to directly connect the floating gate and allow a current flow through it. Clearly, such a method, must not interfere with the sensing unit during measurement phase. Therefore, the circuit shown in figure 5.15a was employed. In particular, two double-diffused MOS (DMOS) act as switches in order to connect/disconnect the floating gate when the potentiostat is operated.

Figure 5.15b shows the simulation of the circuit in figure 5.15a, when V_{CG} = 0.9V, V_{swp} = 1.8V and V_{swn} = 0V, compared to an identical device without the two switches. Obviously, the floating gate potential of the device without the two DMOS is essentially constant, as it is indeed floating. On the other hand, even if the presence of the two DMOS affects the second device during the first 50 seconds, their operation actually guarantee the electrical isolation of the floating gate after such transient response, thus allowing the employment of the structure as a CMFET.

After having verified the feasibility of the proposed approach, the design potentiostat shown in figure 5.16c was realized. The basic working principle of such a circuit rely on the capability of the NMOS transistor to source an adequate current, in order to hold the electrode to a constant potential with respect to the bulk of the solution. For simulation purposes, the microelectrodes in the electrolyte were modeled as a current source in

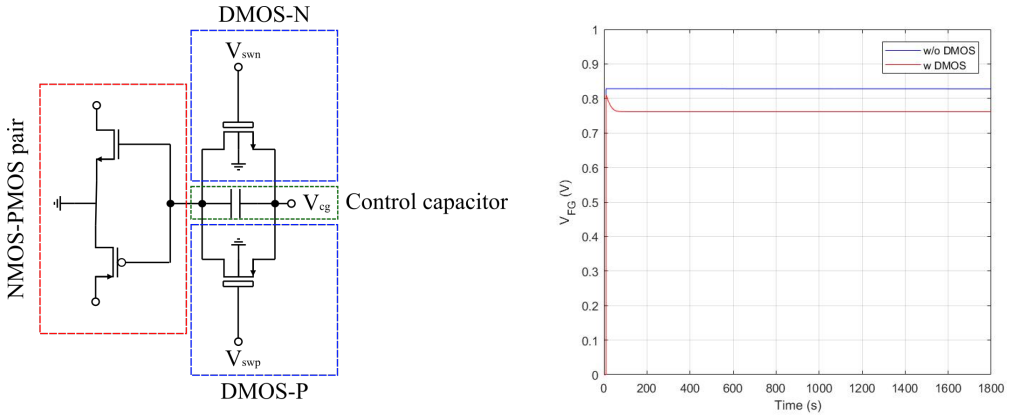

(a) (b)

Figure 5.15 – (a) Circuit schematic of the pixel unit with the addition of the two switches. (b) Electrical simulation of the floating gate potential of the sensing unit with the switches, compared to an identical circuit without the DMOS transitors.

parallel with a fractal parasitic R-C impedance [4].

Stability analyses shown in figure 5.16a have been performed according to [5]: in particular, since R_{CELL} and C_{CELL} vary over a couple of decades, the pole related to the electrode-electrolyte impedance can vary over a couple of decades as well, causing a large shift in the overall phase lag of the potentiostat circuit [5]. Therefore, in order to compensate such an issue, increase the conductivity of the redox medium through an increase in the electrolyte molar concentration or solvent polarity or through a decrease in it's viscosity should be necessary. Inspection of the stability analysis results, however, shows that the potentiostat circuit here discussed is stable for a variation of R_{CELL} in the range $150 \div 1500\Omega$ and C_{CELL} in the range $10 \div 500pF$. Finally, the capability of the circuit to hold the electrode at a desired potential was verified. Figure 5.16b shows the error related to the cell potential with respect to the reference voltage ($V_{REF} - V_{CELL}$).

According to the presented simulations, additional features can be successfully employed to implement in a single electronic platform all the features necessary to perform a measurement without the need for an external instrument, thus allowing to independently address possible electrochemical immobilization, temperature control, as well as telomerase activity measurement.

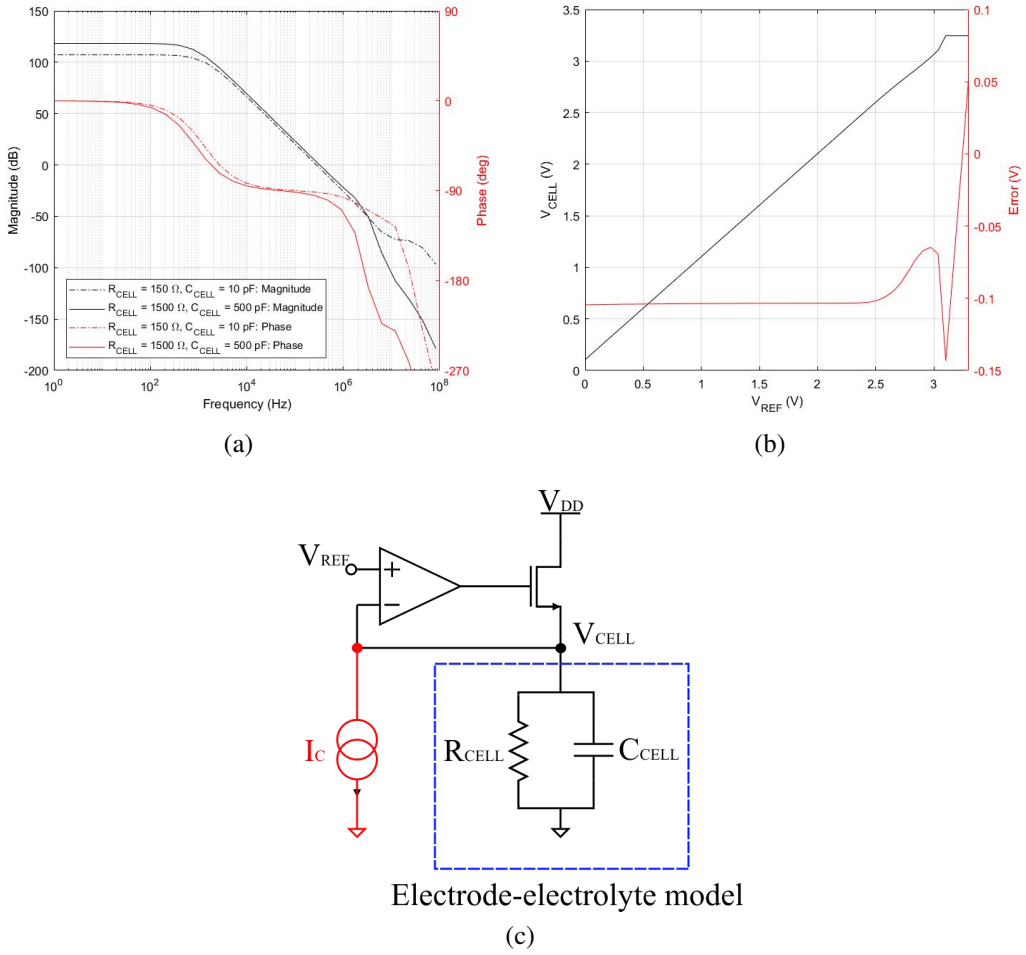

Figure 5.16 – (a) Stability analyses of the potentiostat circuit, for various electrode-electrolyte impedance. (b) cell potential and related error with respect to V_{REF}, as a function of V_{REF}. (c) electrical circuit of the employed potentiostat.

Bibliography

[1] M. Barbaro, A. Bonfiglio, and L. Raffo, "A charge-modulated fet for detection of biomolecular processes: Conception, modeling, and simulation.," *IEEE Trans. Electron Devices*, vol. 53, no. 1, pp. 158–166, 2005.

[2] M. Barbaro, A. Caboni, D. Loi, S. Lai, A. Homsy, P. D. Van Der Wal, and N. F. De Rooij, "Label-free, direct DNA detection by means of a standard CMOS electronic chip," *Sensors and Actuators, B: Chemical*, vol. 171-172, pp. 148–154, 2012.

[3] R. J. Baker, *CMOS Circuit Design, Layout, and Simulation*. 2010.

[4] a. Frey, M. Jenkner, M. Schienle, C. Paulus, B. Holzapfl, P. Schindler-Bauer, F. Hofmann, D. Kuhlmeier, J. Krause, J. Albers, W. Gumbrecht, D. Schmitt-Landsiedel, and R. Thewes, "Design of an integrated potentiostat circuit for CMOS bio sensor chips," *Proceedings of the 2003 International Symposium on Circuits and Systems, 2003. ISCAS '03.*, vol. 5, pp. 9–12, 2003.

[5] S. M. Rezaul Hasan, "Stability analysis and novel compensation of a CMOS current-feedback potentiostat circuit for electrochemical sensors," *IEEE Sensors Journal*, vol. 7, no. 5, pp. 814–824, 2007.

6 Conclusions and outlooks

Since the Nobel Prize-winning discovery of the enzyme telomerase, and the finding of its activity in the pathogenesis of cancer, a strong effort was dedicated to the investigation of telomeres shortening process and telomerase activity regulation. This exertion lay the foundation for the motivation of this PhD work activity: make a breakthrough in current telomerase activity detection methods.

The employment of a bioFET structure allowed the overcoming of the main drawbacks of these approaches, not only avoiding the complex and time-consuming amplification step, but also enabling the possibility to perform a direct, label-free detection of the elongation process, preventing the outbreak of systematic errors caused by the interaction between the label and the process under analyses. Besides the advantages related to the employment of a FET-based device, the Charge-Modulated FET structure further facilitated its employment and miniaturization, enhancing the integration perspective because of the lack of a reference electrode.

In order to exploit novel materials, which proven to be specially interesting in bio-related applications because of their cost-effectiveness and large-area fabrication possibilities, an organic-based implementation of the CMFET was thoroughly studied. The device has proven to precisely detect oligonucleotides of different length, enabling the possibility to distinguish between strands which differ for 6 nucleotides, that is a single repetition of telomere's base sequence. Furthermore, it shown to be suitable for accurately detect and discern telomeres elongation from enzyme presence, and to perform a real-time

measurement of the occurring reaction without the need for sample purification, nor filtration.
Taking advantage of the independence of the proposed approach from the technology actually employed for the device fabrication, a fully CMOS LoC platform was designed in order to achieve a large scale integration, for the development of high-parallel sensing platform conceived for laboratory environment. Finally, according to the results obtained with the organic device and to data reported in literature, the effectiveness of the LoC was addressed through post-layout simulations.

The obtained results clearly demonstrate the feasibility of the proposed approach, and open to the possibility of an application beyond the bare academic proof-of-concept. Therefore, the LoC fabrication and characterization, in order to develop a device for the actual employment in a laboratory environment should be established as a main outlook of this research activity.

A Beyond telomerase activity detection

A.1 OCMFET integration with hairpin-shaped probes for direct detection of DNA hybridization

The results discussed in this manuscript open the possibility to employ the proposed structure to fabricate both a low-cost point-of-care device for clinical applications and an high-parallel sensing platforms for biosensing applications, which span from the detection of DNA hybridization to the measurement of enzyme's expression as indeed discussed in this thesis. In order to further improve device's performances, the integration with a new kind of probe has been examined. In particular, because of the excellent results obtained with the employment of Molecular Beacons (MBs) in different applications, these probes have been evaluated as an interesting alternative to the usually employed linear probes. MBs, originally introduced by Tyagi and Kramer more than two decades ago [1], are oligonucleotide probes with a peculiar stem-loop structure, showed in A.1a.

The stem is a double-stranded structure composed by the two extremities of the oligonucleotide designed to be fully complementary, to ensure the stability of this structure. The loop part acts, entirely or in part, as a probe, allowing the MB to hybridize with a complementary single-stranded DNA or RNA target sequence. In systems with an optical transduction, a quencher and a fluorophore are covalently linked in 3'- and 5'-position. The MB is energetically engineered for maintaining a hairpin shape as long as the loop does not hybridize with a fully complementary target molecule. In this condition,

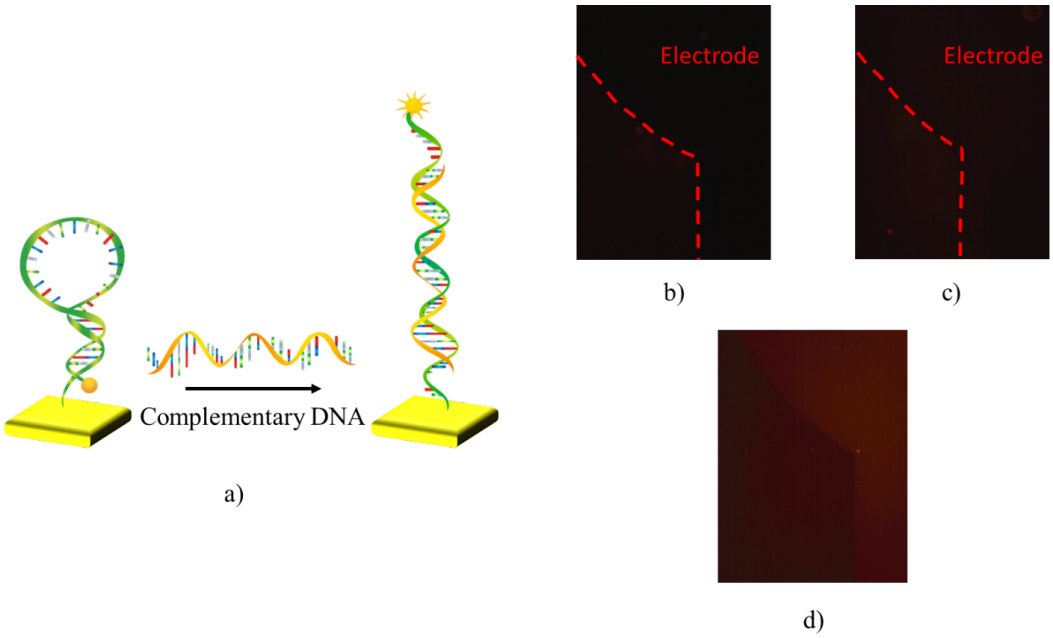

Figure A.1 – a) schematic representation of MBs working principle. Fluorescence microscopy image of the transistor's sensing area before (b) and after (c) MBs immobilization. The fluorescence signal increases after the introduction in solution of fully-complementary ssDNA (d).

the quencher and the fluorophore are close together, thus determining a quenching of the fluorescent signal coming from the latter. Upon hybridization, a conformational change occurs in the molecule and the quencher is moved away from the fluorophore, thus restoring the fluorescence and allowing the detection of the occurred hybridization. The possibility to integrate this technology with the OCMFET was evaluated, anchoring MBs onto the gold sensing area: to this aim, probes were modified in their 3'- end with a thiol (HS) group, which forms a thiol bound with the gold surface. At the 5'- end, a Cyanine3 fluorochrome was employed; in this case, MBs are not labeled with a quencher as the gold surface itself acts as a quenching agent.

Sensors were fabricated as previously discussed, whereas probes immobilization was performed spotting 60 μL of Tris 10 mM pH 8 with the addition of 10 mM $MgCl_2$ (TRIS) containing 100 nM of single-strand DNA molecules (ssDNA) on top of the sensing area. After 90 minutes, 2 μL at 1 mM concentration of solution of 6-mercapto-1-hexanol (MCH, Sigma-Aldrich) was added. MCH molecules act as spacer and blocking agent, leaving probes tethered through the thiols end groups, displacing the weaker adsorptive

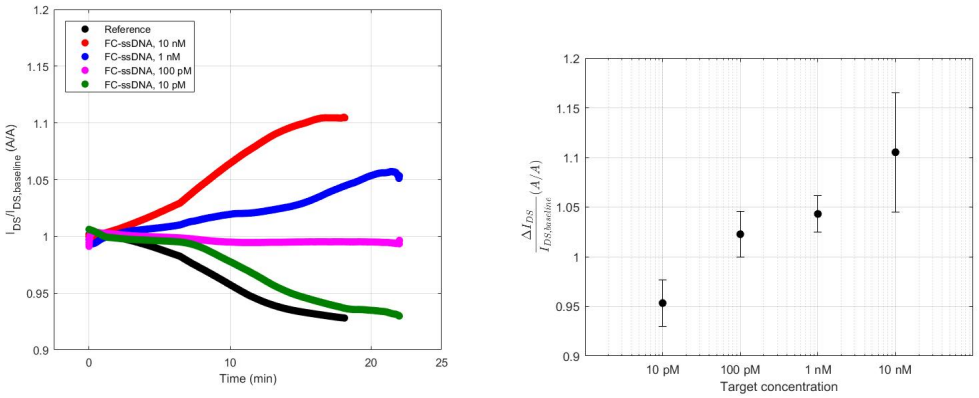

(a) Output current of OCMFET sensors after the addition of different concentrations of FC-ssDNA and of the sole TRIS buffer solution without the FC-ssDNA (black curve).

(b) Output current variation of sensors after the addition of different concentrations of FC-ssDNA

Figure A.2 – Real time electrical characterization of MBs hybridization by means of OCMFETs devices.

contact between DNA and gold [2].

First, the correct immobilization of MB on top of the OCMFET sensing area and their correct functionality upon hybridization was investigated through an optical analysis. Fluorescence images of sensing areas were captured before and after the immobilization of MBs. Figure A.1b and A.1c, show fluorescence microscopy images collected before and after the immobilization, respectively. Because the gold surface acts as quenching agent, as shown in figure A.1a and previously reported in Du *et al.* [3], the fluorescence level is negligible in these images. After that, a target oligonucleotide with a base sequence complementary to the MB loop was inserted on the sensing area. As shown in figure A.1d, an evident increment of the fluorescent signal coming from the sensing area was observed, as an effect of the conformational change of the probe causing the separation of the fluorochrome/quencher pair (cfr. figure A.1a).

Then, electrical transduction of MB hybridization was investigated monitoring OCMFET output current in real-time. Figure A.2a shows the measured output current of OCMFETs devices after the addition of 2 μL of different concentration of MB fully-complementary ss-DNA (FC-ssDNA) molecule, in 60 μL of TRIS solution. The current value is normalized to its value before the introduction of the target molecules ($I_{DS,baseline}$). As a result of the occurring MB hybridization, an increase of the transistor output current

was observed. As a reference, a sensor was exposed to the pure solution employed for diluting the target molecules, showing a significant decrease of the output current (figure A.2a black curve). Such a sensor was employed in order to compensate any non-specific current variation. Therefore, the actual current variation related to the MB hybridization can be estimated by subtracting the non-specific current reduction in the sensor response. The quantitative information about the hybridization process, including the compensation of non-specific effects, is estimated after the saturation of the device response. Finally, the actual response to hybridization, i.e. the difference $I_{DS}/I_{DS,baseline} - I_{DSR}/I_{DSR,baseline}$ evaluated after curves saturation, was estimated with different target concentrations. Figure A.2b shows the obtained results: at least 3 different devices have been measured for each concentration. In order to characterize the actual sensor specificity to the target FC-ssDNA molecule, 4 different sensors have been measured as previously discussed, after the introduction of non-complementary ssDNA molecules at a concentration of 100 nM, which is 10 times higher than the highest target concentration tested. The average current variation measured in this case (0.06 ± 0.01 A/A), shows as electrical transduction of hairpin probes hybridization is possible for a target concentration as low as 100 pM.

Bibliography

[1] S. Tyagi and F. R. Kramer, "© 199 6 Nature Publishing Group http://www.nature.com/naturebiotechnology," *Nature biotechnology*, vol. 14, no. 3, pp. 303–308, 1996.

[2] T. M. Herne and M. J. Tarlov, "Characterization of DNA Probes Immobilized on Gold Surfaces," *J. Am. Chem. Soc.*, vol. 119, no. 13, pp. 8916–8920, 1997.

[3] H. Du, C. M. Strohsahl, J. Camera, B. L. Miller, and T. D. Krauss, "Sensitivity and specificity of metal surface-immobilized "molecular beacon" biosensors," *Journal of the American Chemical Society*, vol. 127, no. 21, pp. 7932–7940, 2005.

B Publications related to the PhD activity

Patents

- Barbaro, M.; Lai, S.; **Napoli, C.** *Metodo per la rilevazione dell'attivitá della telomerasi*, 08/02/2018, 102018000002511

Publications in International Journals

- **Napoli, C.**; Lai, S.; Giannetti, A.; Tombelli, S.; Baldini, F.; Barbaro, M.; Bonfiglio, A. *Electronic Detection of DNA Hybridization by Coupling Organic Field-Effect Transistor-Based Sensors and Hairpin-Shaped Probes*. Sensors 2018, 18, 990.

Conference Proceedings

- **Napoli, C.;** Sonedda, S.; Barbaro, M. *Telomerase activity detection by organic, charge-modulated FET biosensor* 28th Anniversary World Congress on Biosensors, Miami, June 2017.

- **Napoli, C.**; Barbaro, M.; *Optimization of an all-CMOS DNA hybridization biosensor with direct analog to time digital conversion*, Societá Italiana di Elettronica, Palermo, June 2017.

- **Napoli, C.**; Lai, S.; Giannetti, A.; Tombelli, S.; Baldini, F.; Barbaro, M.; Bonfiglio, A. *Organic transistor-based sensor for label-free Molecular Beacons hybridization detection* European Materials Research Society (EMRS), Fall Meeting, Warsaw, September 2016.

- **Napoli, C.**; Lai, S.; Vacca, A.; Mascia, M.; Rizzardini, S.; Palmas, S.; Barbaro, M.; *A device for robust measurement of biospecies in aqueous media* Gruppo Elettronica, Siena, June 2015, 165-166.

- Vacca, A.; Mascia, M.; Rizzardini, S.; Palmas, S.; Lai, S.; **Napoli, C.**; and Barbaro, M.; *Functionalization of Polycrystalline Gold Through the Electroreduction of Aryldiazonium Salts in Ionic Liquids* Chemical Engineering Transactions, 41, 79-84, 2014.